Vertical diffusivity and oxygen concentrations in a fjord basin

A case study of the deep basin in Masfjorden

Master's thesis in physical oceanography

Torunn Sandven Sagen

Geophysical Institute
University of Bergen

June 2021

Acknowledgements

Working on my master's thesis mostly from home has been a challenge, but the last year has also given me many opportunities and learning experiences for which I am grateful.

First and foremost, I want to thank my supervisors, Elin, Kjersti and Ingrid, for the opportunity to work with you for my master's thesis. I am deeply grateful for the valuable guidance, feedback, help and discussions we have on Teams and Zoom (and a few physical meetings), and through the exchange of many emails and documents. You were always encouraging and positive, and I have learned a lot from you regarding oceanography, scientific writing, critical thinking, and structuring my work.

I also want to thank the cruise leaders from the Geophysical Institute, Department of Biological Sciences and Institute of Marine Research for letting me participate in cruises and collect data to use in my thesis, and the crew at Kristine Bonnevie for always being welcoming. Coming along to these cruises were great learning opportunities, and much-needed breaks from home office the last year.

I am thankful for all the friendships I have made during my bachelor and master studies at GFI. Thank you for all the great memories we have together, and for caring at a safe distance through social media when it was required of us.

Last but not least, thank you to my family and friends for supporting me, motivating me, and listening to me when I needed it. Thank you for all the love, the afternoon walks, meals, workouts, and conversations.

Torunn Sandven Sagen
Fana, 31. May 2021

Abstract

The basin layer in a sill fjord is isolated from the coast, and may become hypoxic or anoxic if the renewal frequency is low. Deep water renewals and vertical mixing are the physical processes which affects the oxygen concentration in the basin. The temporal evolution of density and oxygen concentrations in the basin layer in Masfjorden, a sill fjord in western Norway, have been studied based on observations of hydrographic data obtained during February 2019 - March 2021. The vertical diffusivity in the basin layer were estimated from the observations and model results from the hydrodynamic model NorFjords160 by the budget method presented in Stigebrandt and Aure (1989). The observed vertical diffusivity was used in further calculations to find the oxygen consumption rate, and in an attempt to see how a partial renewal affects the oxygen concentrations close to the bottom in the basin. The hydrographic data showed a region with oxygen stressed conditions in the basin layer with concentrations around 2.5 $\mathrm{mL\,L^{-1}}$. Two shallow partial renewals occurred in the upper parts of the basin layer during summer of 2019 and 2020. The the mean oxygen concentration in the basin declined during the observational period, while the oxygen concentration at 450 m increased. The comparison of the volume mean vertical diffusivity in the observations and in the model suggests a realistic, but lower density reduction rate, in the model.

Contents

1 Introduction

Low-oxygen concentrations in a fjord basin will arise naturally over time when the basin layer is not renewed, due to biological activity. One example of such a fjord basin is found in Masfjorden, where low-oxygen concentrations of 2.5 $\mathrm{mL\,L^{-1}}$ (in 2019-2021) is observed close to the bottom in the deepest part of Masfjorden. As a part of my bachelor and master studies, I participated in student cruises to Masfjorden, and collected such oxygen data. This sparked my interest for the physical processes that affect the oxygen concentrations in Masfjorden, such as deep-water renewal and vertical diffusion, and motivated me to further analyze the data from Masfjorden.

Masfjorden is a sill fjord, a type of fjord with its basins separated from the coast by the sill. The basin in a sill fjord is at risk of becoming hypoxic or anoxic if it is not ventilated due to the oxygen consumption by biological activity. Hypoxic and anoxic conditions are terms used to describe low-oxygen and depleted oxygen concentrations, respectively. It is clear that ventilation of fjord basins are important for the ecosystems, as low-oxygen concentration will affect the ecosystems and marine organisms that depend on oxygen (Breitburg et al., 2018; Direktoratsgruppen vanndirektivet, 2018).

The two main processes which bring oxygen to a fjord basin are deep-water renewal and vertical diffusion. During a deep-water renewal event, dense coastal water masses are advected into the fjord. They sink and replace the existing basin water (Gade and Edwards, 1980). As the coastal water masses typically have higher oxygen concentrations compared to the fjord basin, the deep-water renewal event ventilates the fjord basin and increases the oxygen concentration (Aure and Stigebrandt, 1989). In between deep-water renewal events, the stagnant period or stagnation period, the remaining physical process which transports oxygen to the fjord basin is vertical diffusion. Diffusion is the mixing process driven by gradients, and can either be molecular or turbulent. While molecular diffusion is the mixing process of particles within the fluid, turbulent diffusion occurs due to shear in the fluid, and is more rapid than molecular diffusion (Honrath, 1995). Diffusion can be described in terms of a diffusion coefficient, also called diffusivity. This is a proportionality constant between the diffusive flux and the gradients within the fluid, and it describes the mixing intensity. When the diffusivity is known, we can estimate the transport of properties, for instance salt or oxygen, due to diffusive mixing.

A long-term trend showed decreasing oxygen concentrations between 1975 - 2017 in the deepest basin in Masfjorden, and it has been linked to the reduction of high density coastal water masses at sill depth and deep-water renewal events (Aksnes et al., 2019; Darelius, 2020). Observations of low-oxygen concentrations had consequences for aquaculture in Masfjorden, as fish farms needed to reduce their production and two farms were shut down (Aarre, 16.05.2017). Currently, there are no commercial fish-farming in the inner

part of the fjord, but Institute of Marine Research are still active.

Most of the recent fjord research has focused on the circulation and water exchange in the upper parts of the fjord, as this is where salmon lice lives. For instance, the Institute of Marine Research (IMR) operates a salmon lice model, which is used to gather information and advise the aquaculture industries along the Norwegian coast regarding the development and dispersion of salmon lice. The salmon lice model is based on the hydrodynamic model NorKyst800, a ROMS model with horizontal grid of 800 m$\times$800 m and 35 terrain-following layers. In addition, the IMR has another model set-up, NorFjords160, which offers a finer resolution of fjord regions (160m) (Sandvik et al., 2019). The model results show that deep-water renewal events occur more often than observed in the basin layer in Masfjorden. Since the basin layers have not been paid much attention to, it is interesting to look into the results and compare them to the observations.

The aim of my thesis is to further investigate the hydrographic and oxygen data from Masfjorden, focusing on oxygen concentrations and how they relate to the physical ventilation processes. The hydrographic and oxygen data were collected with CTD and mooring instruments during the time period February 2019 - March 2021. I estimate the vertical diffusivity with the method presented in Stigebrandt and Aure (1989), which is valid a fjord basin during stagnant periods. The hydrographic and oxygen data show no sign of a deep-water renewal event in the observation period, only shallow partial renewals. After I determine the vertical diffusivity in the fjord basin, I use it in calculations of oxygen concentrations, and to estimate oxygen consumption rates in the basin. I also the estimate the vertical diffusivity in NorFjords160 with the method in Stigebrandt and Aure (1989) to compare the and investigate if the model produces realistic vertical diffusivity results.

The topic of this thesis can be linked to United Nations' Sustainable Development Goals number 14 (SDG14), 'Life below water'. The aim for SGD14 is to "*conserve and sustainably use the oceans, seas and marine resources for sustainable development*" (United Nations, n.d.). Low-oxygen concentrations in fjords are of concern since fjords are important marine resources due to their ecosystem services and central role in aquaculture. Oxygen is vital for marine life and ecosystems, and low concentrations may have implications for aquaculture, production, and potentially the local communities. Additional organic matter and waste from fish farms may also increase the oxygen consumption rate in the basin (Stigebrandt, 2012), as more organic matter are available to be decomposed by respiration (Breitburg et al., 2018). Thus, renewal in fjords are important to understand, since it both flushed out waste from fish farms and ventilates the basin.

Increasing our knowledge about the physical processes in Masfjorden and how it affects oxygen concentrations is an important step to sustainably use fjords as a marine resources

and to care for the ecosystems and fjord environments. The findings from Masfjorden may also be of interest for other sill fjords that suffer the same fate (Andersson, 06.07.2020, 24.01.2021). Similar trends in low-oxygen concentrations have been observed in other sill fjords around Bergen, such as for instance Sørfjorden south of Osterøy, where low-oxygen concentrations have been observed in the deepest basin (Dale et al., 2019; Bye-Ingebrigtsen et al., 2019).

2 Background

2.1 General characteristics of fjords

A fjord is a long, narrow and deep inlet of coastal waters (Stigebrandt, 2012). The development of the fjord structure is linked to glacial erosion and carving. This explains why fjords are found along coastlines at higher latitudes, with steep-sided topography as the surrounding landscape and deep bathymetry (Farmer and Freeland, 1983). Fjords may contain one or multiple 'sills'. A sill is a shallow area, often located close to the fjord opening at the coast. It acts as a barrier between the coastal water and fjord water. When multiple sills are present, they create several basins within the fjord which results in varying depth along the fjord(Figure 2.1). In other words, a fjord can be described as a semi-enclosed basin constricted by topography (Inall and Gillibrand, 2010).

The constrictions in a fjord, such as the depth and width, are important to consider when we want to understand the physical oceanography in fjords. In nature, we can find fjords to be long or short, narrow or wide, deep or shallow, with or without sills. All these factors influence the dynamics and hydrography. Therefore, the fjord dynamic will vary between different fjords, and results that apply to one fjord may not be the case for another. I begin with a general introduction of physical fjord oceanography, before I specify which processes are relevant for Masfjorden and for this thesis.

Fjord systems are complex, where both local and non-local forcing affect fjord dynamics. Local forcing refers to the mechanisms within the fjord region, and non-local forcing are mechanisms which take place outside the fjord, i.e. the coastal region. Examples of local forcing are fresh water input, local wind stress and breaking of internal waves. Non-local forcing examples are non-local (or coastal) winds and horizontal density gradients between fjord and coast (Stigebrandt, 2012). We will see that currents driven by the different types of forcing are often confined to certain depth levels, or layers, in the fjord (Figure 2.2). This affects the hydrography in the fjord and gives rise to the typical water masses found in the fjord (Figure 2.1).

The fresh water input gives rise to *the surface layer* (Figure 2.1), where we find the lightest water masses in the fjord. These water masses are less saline compared to coastal and oceanic water masses due to the fresh water input. The fresh water input typically occurs in form of river runoff, which originates from rainfall or snow melt. The largest river runoff is often found at the fjord head, but sources can also be found at any point along the fjord. The surface layer is also referred to as the brackish layer. The typical depth of the layer is between 1-5 meters, depending on the intensity of the fresh water input relative to the fjord size (Aksnes et al., 2019).

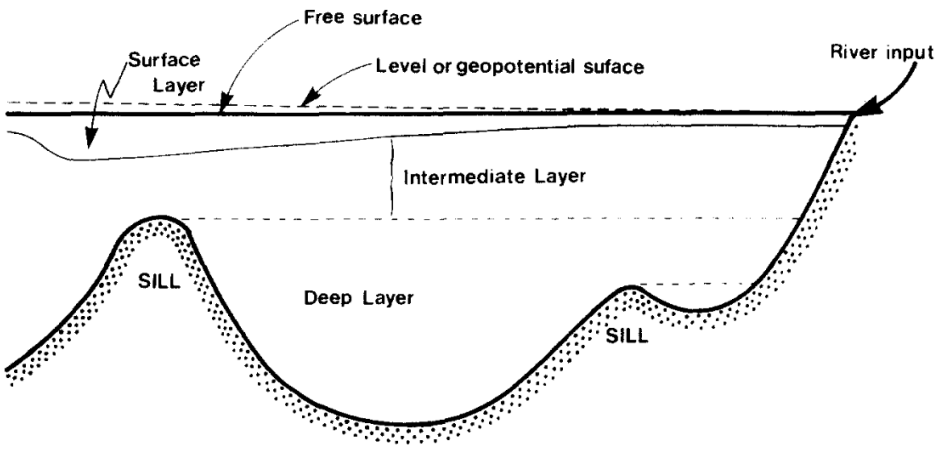

Figure 2.1: Schematic of typical water masses in sill fjords. The schematic shows an along-fjord section, from the fjord the mouth to the head. Two sills create two basins in the fjord. From Farmer and Freeland (1983)

.

The local forcing factors that influence the dynamics in the surface layer are fresh water input and local wind stress. The fresh water input introduces a mean estuarine circulation in the upper part of the fjord (Figure 2.2). Averaged over a tidal cycle, the fresh water input in the surface layer set up a current of fresher water directed out of the fjord. A compensating current of higher salinity water arises to conserve the fjord water volume (Inall and Gillibrand, 2010). The local wind stress is normally directed along-fjord, and sets up wind-driven currents in the surface layer. The wind-driven currents fuel vertical mixing in the upper layers (Stigebrandt, 2012), and it may enhance or dampen the estuarine circulation depending on the direction of the wind and the wind-driven currents. Wind events may also contribute to water exchange in the surface layer of the fjord (Spall et al., 2017). The wind driven currents are typically a few percent of the wind speed (Inall and Gillibrand, 2010). If the wind driven currents are 2 % of the wind speed, the wind driven current will be 0.1 $\mathrm{m\,s^{-1}}$ when the wind speed is 5 $\mathrm{m\,s^{-1}}$. Stronger winds increase the wind driven currents. The effects of local winds also depend on whether the fjord is narrow or wide. A narrow fjord has a fjord with smaller than the internal Rossby radius of deformation. In this case, the effects of Earths rotation can be neglected in the fjord, and the wind forcing is balanced by friction (Spall et al., 2017). For a wide fjord, the fjord width is larger than the internal Rossby radius of deformation, and Coriolis effects must be considered. Wind forcing may cause upwelling-downwelling response in wide fjords (Cushman-Roisin et al., 1994).

The intermediate layer is found below the surface layer and above the sill depth (Figure 2.1). The thickness of the layer depends on the sill depth. The layer can be absent if the sill is very shallow, or be several meters thick if the sill is deep (Inall and Gillibrand, 2010). In the case where the intermediate layer is present, the stratification and properties are

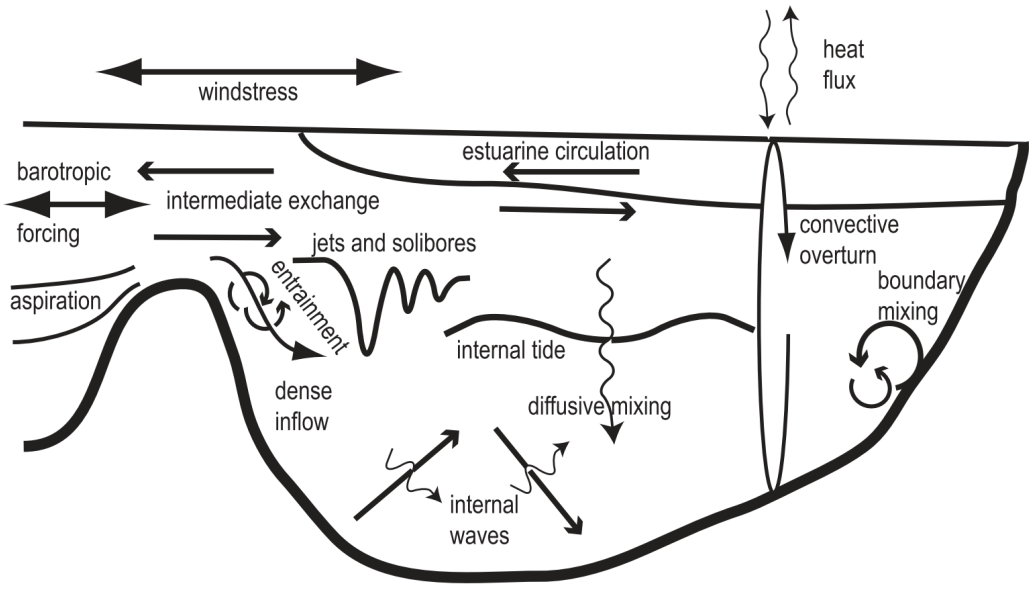

Figure 2.2: Schematic of common physical processes in sill fjords. The schematic shows an along-fjord section. From Inall and Gillibrand (2010)

.

determined by the coastal water masses outside the sill. The changes in temperature, salinity and other properties are found in the intermediate layer, with some phase delay (Stigebrandt, 2012).

Horizontal density gradients between the fjord and coast exist set up currents in the intermediate layer to reduce the gradients. This type of circulation is often referred to as the intermediate exchange (Stigebrandt, 2012). This is an example of how non-local forcing influences the fjord region. In fjords where tidal forcing is weak, the density gradients and the exchange of water masses are caused by vertical movement of the pycnocline at the coast. The vertical movement of the pycnocline is affected by e.g. coastal up- or downwelling, which is determined by coastal winds (Inall and Gillibrand, 2010).

In this thesis, I focus on the physical processes related to *the basin layer*, which is defined as the layer below sill depth. We have seen that water exchange takes place continuously in the surface and intermediate layer through mentioned processes like estuarine circulation and intermediate water exchange. The sill acts as a barrier between the coastal water and the basin water, which isolates the basin layer (Inall and Gillibrand, 2010; Stigebrandt, 2012). Given the right conditions, water exchange between coast and basin can occur. This type of water exchange is described in Chapter 2.2, together with its effect on oxygen concentrations.

2.2 Deep-water renewal

A *deep-water renewal (DWR) event* refers to the phenomenon where the basin layer has been renewed with coastal water masses (Figure 2.3). Without DWR events, the isolated basin layer is cut off from circulation and from its oxygen supply though renewal, and becomes stagnant over time. One effect of a long-term stagnation period is oxygen depletion in the basin layer. As oxygen is important for several organisms, it is clear that DWR events are important for maintaining a habitable environment in the fjord basin.

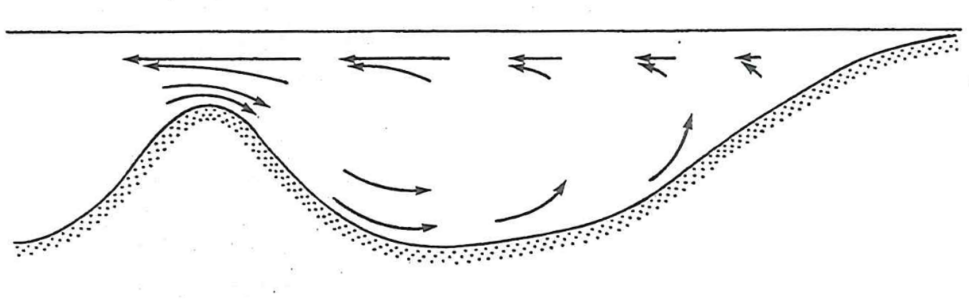

Figure 2.3: Schematic of a deep-water renewal event. Dense water enter at the sill, sinks and replaces existing water in the basin. Figure from Gade and Edwards (1980)

.

It is the density of the coastal waters compared to the basin water density that determines if a DWR event occurs. Coastal water masses are advected in and out the fjord through intermediate exchange. The basin layer remains unaffected by the intermediate exchange as long as it is denser than the coastal waters in the intermediate layer. When the coastal water density is equal or greater than the basin water density, coastal water sinks and renews the basin layer (Gade and Edwards, 1980). A DWR event can be full, where the entire basin layer has been renewed, or partial, where only parts of the basin has been renewed. A partial renewal occurs if the density of coastal waters is somewhere in between the density at the sill level and density at the basin bottom, or if the period of inflow is not sufficiently long. How quickly the basin is filled with new water depends on the transport capacity at the mouth and the volume of the basin. For fjords with large basin volumes, the time it takes to fill up the basin may last longer than the density fluctuations at the coast (Aksnes et al., 2019; Stigebrandt, 2012; Inall and Gillibrand, 2010). The DWR event itself is a relatively rapid process, and occurs on the time scale of about a few weeks (Gade, 1973).

How often a DWR event occurs is determined by the renewal frequency of the basin layer. The renewal frequency depends on the rate of density reduction (i.e. vertical mixing rate) in the basin and the coastal density variability (Gade, 1973; Darelius, 2020),

particularly at sill level of the fjord. The basin water density is reduced over time due to vertical mixing. A greater vertical mixing rate will increase the renewal frequency, as lighter water mixes down and reduces the density quicker. Thus, vertical mixing is a precondition for renewal, as it reduces the density difference between coastal and basin water (Gade and Edwards, 1980). The vertical mixing process in a fjord basin is discussed more in detail in Chapter 2.2.1.

The coastal density variability follows the variations in the oceanic climate, which depends on the season, weather events and meteorological conditions, interannual variability, and internal waves. All these factors affect the density of water masses found at the sill depth and the intermediate layer (Gade and Edwards, 1980). Studies from Gullmarsfjorden on the west coast of Sweden link DWR events to the North Atlantic Oscillation (NAO) (Nordberg et al., 2000; Polovodova Asteman and Nordberg, 2013). When the NAO index is negative, the sea level pressure over Iceland is higher compared to over the Azores. Northeasterly winds over Europe are more common during such conditions, and it drives coastal upwelling along the west coast of Sweden (Polovodova Asteman and Nordberg, 2013). Northerly winds are also of interest in regards to DWR events in fjords along the Norwegian coast line. Intrusions of dense waters into Norwegian fjords have been connected to northerly winds and coastal upwelling (Gade and Edwards, 1980; Asplin et al., 1999). Northerly winds set up an Ekman transport directed away from the coast line, lifting denser water up to towards the surface near the coast (Asplin et al., 1999; Cushman-Roisin and Beckers, 2011), and the sill.

Observations from Norwegian fjords have shown some regularity in the occurrence of DWR events. But the duration between each event and time of year they occur varies between different fjords. In the innermost basin in Oslofjorden, renewal occurs during winter time every 3-6 years. In Hardangerfjorden and Sognefjorden, they occur less frequent and preferably during summertime (Gade, 1973).

Even though a regularity of DWR events in fjords can be established, the regularity will be affected by changes in the oceanic climate and the density structure. Such changes may reduce or prevent the occurrence of DWR events. Ocean warming has been linked to reduction in the occurrence of DWR events in fjords along the Norwegian coast (Aksnes et al., 2019; Darelius, 2020), and coastal freshening has prevented renewal of fjord basins in Northeast Greenland (Boone et al., 2018).

2.2.1 Vertical mixing

Mixing is the irreversible process which changes the properties of fluids, and it occurs both vertically and horizontally. In this thesis, I will study mixing in form of vertical diffusion. Diffusion is a down-gradient, random process in which fluid properties are transported

from regions of higher concentration towards lower concentrations. The results is a diffusive flux which homogenizes the fluid over time, as properties spreads out and reduces the gradients (Cushman-Roisin and Beckers, 2011). Horizontal mixing is larger than vertical mixing because stratification and gravity works against mixing in the vertical direction. This is illustrated by the globally averaged vertical and horizontal (turbulent) diffusivity. The vertical (turbulent) diffusivity is found to be $\kappa_V = 10^{-4}\ \mathrm{m^2\,s^{-1}}$, while the horizontal (turbulent) diffusivity κ_H tends to be between 10^3 and $10^4\ \mathrm{m^2\,s^{-1}}$ (Talley et al., 2011).

The *diffusivity* (κ), or the diffusion coefficient, is a proportionality constant between the diffusive flux and the gradients in the fluid, and is used to quantify the effects of diffusion. It is a measure of the rate at which diffusion occurs and the intensity of mixing, and has SI-unit of $\mathrm{m^2\,s^{-1}}$. As an example, the expression for vertical turbulent (eddy) flux of density is given by

$$\kappa \frac{\delta \rho}{\delta z} = \overline{w'\rho'}$$

where $\overline{w'\rho'}$ is the vertical turbulent flux of density, $\frac{\delta \rho}{\delta z}$ is the vertical gradient of the density, and κ is the turbulent (eddy) diffusivity (Stigebrandt, 2012).

In addition for diffusion to be either vertical or horizontal, it can also be either molecular or turbulent. Molecular diffusion is the mixing process of the particles within the fluid, while turbulent diffusion is the mixing process which occurs due to shear and presence of eddies in the fluid (Honrath, 1995). Molecular diffusion is a slow process, and can exists without the presence of turbulence. The molecular diffusivity depends on the properties and the fluid, and will be different for specific substances, e.g. the molecular diffusivity for heat is larger than the molecular diffusivity for salt in sea water ($10^{-7}\ \mathrm{m^2\,s^{-1}}$ compared to $10^{-9}\ \mathrm{m^2\,s^{-1}}$ at salinity = 35) (Talley et al., 2011).

When turbulent motions are introduced, shears are created in the fluid. This accelerate and enhance mixing in the fluid (Thorpe, 2007), and makes turbulent diffusion a more rapid process compared to molecular diffusion (Honrath, 1995). While the molecular diffusivity depends on the quantity in question, the turbulent diffusivity mixes all quantities similarly. Thus, it is the turbulent diffusion that we are interested in with regards to supply oxygen to and density reduction in fjord basins.

The vertical diffusivity will vary among fjord basins, and with depth within a basin. From observations, typical values for vertical diffusivity in Norwegian fjords were found to be around $10^{-4}\ \mathrm{m^2\,s^{-1}}$, with the lowest values around $10^{-6}\ \mathrm{m^2\,s^{-1}}$(Gade and Edwards, 1980). The turbulent motions in fjords that feed into mixing processes stem from tidal forcing, wind forcing at the surface or instabilities in circulation near the surface (Farmer and Freeland, 1983). The effects of tides can be felt in the basin interior, while the currents

and turbulence generated by winds are found closer to the surface, and are reduced with depth (Farmer and Freeland, 1983; Gade and Edwards, 1980). Mixing can occur at the boundaries or be felt in the interior of the basin due to breaking of internal waves. In fjords where tidal forcing is weak, wind-induced mixing may dominate (Inall and Gillibrand, 2010).

2.2.2 Dissolved oxygen

The concentrations of dissolved oxygen in the ocean depend on both biogeochemical and physical processes. Air-sea gas exchange of oxygen occurs at the surface, and photosynthesis by primary producers occurs close to the surface in the euphotic zone. As a result, higher oxygen concentrations are typically found close to the surface. Subsurface, oxygen is consumed by organisms as they decompose organic matter, a process known as aerobic remineralization (Sarmiento and Gruber, 2006). Within the ocean, oxygen is redistributed through physical processes such as diffusion, upwelling- downwelling events and currents. Dissolved oxygen is a useful tracer for circulation (Broecker and Peng, 1983; Sarmiento and Gruber, 2006), even though it is not a conserved quantity. Low-oxygen concentrations indicate that the water masses have not been in contact with the atmosphere recently, and is used as an indicator for ventilation and mixing in the ocean, such as coastal upwelling and DWR events (Thomson and Emery, 2014).

In a sill fjord where the sill depth is greater than the euphotic zone, sources of oxygen in the basin are limited. Photosynthesis will not take place as light does not reach the layer, and the air-sea gas exchange is limited to the surface. Hence, the three governing processes for oxygen concentration in a fjord basin are oxygen consumption due to the biochemical decomposition of organic matter, vertical diffusivity, and DWR events (Aksnes et al., 2019). During stagnant periods, the oxygen concentration depends on the oxygen consumption rate and the vertical diffusivity. When the oxygen consumption rate exceeds the physical transport of oxygen (and photosynthesis), oxygen concentrations will naturally be reduce over time (Breitburg et al., 2018).

When we know that the oxygen concentration and the density in an isolated basin layer decrease over time, we can identify a DWR event by these two parameters. After a DWR, the oxygen concentration and the density in the basin layer is expected to have increased since the inflowing coastal water usually has higher concentrations of oxygen compared to the basin water (Aure and Stigebrandt, 1989), and it must be denser in order to renew the layer.

The basin layer is prone to become hypoxic, or anoxic, due to the natural decrease of oxygen. This may occur in basins were the vertical diffusive oxygen transport is weak, and stagnant periods are long. In hypoxic conditions, the oxygen concentrations are

sufficiently low to affect sensitive processes in the ecosystem (Breitburg et al., 2018). In anoxic conditions, the water is fully depleted of oxygen. There are consequences for ecosystems related to hypoxic and anoxic conditions, and the consequences will vary since the oxygen tolerance varies among different organisms. Generally, low-oxygen concentrations and hypoxic conditions can alter growth and behaviour, increase disease and reduce survival for organisms (Breitburg et al., 2018), and loss of species diversity and bio mass is expected in (Chu et al., 2018). A common limit for hypoxic conditions in literature is set to be below 2 $\mathrm{mg\,L^{-1}}$, or 1.4 $\mathrm{mL\,L^{-1}}$ (Breitburg et al., 2018; Conley et al., 2011; Chu et al., 2018). I use $\mathrm{mL\,L^{-1}}$ in this thesis, but both units are included in Table 2.1. Limits for serve hypoxia (Chu et al., 2018) and oxygen stressed conditions (Conley et al., 2011) are also included.

Unit	**Serve hypoxic conditions**	**Hypoxic conditions**	**Oxygen stressed conditions**
$\mathrm{mL\,L^{-1}}$	$[O_2] < 0.5$	$0 < [O_2] < 1.4$	$1.4 < [O_2] < 2.8$
$\mathrm{mg\,L^{-1}}$	$[O_2] < 0.7$	$0 < [O_2] < 2$	$2 < [O_2] < 4$

Table 2.1: Oxygen concentrations, O_2, limits for classifying hypoxic, serve hypoxic or oxygen stressed conditions for units $\mathrm{mg\,L^{-1}}$ and $\mathrm{mL\,L^{-1}}$ (by unit conversion: $1\mathrm{mg\,L^{-1}} = 0.7\mathrm{mL\,L^{-1}}$ (ICES, n.y)).

A classification of ecological conditions at different oxygen concentrations in deep waters in fjords is given in Table 2.2, from "Veileder 02:2018" (Direktoratsgruppen vanndirektivet, 2018). Table 2.2 lists what state an ecosystem is at different concentrations of oxygen, where the ecological conditions range from "Very poor" to "Very good". Following this classification, the environment is considered to be good when oxygen concentrations above 3.5 $\mathrm{mL\,L^{-1}}$. Below 2.5 $\mathrm{mL\,L^{-1}}$, the ecological conditions are "Poor" and "Very poor". In such conditions, the ecosystem is considerably affected by the low-oxygen concentrations. In comparison with Table 2.1, "Poor" overlaps with oxygen stressed conditions, and "Very Poor" ecological state overlaps with hypoxic conditions.

	Very Poor	**Poor**	**Moderate**	**Good**	**Very good**
Oxygen $[\mathrm{mL\,L^{-1}}]$	< 1.5	1.5 - 2.5	2.5 - 3.5	3.5 - 4.5	> 4.5

Table 2.2: Classification system for ecological conditions based on oxygen levels in a basin layer (deep-water), modified from "Veileder 02:2018" (Direktoratsgruppen vanndirektivet, 2018).

2.3 Masfjorden

The study area for this thesis is Masfjorden, a fjord located on the Norwegian west coast. Masfjorden is a fjord arm of Fensfjorden, and Fensfjorden is connected to the North Sea (Nerheim and Lusher, 2020). Masfjorden is split into two smaller fjord branches; Matrefjorden and Haugsværfjorden. Matrefjorden reaches eastward, and Haugsværfjorden northeastward (Figure 2.4). Masfjorden is about 24 km long from its mouth to its head in Matrefjorden, and between 0,5 - 2 km wide (Darelius, 2020).

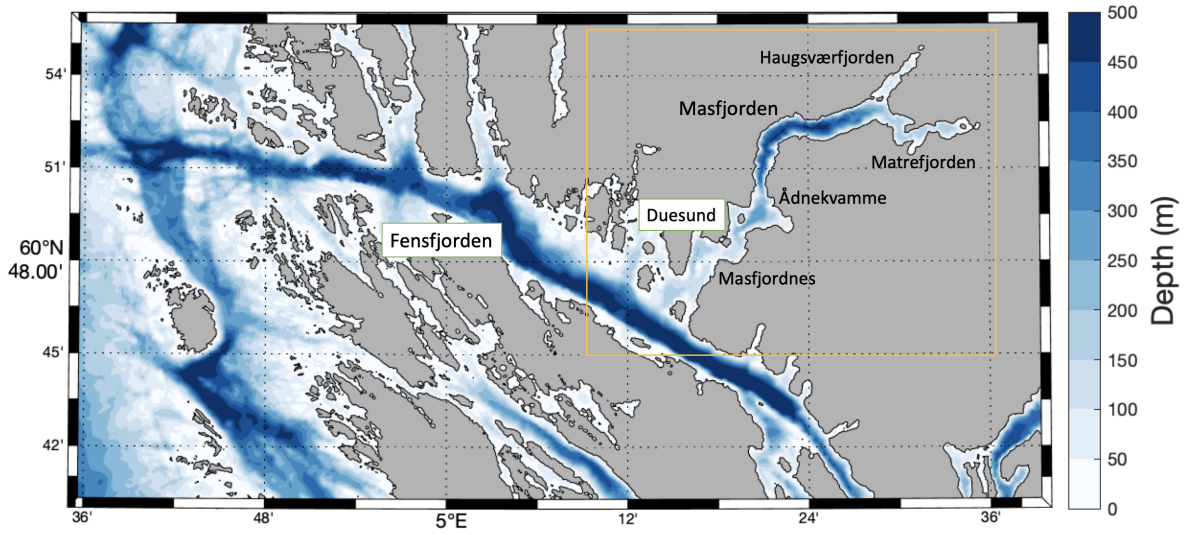

Figure 2.4: Map of Fensfjorden and Masfjorden with its fjord branches (Haugsværfjorden and Matrefjorden). The bathymetry is shown, where light blue represent shallow areas and dark blue represent deep areas. Locations mentioned in the text are shown on map. The orange box defines the area of Masfjorden, and is further explained in Figure 2.5

I examined bathymetric charts of Masfjorden to identify and locate sills and basins, and I identified two sills central for my thesis (Figure 2.5). The first sill (70 m) is located close to Masfjorden's mouth, between the Masfjordnes and Duesund. It separates the Masfjorden basin from Fensfjorden and the North Sea. I refer to this as the Outer Sill. The second sill, hereafter the Inner Sill, is found near Ådnekvamme. The depth of this sill varied between 140 m and 180 m due to what can be described as a trench at the sill. The deepest connection at 180 m is defined as the sill depth of the Inner Sill. A third sill (about 25 m) is located in the mouth of Haugsværfjorden, separating the basin in Haugsværfjorden from Masfjorden.

The Inner and Outer sill give rise to two basins in Masfjorden. The basin located between the Outer and Inner Sill is about about 295 m, from now on called The Shallow Basin. The second basin is located between the Inner Sill and the intersection of Haugsværfjorden and Matrefjorden (Figure 2.5). This basin is is 489 m deep, which is the maximum depth of Masfjorden (Aksnes et al., 2019), and therefore called the Deep Basin.

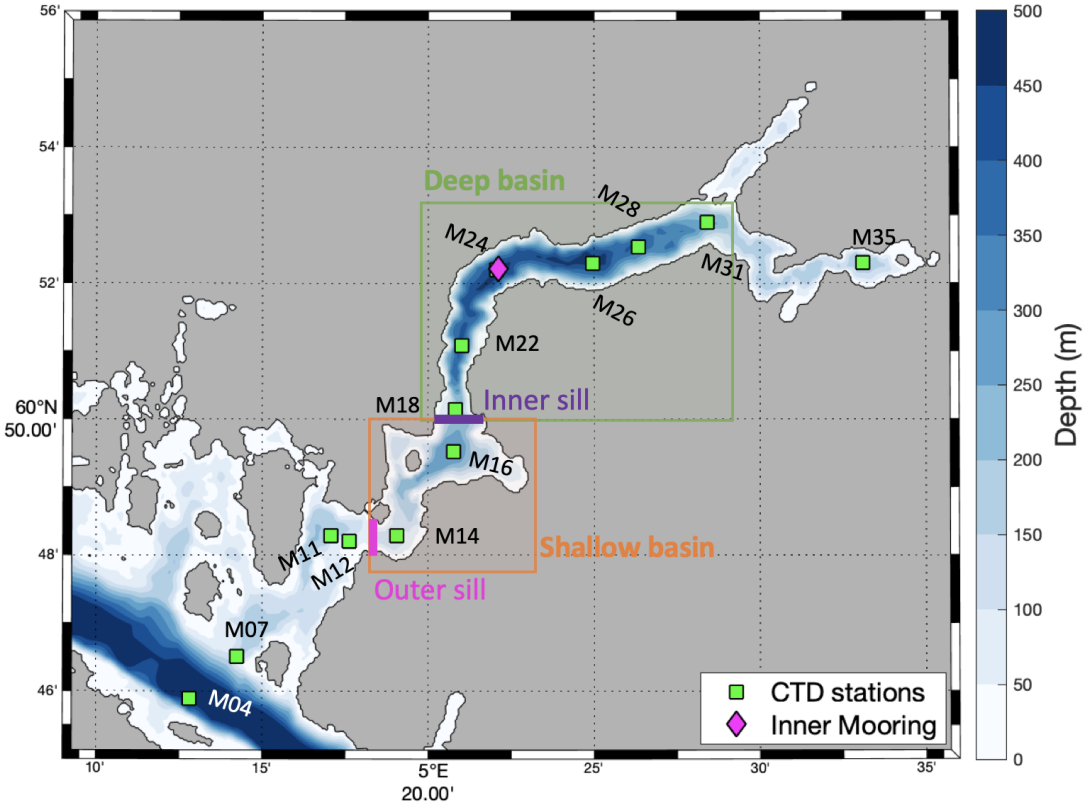

Figure 2.5: Map of Masfjorden with central fjord features and location of CTD stations and Inner Mooring marked. The bathymetry of the fjord is shown, the basins are marked as squares and the sills are represented by lines.

By following the general characteristics of fjord hydrography described in Chapter 2.1, the basin layers in the Deep and Shallow basin are expected to be found below the Inner Sill depth (180 m). Between the Outer Sill depth (70 m) and the surface layer (upper 1-5 m) we expect the intermediate layer to be found. A layer between 70-180 m remains to be classified, as this by definition is not a part of neither the intermediate nor the basin layer. This layer will probably be more influenced by coastal water masses than the basin layer, but sill more isolated than the intermediate layer (Figure 2.6).

Similarly to other fjords along the western coast of Norway, the surface and intermediate layer in Masfjorden are influenced by fresh water input, the Norwegian Coastal Current, and the coastal wind patterns (Nerheim and Lusher, 2020; Aksnes et al., 2019; Asplin et al., 1999). The large remaining basin layers in the Deep and Shallow basin are separated from the coastal waters, and are ventilated and renewed during DWR events. The water masses at 70 m in Fensfjorden are of interest when DWR events are in question, as the Outer Sill separates Masfjorden from Fensfjorden.

We find several industries, especially aquaculture industries, located in fjords along the

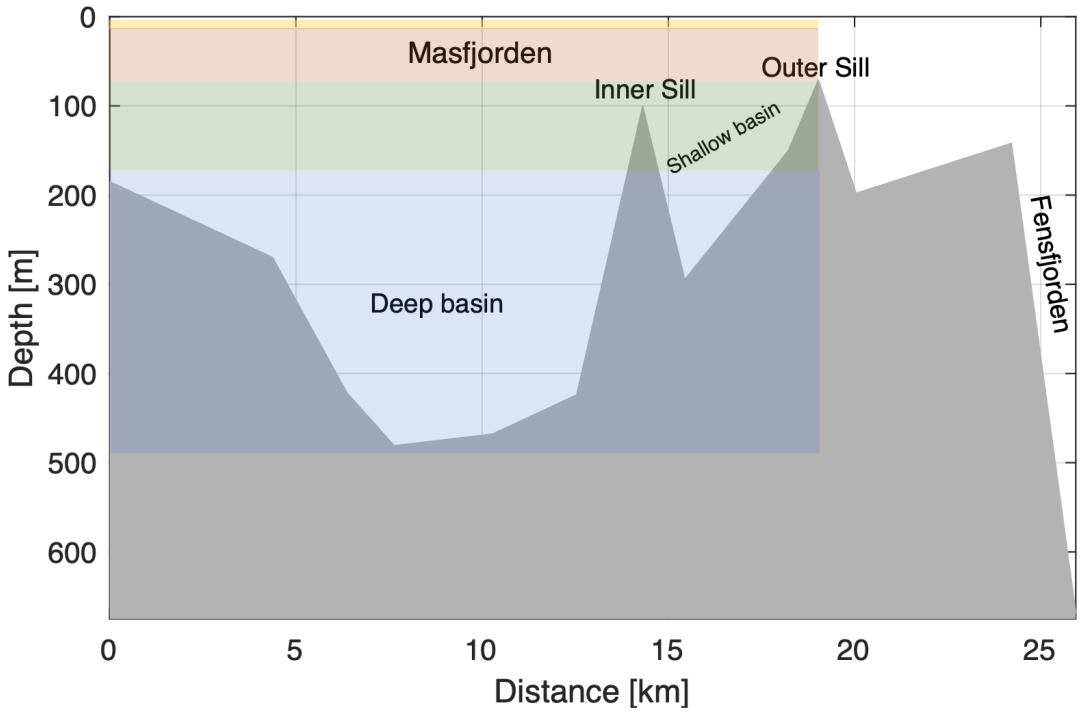

Figure 2.6: An illustration of the bottom bathymetry in Masfjorden based on CTD profiles. The section starts in Matrefjorden and reaches out towards Fensfjorden. The expected depths of the surface layer (yellow), intermediate layer (red) and basin layers (green and blue) are indicated. Note that the bottom bathymetry is based on the depth registered with the CTD, and does not represent the exact depth in the fjord.

coast line of Norway, which provides local communities with work (Nerheim and Lusher, 2020). Masfjorden is no exception, and several fish farms have been located along the fjord. A hydropower plant owned by BKK is located in Matre (BKK, 2021). The Institute of Marine Research (IMR) has a research station in Matre, dedicated to aquaculture research and fish experiments related to reproductive biology, fish welfare, salmon sea lice and fish nutrition (IMR, 2020).

A multi-decadal decline in dissolved oxygen in Masfjorden has been observed in the period 1975-2017, and since 2011, the oxygen concentration have been decreasing in the deeper parts of the basin in Masfjorden (Aksnes et al., 2019). The low-oxygen concentrations gained attention in the media as the they might cause difficulties for the marine life in the fjord. The consequences of low-oxygen observations, and Masfjorden being "suffocated", were that two fish farms in Masfjorden were shut down, and other fish farms had to reduce their activity (Andersson et al., 13.02.2017; Aarre, 16.05.2017).

During the spring of 2019 and 2020, I participated in two student cruises as a part of the courses GEOF232/GEOF337 at Geophysical Institute (GFI). We collected the standard hydrographic measurements, such as temperature and salinity, and oxygen, carbon and nutrient measurements. In both 2019 and 2020, we observed low-oxygen in the Deep

basin in Masfjorden of $\simeq$ 2.5 mL L^{-1}. Anoxic conditions were found below 60 m in Haugsværfjorden during both cruises. An interesting observation was the development of foul-smelling water samples. In 2019, the water samples from Haugsværfjorden were fully depleted of oxygen, but did not have any kind of smell. A year later, the water samples were both depleted of oxygen and foul-smelling. This indicated that anaerobic microorganisms had started to degrade dissolved organics into odorous organic acids and reduced sulfur, such as H_2S, causing the foul-smelling water samples (Liang et al., 2018). During a student cruise in March 2021, black particles were observed in the water samples, indicating a further development in anoxic conditions. Haugsværfjorden serves as the example and illustration of what can happen in the Deep basin in Masfjorden if DWR events and ventilation of the basin layer does not occur.

3 Methods and data

3.1 CTD data

In this thesis, I use CTD data from seven cruises from the time period February 2019 to March 2021 (Table 3.1). The CTD data is used to study the hydrography, to establish stagnant periods and to calculate the vertical diffusivity in Masfjorden. The cruises were organized by either Geophysical Institute (GFI) or Department of Biological Sciences (BIO) at University of Bergen. For convenience, I named each cruise after the month and year they took place (Table 3.1). From each cruise, there were between 10 and 100 CTD casts available.

The CTD sections from Mar19, Mar20 and Mar21 consist of 35 stations reaching from Masfjorden's mouth to its head in Matrefjorden, and provide very detailed CTD sections. In addition, CTD stations from Fensfjorden and Haugsværfjorden were also obtained. The CTD sections from the remaining cruises consist of fewer stations spread out along Masfjorden.

Cruise name	**Cruise ID**	**Time period**	**Organized by**	**Stations covered**
Feb19	KB2019602	1.-4. February 2019	GFI student cruise	12 / 13
Mar19	KB2019604	28. February - 3.March 2019	GFI student cruise	13 / 13
Oct19	GS2019114	1.-4. October 2019	BIO cruise	6 / 13
Mar20	KB2020603	2.-8. March 2020	GFI student cruise	13 / 13
Jun20	KB2020610	2.-8. June 2020	BIO cruise	10 / 13
Sept20	GS2020112	15.-16. September 2020	BIO cruise	11 / 13
Mar21	KB2021605	24. February - 02. March 2021	GFI student cruise	13 / 13

Table 3.1: Information about cruises which provided CTD data. The column "Stations covered" indicated how many of the 13 selected stations were obtained during the different cruises.

I chose 13 stations from the CTD sections with 35 stations, which were the ones I found the most relevant and useful with respect to the analysis. They were chosen based on their location so that main features of the fjord, such as the basins and sills, were included in the section. The chosen CTD stations are listed in Table 3.2, and shown in Figure 2.5. Most of these stations were repeated during all cruises, so times series from different important locations in the fjord are available. In Table 3.1 its indicated how many of the 13 selected stations were obtained during each cruise.

Station name	Feb19	Mar19	Oct19	Mar20	Jun20	Sept20	Mar21
M35	118 (157)	268 (267)	386	169		306	241
M31	122 (161)	275 (271)		173		304	245
M28	123	277		176			247
M26	125 (138)	279	384 (385)	218 (179)	461 (462)	303	251
M24	117	283	382	181 (168)	469	301	250
M22	127	285		183	468	300	255
M18	129	289		187	468		259
M16	130 (156, 176)	291	381 (387)	189	460	299	261
M14		302		194	459	298	263
M12	133 (116)	301	388	220	467 (458)	297	265
M11	134	298 (299)		221	457	296	266
M07	136	265		198	456	295	270
M04	141 (173)	319 (260)	380	201	455	294	273

Table 3.2: List of the 13 CTD stations in Masfjorden used in this thesis. The station names are listed in the first column. The rest of the table contains information about which cast(s) from each cruise represent the different stations. If several casts where taken at one station, the cast I have used for the analysis is listed first, and the other casts are listed in parenthesis.

The oxygen and conductivity sensors on CTD were calibrated with water samples. The oxygen samples were analyzed by manual or automatic Winkler titration on board or immediately after the cruise since oxygen is reactive and not conserved, and the oxygen concentration changes over time. The water samples for conductivity could be analyzed later, as salt is conserved. The CTD measurements were corrected accordingly to the results from each calibration analysis.

All corrections applied to conductivity data for this thesis are based on the results from IMR's conductivity calibration analysis, except for Mar21 which is based on an analysis by GFI students. The oxygen calibration were performed by GFI. The corrections for both oxygen and conductivity were mean offsets (Table 3.3). I calibrated and corrected the oxygen data from Feb19 and Jun20, and added conductivity corrections to Jun20, Sept20, and Mar21. A detailed description of the calibration work for oxygen is found in Appendix A (Chapter 7.1).

	Feb19	**Mar19**	**Oct19**	**Mar20**	**Jun20**	**Sept20**	**Mar21**
dC [$\mathrm{S\,m^{-1}}$]	-0.012	-0.006	0.003	-0.008	-0.007	-0.014	0.013
dO ± std [$\mathrm{mL\,L^{-1}}$]	0.243 ± 0.088	0.2 ± 0.063	0.28 ± 0.084	1.04*Ox + 0.035 ± 0.09	0.135 ± 0.098	0.128 ± 0.016	1.016*Ox + 0.071 ± 0.049
Number of O_2 samples	96	119	22	130	91	7	163
Winkler titration	Manual	Manual	Auto.	Manual	Auto.	Auto.	Manual

Table 3.3: List of corrections applied to conductivity and oxygen measurements from calibration results. dC and dO are the mean offsets for conductivity and oxygen. Number of O_2 samples are the total number of available oxygen water samples from each cruise. The Winkler titration method used is also stated (Manual vs Automatic).

3.2 Data from the Inner Mooring

In addition to the CTD data, I use mooring data from Masfjorden from the time period 2. February 2019 to 1. March 2020 were available. Two moorings were deployed in Masfjorden during the Feb19 cruise, and were recovered during the Mar20 cruise. One mooring was placed on the Outer Sill (70 m), and the other was placed in the Deep Basin (about 465 m), in the inner part of Masfjorden (Figure 2.5). Hence, the names Sill Mooring and Inner Mooring. Several of the instruments on the Sill Mooring turned out the not provide reliable data after first round of analysis. During the recovery of the Sill Mooring, we found marine plants growing on some of the instruments, which most likely interfered with sensors on the instruments. Since the focus of my thesis is the Deep Basin, I do not work with the available data from the Sill Mooring.

The Inner Mooring was made up of 4 Sea Bird instruments of the type SBE37 (Table 3.4). At 190m, 340 and 455m, SBE37 ODO instruments were located, and a SBE37 at 265m. When analyzing the data, the SBE37 at 265 m showed dubious spikes in conductivity and temperature, and were not used in further work. Thus, the Inner Mooring provide times series of temperature, salinity and oxygen at 190m, 340 and 455m in the Deep Basin, which I use in the hydrography analysis.

I calibrated the Inner Mooring instruments against calibrated CTD profiles from Feb19, Mar19, Oct19 and Mar20, for conductivity, temperature and oxygen as described in Appendix A (Chapter 7.2). A linear or constant correction was applied to each instrument based on the temporal evolution of the offset between CTD and mooring instruments (Tabel 7.1). For the analysis of the Inner mooring time series, I calculated the conservative

temperature, absolute salinity and potential density anomaly with reference pressure of 0 dbar (σ_0) before I applied a low-pass filter (7 days) to the time series.

Depth	190 m	265 m	340 m	455 m
Instrument (serial nr)	SBE37 ODO (12340)	SBE37 (8974)	SBE37 ODO (12338)	SBE37 ODO (12339)
Measured parameters	T, C, O_2	T, C	T, C, O_2	T, C, O_2
Sampling interval	30 min	5 min	30 min	30 min
Time period	02.Feb.2019 - 01.Mar.2020	02.Feb.2019 - 01.Mar.2020	02.Feb.2019 - 01.Mar.2020	02.Feb.2019 - 10.Mar.2019

Table 3.4: Information about the Inner Mooring instruments; the depth of each instrument, the parameters measured by the instrument, the sampling interval and measuring period.

3.3 Data from NorFjords160

The third data set I use is the model results of temperature and salinity from NorFjords160. NorFjords160 is a model set-up by the IMR of the hydrodynamic model ROMS (Regional Ocean Modeling System) for a coastal area of West Norway(Sandvik et al., 2019), which includes Masfjorden and Fensfjorden (Figure 3.1). A hydrodynamic model solves the primitive equations by numerical methods for a grid. The model results give a description of how fluids move on a rotating sphere, such as water masses in the ocean. With realistic bathymetry data, forcing, initial and boundary conditions, the model provide information about the dynamics and physical environment, such as currents, water level and hydrography within the defined grid (Albretsen et al., 2011; Sandvik et al., 2019).

NorFjords160 has a horizontal grid size of 160 m×160 m, and the vertical grid uses terrain-following sigma coordinates. There are 35 vertical layers in total, and the depth of each vertical layer varies depending on the bathymetry (Sandvik et al., 2019). In shallow area, the vertical distance between each grid cell is small, and when the depth increases so does the distance between the grid cells. This is different from z-coordinates, where the distance between each grid cell is constant, unaffected by varying depth. The model receives the open boundary values from NorKyst800. The atmospheric forcing and the fresh water input comes from results from Norwegian Meteorological Institute (MET) and Norwegian Water Resources and Energy Directorate (NVE). The fresh water input is the results from a hydrological model by NVE which gives the daily runoff from about 100 rivers, and the atmopheric forcing is from the the 2.5 km × 2.5 km AROME MetCoOp forecasting system by MET. (Asplin et al., 2014; Müller et al., 2017).

The temperature and salinity data I use from NorFjords160 are from a model run for

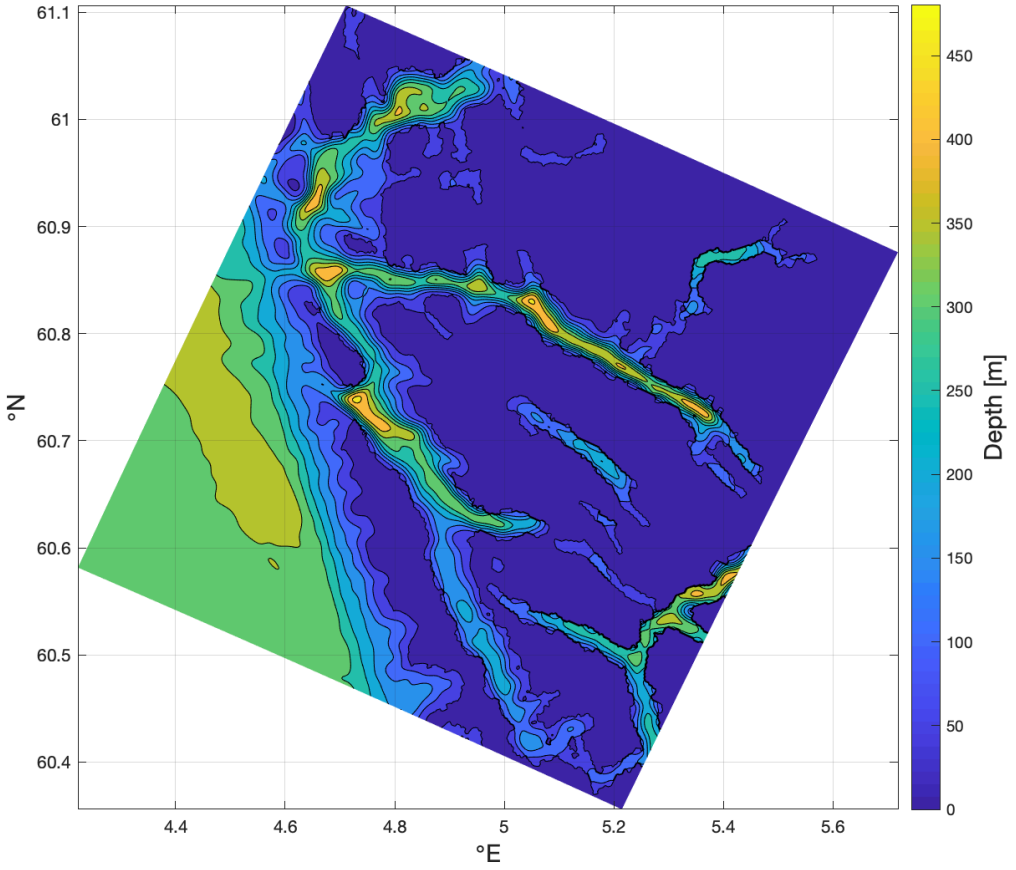

Figure 3.1: Model area for NorFjords160. The area includes Masfjorden (ca 60.9 °N, 5.4 °E) Fensfjorden, the coastal area outside of Fensfjorden.

Dates in 2015	Index in model
18. / 25. February	6980 / 8000
12. / 19. April	14660 / 15620
14. / 17. May	19290 / 19600
8. / 22. August	31900 / 33630
5. / 12. October	40000 / 41000
25. / 28. December	51600 / 52000

Table 3.5: Information about the point of time (date and model index in NorFjords160) the vertical temperature and salinity profiles were extracted from station 1 (M24). Data were extracted from two dates from the beginning and end of each stagnant period.

1. January 2015 - 31. December 2015. All data are extracted from the same location as station M24 has in the Deep Basin. I converted the model data to conservative temperature and absolute salinity, from which I calculated potential density (σ_Θ). To begin with, I extracted time series from 150 m, 200 m and 280 m of temperature and salinity to identify stagnant periods. After I determined the stagnant periods (as described in

Chapter 4.3), I extracted vertical profiles from suitable points of time (Table 3.5).

I use the vertical profiles from NorFjords160 in the calculations of vertical diffusivity. In combination with results from the observations, I determine if if the model manages to give realistic results for vertical diffusivity in the Deep Basin, or if adjustments of the mixing coefficients are needed.

3.4 Method for estimating vertical diffusivity in fjord basins

I will calculate the vertical diffusivity κ [$\mathrm{m^2\,s^{-1}}$] in the Deep Basin by using the CTD and NorFjords160 data presented. I find the vertical diffusivity by using the budget method presented in Stigebrandt and Aure (1989). The budget method uses observations of two vertical density profiles from different points in time and the horizontal surface area in the basin to find the vertical diffusivity. The requirements for the budget method to work are observations from a stagnant period, no exchange of heat or salt with the bottom sediments, and no radiation of heat from above. In other words, the method does not work if a DWR event occurs in the time between the density profiles were obtained. An analysis of hydrographic and oxygen data is important to do before the vertical diffusivity is calculated in order to find stagnant periods where the requirements are fulfilled.

The starting point for the method is the horizontally averaged conservation equation for the density in the basin water.

$$\frac{\delta\rho}{\delta t} = \frac{1}{A}\frac{\delta}{\delta z}\left(A\kappa\frac{\delta\rho}{\delta z}\right) \tag{1}$$

where t is time, z is the vertical coordinate, $\rho = \rho(z,t)$ is the horizontally averaged density, $A = A(z)$ is the horizontal surface area of the basin, and $\kappa = \kappa(z)$ is horizontally averaged vertical diffusivity. The parameters $\frac{\delta\rho}{\delta t}$ and $\frac{\delta\rho}{\delta z}$ can be found from observations of temperature and salinity, as density can be calculated from temperature and salinity. $\frac{\delta\rho}{\delta z}$ can be found from the vertical profile, and $\frac{\delta\rho}{\delta t}$ is found from two profiles from different points in time. $A = A(z)$ is calculated from bathymetric maps of the fjord.

By integrating Equation (1) from the bottom, b, to an given depth, u, an expression for κ is found (Equation (2)). There is no diffusive flow at the bottom b.

$$\kappa_{z=u} = \frac{1}{\left(A\frac{\delta\rho}{\delta z}\right)_{z=u}}\int_b^u \frac{\delta\rho}{\delta t}A\,dz \tag{2}$$

3.4.1 Applying the method to the Deep Basin

In the following description I describe how I applied the method from Stigebrandt and Aure (1989) to the CTD (observed) data and the NorFjords160 (model) data from the Deep Basin in Masfjorden. I use Equation 2 to find the vertical diffusivity in the data and the model. It is important to note that before this method can be applied any of the data sets, the stagnant periods have to be identified.

First, I found the surface area $A(z)$ in the Deep Basin. I defined the region that represented the Deep Basin in the bathymertic maps and in the model grid (Figure 3.2). The bathymetric data I have used in this thesis are from IMR. These data have a 50 m $\times$ 50 horizontal resolution on an irregular grid. The bathymetric data were collected from the online data source established by the Norwegian Mapping Authority, the Hydrographic service (`http://www.norgedigitalt.no`).

The depth of the Deep Basin is 288 m in the NorFjords160 model grid, which is about 200 m shallower than the real fjord depth (489 m). The depth of the fjord in the model grid has been lifted in order to smooth the boundary, as the narrow and steep bathymetry of fjords are difficult to model. I defined the Deep Basin as the basin below the Inner Sill depth (180m). In the model grid, this sill is 130 m. Due to varying CTD casts I set a fixed depth for the bottom to be 460 m, a depth most CTD casts reached (Table 3.6).

Deep Basin	**Bathymetric map**	**Model grid**
Inner sill depth	180 m	130 m
Bottom depth	460 m	270 m
Horizontal grid size	50×50 m	160×160 m
Vertical grid size, dz	20 m	20 m
Volume	1.345×10^9 m^3	1.322×10^9 m^3

Table 3.6: The parameters used to define the Deep Basin in the observations (bathymetric map) and in NorFjords160 (model grid).

The surface area $A(z)$ was calculated at every 20 m between the sill level and bottom depth in both the bathymetric map and the model grid. This was done by counting all grid points where the depth was greater than a level z. I compared the basin volume in each case by calculating volume for every 20 m with the known $A(z)$, and found the total volume between sill depth an bottom boundary (Table 3.6).

Second, I used two vertical density profiles of potential density from a stagnant period in order to find $\frac{\delta\rho}{\delta t}$ and $\frac{\delta\rho}{\delta z}$, so I used $\rho = \sigma_\Theta$. I followed the same procedure for the observed and the model data, adjusting the parameters, e.g. sill depth, bottom depth etc., as needed (Table 3.6). I applied a moving mean (20 m) to the profiles to smooth out any

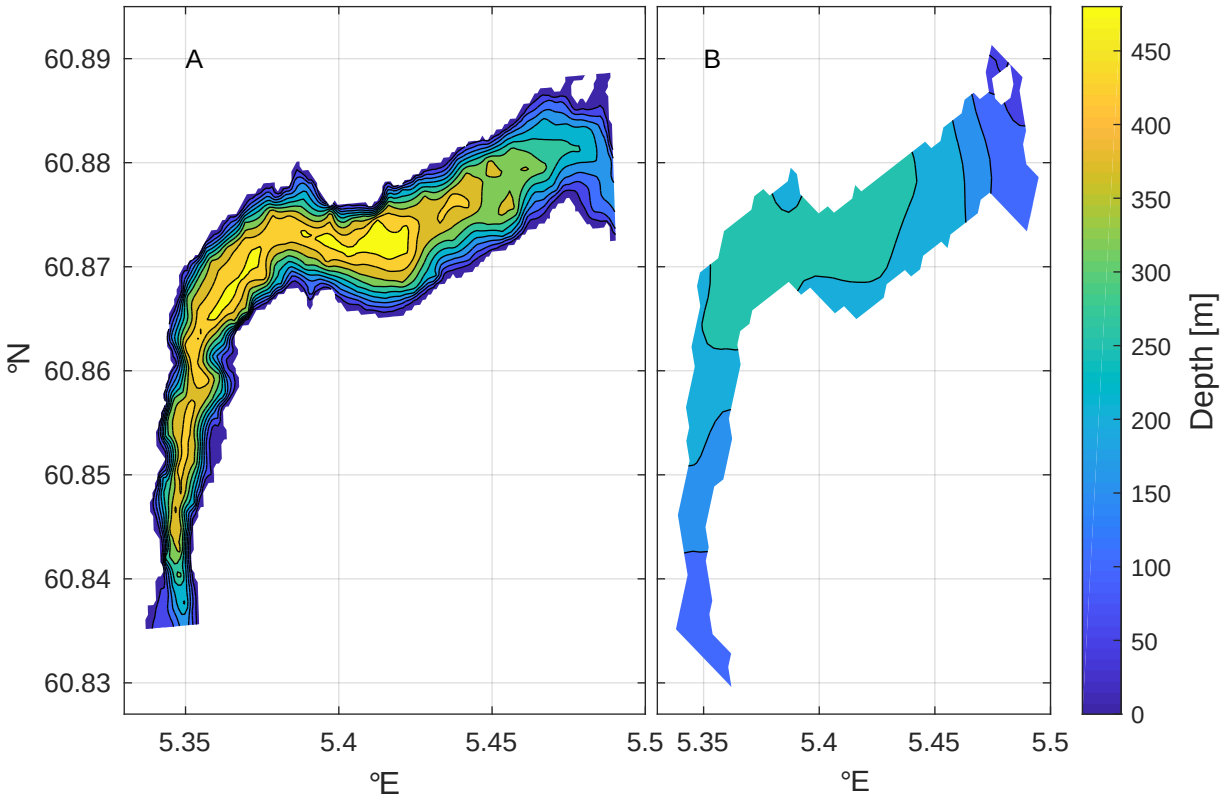

Figure 3.2: The defined regions for Deep Basin in the bathymetric map (A) and in the model grid (B).

spikes in the data, before the profiles were sub-sampled to the same depths as $A(z)$ had been calculated at. In order to find the time derivative of the density, $\frac{\delta\rho}{\delta t}$, I divided the density difference between the profiles at each depth by δt, the length of the time period between two profiles. The vertical derivative of the density, $\frac{\delta\rho}{\delta z}$, was calculated at each depth by dividing the center difference between two z-levels with the vertical grid size of 20 m.

When $\frac{\delta\rho}{\delta t}$, $\frac{\delta\rho}{\delta z}$ and $A = A(z)$ were known, I calculated the vertical diffusivity for different stagnant periods using Equation 2. An example of the parameters used in and results from Equation 2 are shown in Figure 3.3. The example shows two density profiles from observations in different colors. The profiles of $A(z)$, $\frac{\delta\rho}{\delta t}$ and $\frac{\delta\rho}{\delta z}$ are included, and we see how they influence the final results of the vertical diffusivity. $\frac{\delta\rho}{\delta z}$ largely determine the shape of κ.

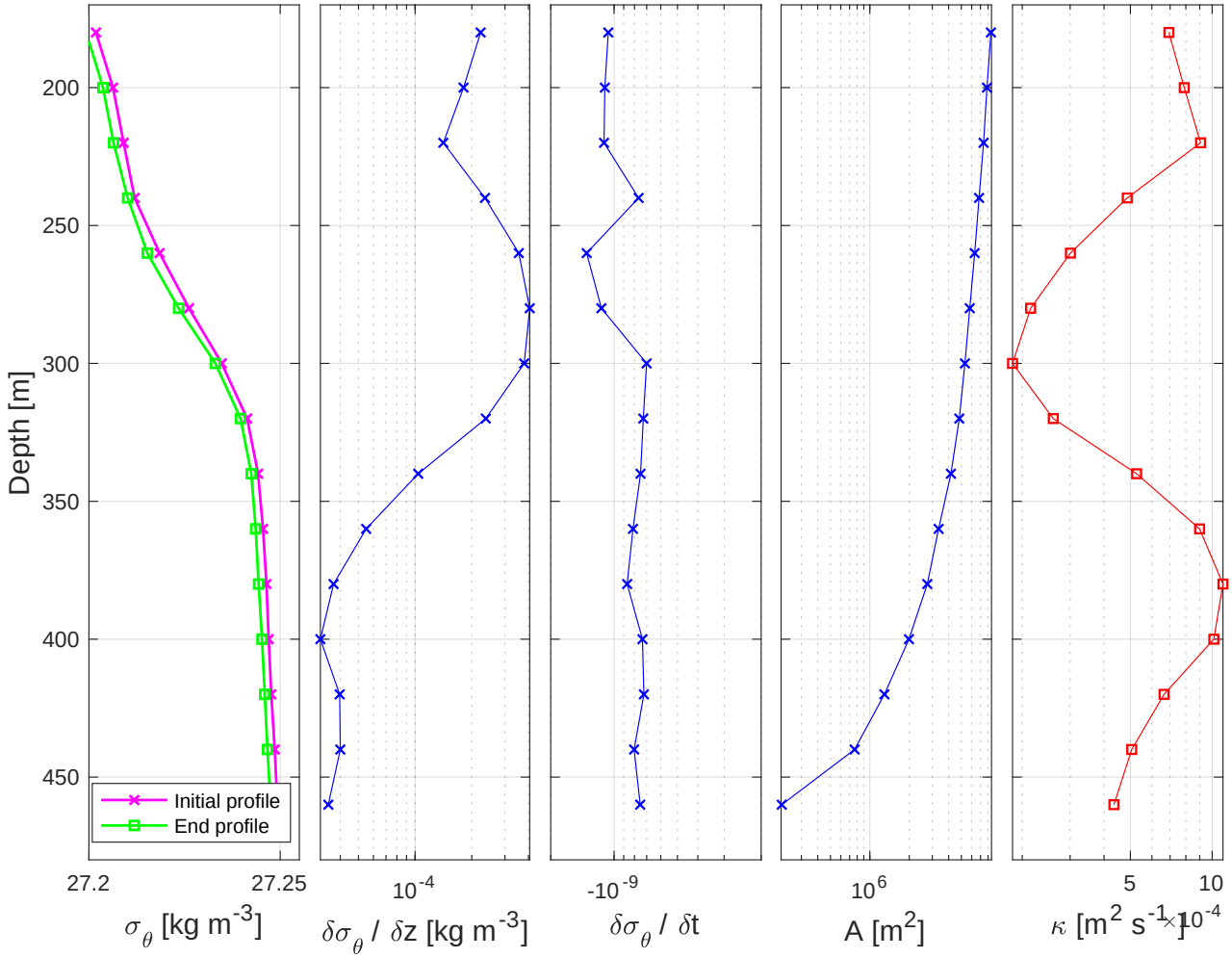

Figure 3.3: An example of the parameters used in in Equation 2 used to calculate the vertical diffusivity, κ, in the fjord basin. Initial profile is the first profile and end profile is the second profile in the stagnant period.

3.5 Calculations of oxygen concentrations in the basin layer

I used κ estimated from observations for further calculations of oxygen concentrations in the Deep Basin. By changing the density parameter to oxygen in Equation 1, oxygen concentration can be estimated with the following equation

$$\frac{\delta O}{\delta t} = \frac{1}{A}\frac{\delta}{\delta z}\left(A\kappa\frac{\delta O}{\delta z}\right) \tag{3}$$

where t is time, z is depth, $O = O(t, z)$ is the oxygen concentration and $\kappa_z = \kappa(z)$ is the vertical diffusivity at level z.

In Equation 3, the oxygen concentration is treated as a conserved quantity, and the equation describes how the oxygen concentration changes over time solely due to vertical diffusion during stagnant periods. Since oxygen is not conserved due to biological oxygen

consumption, we need to add a sink term in order to fully describe how the oxygen concentration changes in the basin layer

$$\frac{\delta O}{\delta t} = \frac{1}{A}\frac{\delta}{\delta z}\left(A\kappa\frac{\delta O}{\delta z}\right) - b_{t,z} \tag{4}$$

where $b_{t,z}$ is the terms which includes the biological consumption rate. Now, Equation 4 describes how the oxygen concentrations change due to vertical diffusion and biological consumption.

Since no information about the biological consumption rate was directly available from the data, I treated oxygen as a conserved quantity and worked with Equation 3 for my calculations. With an initial oxygen concentration O_n and κ known from calculations, I used Equation 5 to predict the oxygen concentration O_{n+1} at each depth level z forward in time. The horizontal surface area, $A(z)$, and $\frac{\delta O}{\delta z}$ were found as described in Chapter 3.4.1. The oxygen concentrations can only be estimated during stagnant periods since it is an assumption behind the calculations of κ.

$$O_{n+1} = O_n + \frac{\delta t}{A}\frac{\delta}{\delta z}\left(A\kappa\frac{\delta O_n}{\delta z}\right) \tag{5}$$

I ran the calculations m times with a time step $\delta t = 12$ hours, where $m = \frac{\Delta time}{\delta t}$ and $\Delta time$ is the time between the observed profiles, unless stated otherwise.

The lower boundary condition was set to be $O_{n+1}(bottom) = O_{n+1}(bottom - 1)$, meaning that there is no flux through the bottom. For the upper boundary condition I had to assume a behaviour, as I did not have information about how the upper boundary changed over time. Since I knew the oxygen concentration from the two vertical observed profiles, I assumed oxygen behaved linearly between the observed profiles. The upper boundary condition was written as $O_{n+1}(top) = O_n(top) + \frac{O_{end}(top) - O_{initial}(top)}{m}$. This boundary condition is limited by the need of an additional observed profile from the end of a stagnant period, and that a linear change may not be a realistic behaviour for the oxygen concentration at sill depth. If the calculations run for a longer period than the stagnant period, meaning that $\Delta time$ has been been increased, the upper boundary condition does not show the correct oxygen concentration value at time step m.

There are several profiles in question when working with these oxygen calculations. Therefore, I introduce names for the different profiles. The profile from the beginning of the stagnant period is the *initial profile*. The initial profile can either be an observed profile from CTD data, or it can be an altered and modified, then called an artificial initial profile. The profile from the end of the stagnant period is the *end profile*, and is also an observed profile from the CTD data. The *estimated profile* is the profile calculated from

Equation 5.

3.5.1 Oxygen profiles and oxygen consumption rate

In the case where I used the (observed) initial profile, I estimated the biological oxygen consumption rate in the basin layer from difference between estimated profile and the end profile (The first method). In order to test and qualify the findings, I also followed the method presented in Aure and Stigebrandt (1989), which estimates the mean oxygen consumption rate for the entire basin, CONS (The second method). What essentially separates the methods is that the first method is used to calculated the oxygen concentration and the oxygen consumption rate at each depth z, resulting in a vertical profile. The second methods finds a volume mean of the basin, without finding a vertical profile.

The first method: When $O_{Est}(z)$ is the estimated profile from the (observed) initial profile, $O_{Est}(z)$ and the end profile, $O_{End}(z)$ represent the oxygen concentration at the same time. We except the concentrations to differ since oxygen is conserved in the calculation of $O_{Est}(z)$, but not in $O_{End}(z)$. Both diffusion and biological oxygen consumption is present in real life and in $O_{End}(z)$, as seen in Equation 4. Therefore, we assume the difference $O_{Est}(z) - O_{End}(z) = \Delta O_2$ to be due to oxygen consumption, which can be used to find oxygen consumption rate profile, $b_{t,z}$.

I found the oxygen consumption rate profile, $b_{t,z}$, during the stagnation period by dividing ΔO_2 by $\Delta time$. The rate was given in $\mathrm{mL\,L^{-1}\,month^{-1}}$. For the conversion of the unit from $\mathrm{mL\,L^{-1}\,s^{-1}}$ to $\mathrm{mL\,L^{-1}\,month^{-1}}$, where one month is 30 days.

The total oxygen consumption rate in the basin was found by summing together $b_{t,z}$ between 300 m and 460 m, and the mean oxygen consumption rate in the basin was found by finding the mean of $b_{t,z}$ between 300 m and 460 m. This oxygen consumption rate was comparable with the oxygen consumption rate found with the second method.

The second method: In Aure and Stigebrandt (1989), a mean oxygen consumption rate for the entire basin was found by introducing new parameters; the volume mean oxygen depletion rate, DEPL, the volume mean contribution DIFF from the diffusive flux of oxygen into the basin layer, and the volume mean oxygen consumption rate, CONS (all in $\mathrm{mL\,L^{-1}\,month^{-1}}$). CONS is found by

$$CONS = DEPL + DIFF \tag{6}$$

To find each parameter in Equation 6, they introduce and upper (hu) and lower (hl) boundary of the basin layer. The upper layer is set to be about 10 m below sill depth, and the lower layer was set to exclude data with oxygen concentrations below 2 $\mathrm{mL\,L^{-1}\,month^{-1}}$.

The volume of the basin, V_b, was defined to be between hu and hl. The mean volume is needed in order to find the mean depth of the basin to be $V_b = A(hu) * H_b$, which DIFF is defined from

$$DIFF = \frac{\kappa\left(\frac{\delta O}{\delta z}\right)_{hu}}{H_B} \tag{7}$$

I set the upper and lower limit to be 300 and 460 m, and found the mean volume between these limits and $H_b = V_b/A(300m)$. Then DIFF was found as in Equation 7. DEPL was found by finding the mean of $\frac{\delta O}{\delta t}$ between the upper and lower layer, which is known from CTD measurements. Then, CONS were calculated using Equation 6.

3.5.2 Oxygen profiles and partial renewals

By using of artificial, or idealistic, initial profiles it is possible to investigate how a partial renewal would effect the oxygen concentration in the basin. I made three artificial initial profiles by altering the oxygen concentration of the initial profile from Sept20-Mar21. I altered the initial oxygen profile by assigning specific values for oxygen concentrations to certain depths (Table 3.7).

Depth [m]	Original O_2 [mL L^{-1}]	No renewal [mL L^{-1}]	Partial renewal [mL L^{-1}]	Deep partial renewal [mL L^{-1}]
180	3.71	**3.70**	**4.68**	**4.68**
200	3.99	**3.71**	**4.70**	**4.70**
220	3.99	**3.71**	**4.70**	**4.70**
240	3.71	**3.70**	**4.68**	**4.68**
260	3.51	3.51	**4.00**	**4.50**
280	3.28	3.28	**3.5**	**4.00**
300	2.95	2.95	2.95	**3.50**
320	2.67	2.67	2.67	**2.95**

Table 3.7: Original O_2 is oxygen concentrations [mL L^{-1}] from the initial profile of Sept20-Mar21. The three remaining cases are the artificial initial profiles, which is an altered version of Original O_2. The values in **bold text** are the altered values I have assigned the certain depths in each case.

I made three different scenarios; no partial, a partial renewal and a deep partial renewal. The partial renewal and deep partial renewal differs from each other between 260 m and 320 m, where the layer affected by the partial renewal in the latter case reaches further down in the water column. The different values for oxygen concentration at the

different depths were tested to represent a somewhat realistic environment, and to get stable results. If the gradients in the oxygen profile could not be too sharp, otherwise instability would be seen in the estimated oxygen profile.

It would not have been a problem to use the data from Oct19-Mar20 period, but I chose the Sept20-Mar12 period since the stagnation period was a little bit longer. The Feb19-Mar19 did not seem like an interesting period to do the calculations for due to its short length.

4 Results

4.1 Hydrography in Masfjorden

4.1.1 Results from CTD data

I begin with a presentation of the hydrography in Masfjorden (Figure 4.1 and Figure 4.2). The CTD data are from March 20, and the section is made up of the 13 selected stations (Figure 2.5), which captures the main features of Masfjorden, such as the the Inner and Outer Sill and the Deep and Shallow Basin. The sections illustrate the layers in Masfjorden and the difference between the environment inside and outside the sills nicely.

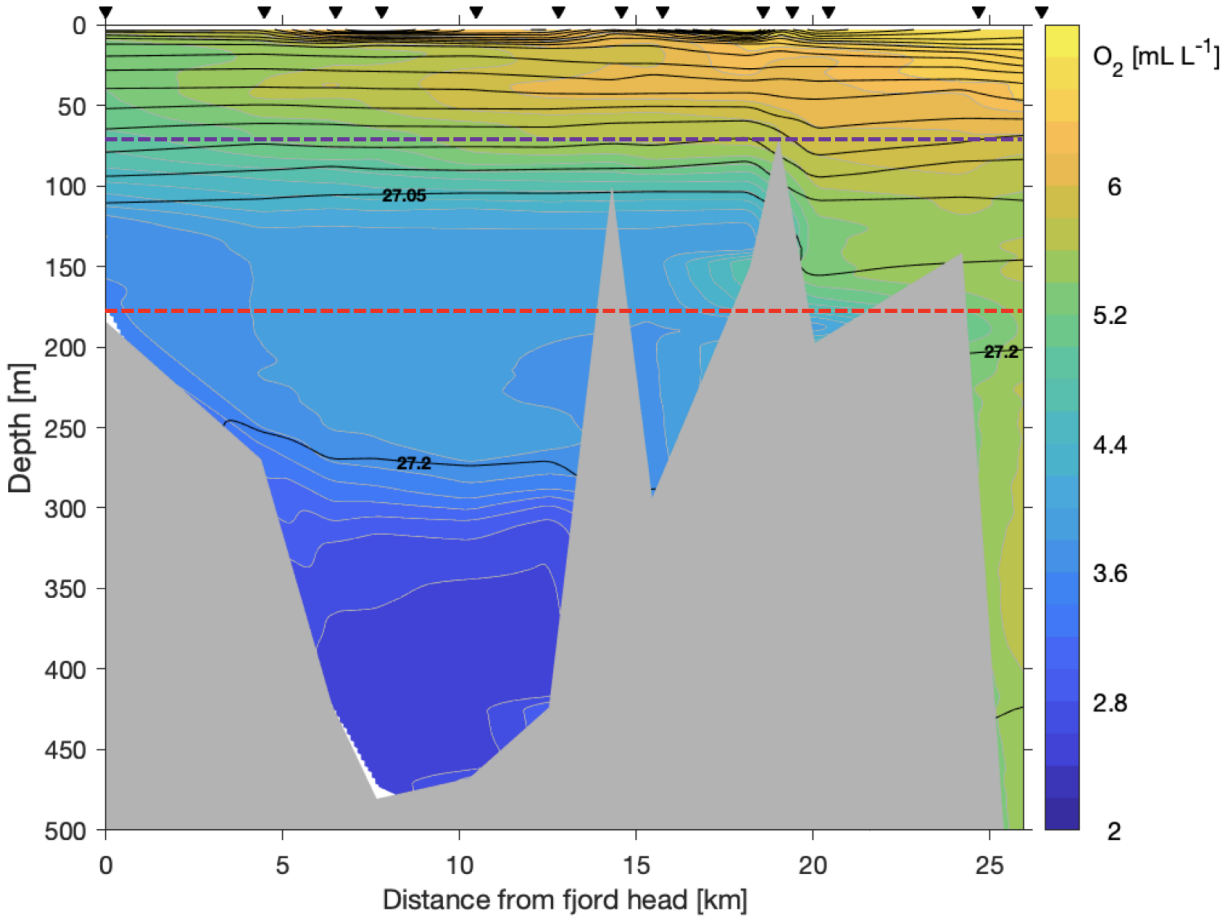

Figure 4.1: CTD section from Masfjorden showing dissolved oxygen concentrations. The potential density (σ_0) contours are plotted with 0.15 kg m^{-3} interval. Data are from March 20. The leftmost station is M35 in Matrefjorden, and the rightmost station is M04 in Fensfjorden. The vertical dashed lines indicate the sill true depths of the Outer (purple) and Inner (red) Sill.

From the oxygen, temperature and salinity sections, we identify the basin layer below ca 120 m depth, and note that there are two layers present; The Upper layer and the Lower layer. We observe low-oxygen concentrations in the Deep Basin where the lowest oxygen concentration (>2.5 mL L^{-1}) are found below 300 m. This is the Lower layer, where we

also find the coldest and most saline water is found, with CT around 8.1 °C and SA of 35.14 g kg^{-1}. In the Upper layer, between ca 120 m and 300 m, we find slightly higher oxygen concentrations of $\simeq$ 3.8 mL L^{-1}, CT of 8.2 °C and SA around 35.08 g kg^{-1} (Figure 4.1 and 4.2).

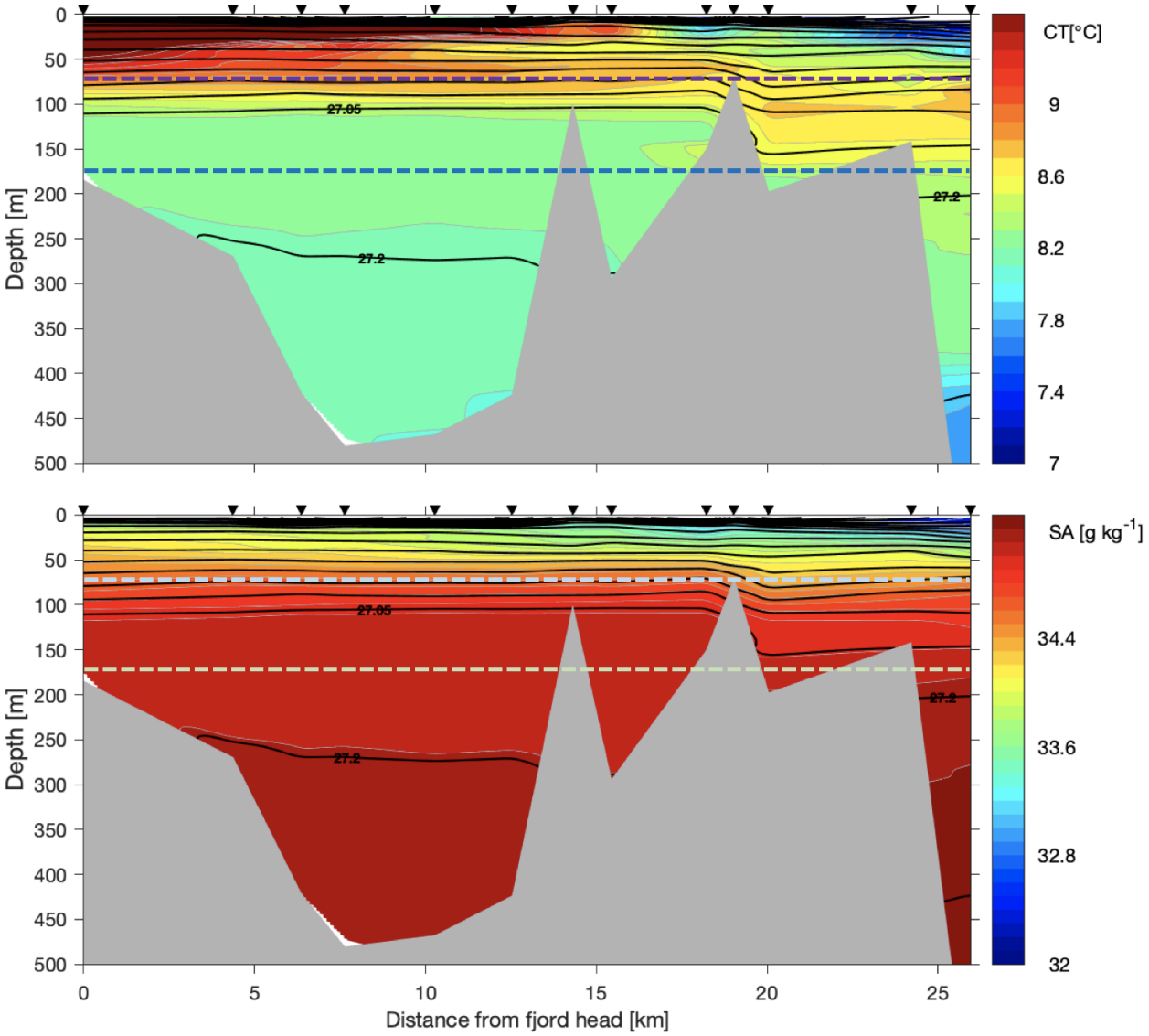

Figure 4.2: CTD section from Masfjorden showing showing conservative temperature (CT) and absolute salinity (SA). The potential density (σ_0) contours are plotted with 0.15 kg m^{-3} interval. Data are from March 20. The leftmost station is M35 in Matrefjorden, and the rightmost station is M04 in Fensfjorden. The vertical lines represent the sill depths of the Outer (70 m) and Inner (180m) Sill.

The surface layer is seen by the rapid change in density contours and low salinity observations close to the surface. The intermediate layer is found between the surface and basin layer, and where oxygen concentrations are between 4 and 6 mL L^{-1}, and varies both vertically and horizontally. The highest oxygen concentrations are found close to surface

around the mouth of Masfjorden. A tongue of more oxygen-rich water reaches from the mouth towards the head in Masfjorden at 40 m depth. Temperature and salinity also varies vertically and horizontally in the intermediate layer (Figure 4.1 and4.2).

To capture the time evolution in Masfjorden and define stagnation periods, I plotted CTD casts from the deepest stations in the Deep Basin (M26, Figure 4.3) and in the Shallow Basin (M16, Figure 4.4). If oxygen, O_2 and potential density, σ_Θ, increases below sill depth between cruises, a renewal event has taken place in the time period between the cruises.

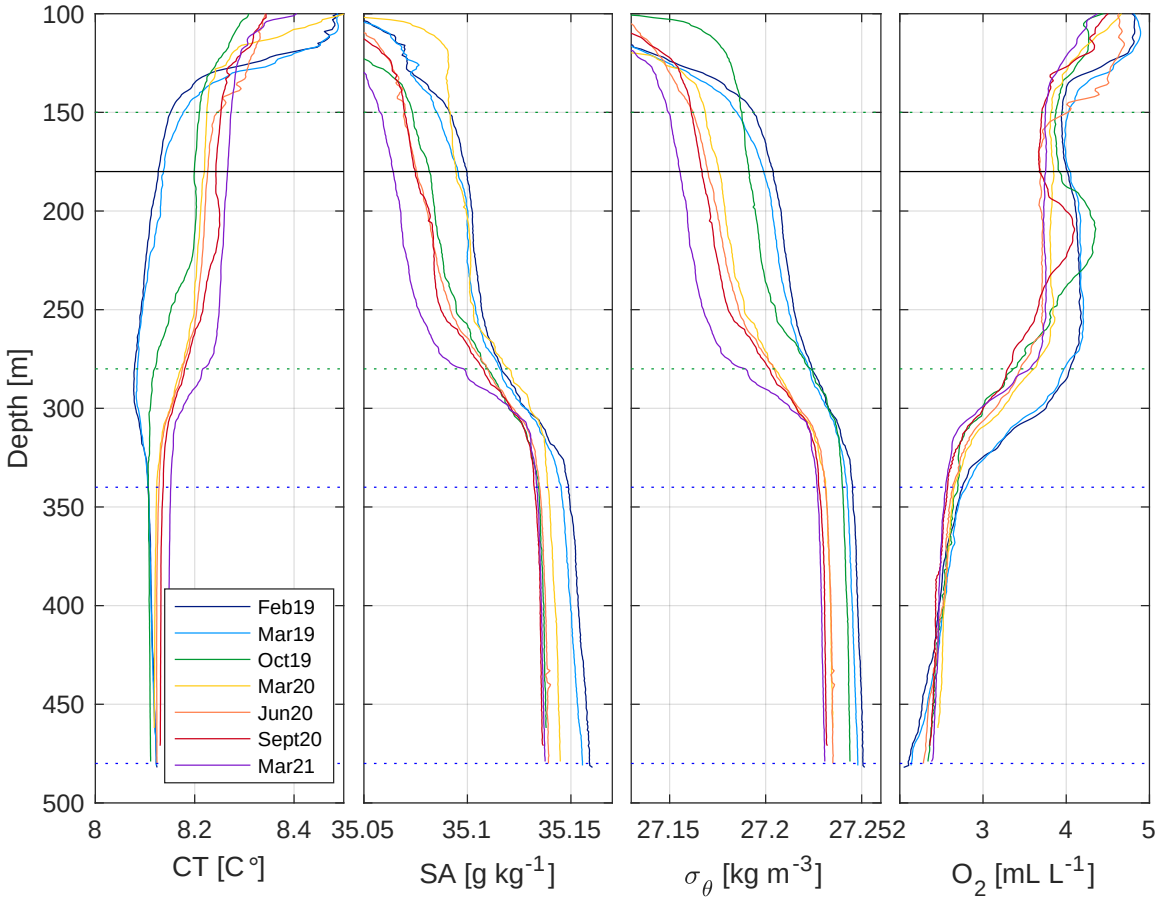

Figure 4.3: Profiles from CTD station M26, located in the Deep Basin in Masfjorden. The profiles show CT, SA, σ_Θ) and O_2. Each cast is color coded with respect to time. The depth of the Inner Sill (180 m) is marked as the black horizontal line. The blue, dotted lines represent the Lower layer, and the green, dotted lines represent the Upper layer.

The Upper and Lower layer identified from the CTD sections are also seen in the CTD profiles, but at slightly different depths. The Upper layer is found between ca 150 m and 280 m, and the Lower layer is found between 340 m and the bottom. In these layers the parameters CT, SA, σ_Θ and O_2 are homogeneous and constant with depth. Between 280 m and 340 m, the water masses changes gradually, where σ_Θ increases and O_2 decreases (Figure 4.3). In the Shallow Basin, only one layer is found below sill depth, and its density

overlaps with the Upper layer in the Deep Basin at around 27.2 kg m^{-3}. The density of the Lower layer is about 27.25 kg m^{-3} (Figure 4.4). Over time σ_Θ decreases in both the Shallow and Deep Basin.

CT increases gradually over the observation period, from February 2019 to March 2021 in the Deep and Shallow Basin. Between February 2019 and October 2019, CT increases with 0.1 °C at 250 m in the Upper layer and in the Shallow basin (from 8.1 °C to 8.2 °C). In the Lower layer, CT increases gradually, but less compared to the Upper layer. SA show an overall decrease over the observation period in both the Shallow and Deep basin. SA decreased with about 0.02 g kg^{-1} at 250 m and 470 m in the Deep Basin (Figure 4.3 and 4.4).

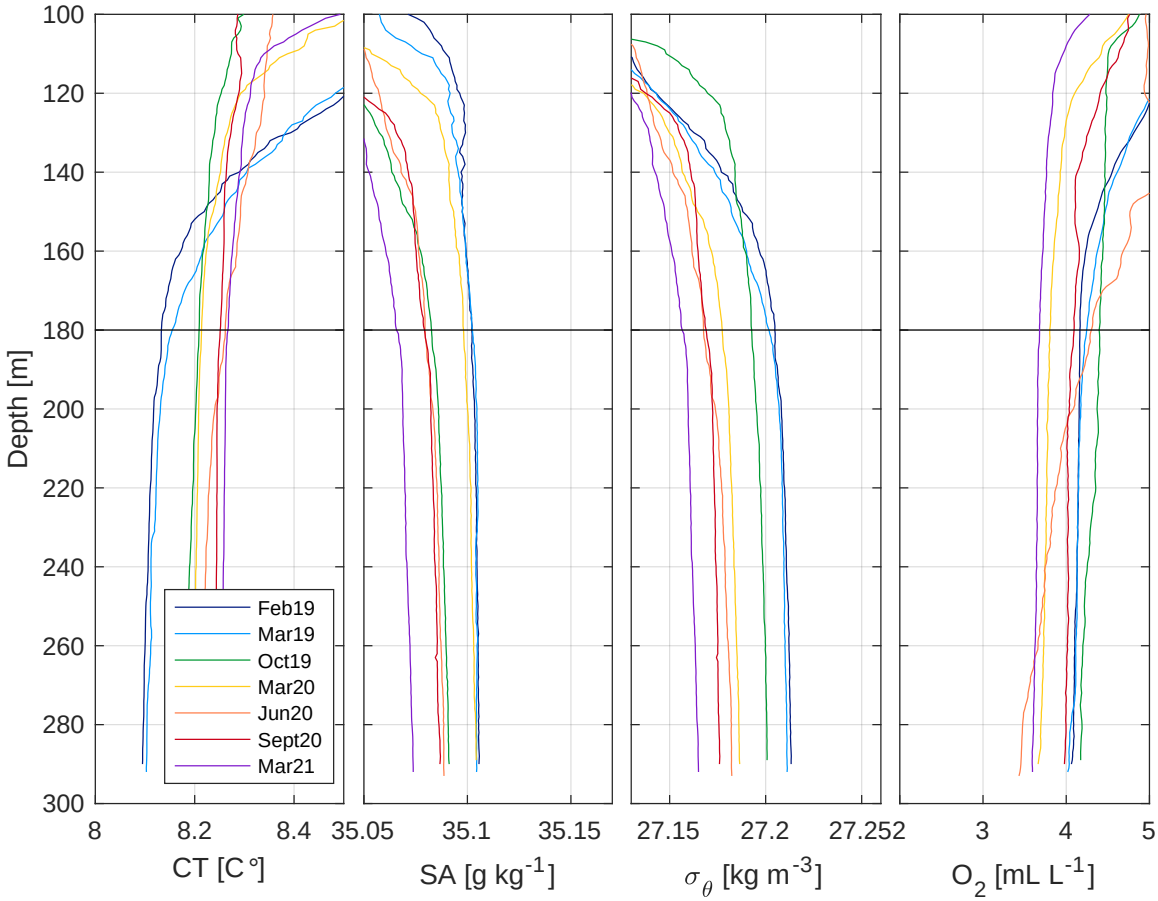

Figure 4.4: Profiles from CTD station M16, located in the Shallow Basin in Masfjorden. The profiles show CT, SA, σ_Θ and O_2. Each cast is color coded, representing the cruises, and time, from which they were obtained. The sill depth of 180 m, separating the Shallow basin from the Deep basin, is marked as a black horizontal line.

Since there is an interesting development in O_2 around 220 m in the Deep Basin (Figure 4.3), I plotted the time evolution of O_2 and σ_Θ at specific depths (Figure 4.5). The uncertainty of the parameters is included, where the uncertainty in the oxygen concentration is the standard deviation from the oxygen calibration (Table 3.3). The standard

deviation for the density measurements are the based on the typical standard deviation (0.006 $\mathrm{S\,m^{-1}}$) from the conductivity calibration, which gives an standard deviation of 0.005 $\mathrm{kg\,m^{-3}}$) for the potential density (Figure 4.5). In addition to the observations and their uncertainties, I included the density reduction rates during stagnant periods at the bottom of Masfjorden, D = 0.01, 0.0125 and 0.015 $\mathrm{kg\,m^{-3}\,yr{-}1}$ used by Darelius (2020), the observed long-term oxygen decline rate of 0.014 - 0.047 $\mathrm{mL\,L^{-1}\,yr{-}1}$ and the estimate for oxygen consumption b = 0.52 $\mathrm{mL\,L^{-1}\,yr{-}1}$ in the Deep Basin used by (Aksnes et al., 2019).

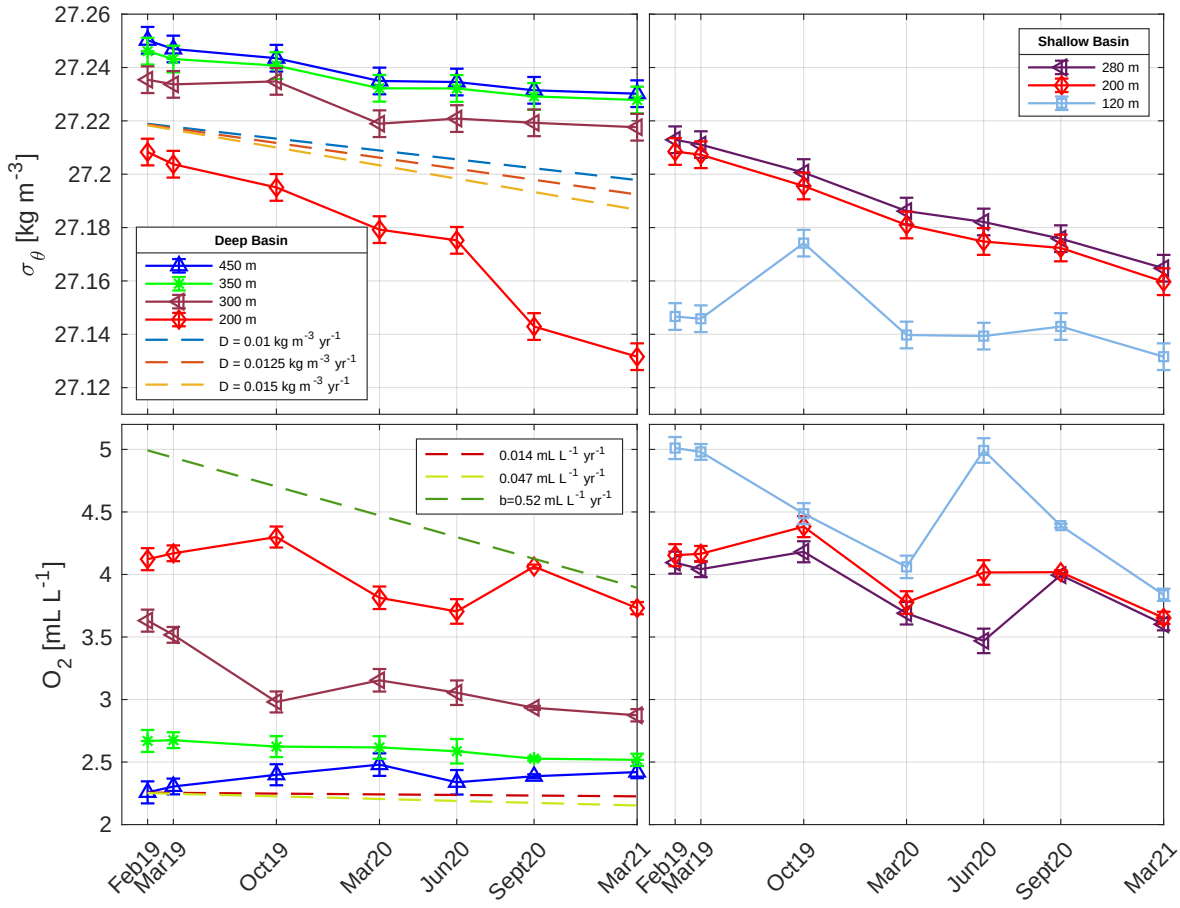

Figure 4.5: Temporal evolution of σ_Θ and O_2 at 200, 300, 350 and 450 m in the Deep Basin, and at 120, 200 and 280 m in the Shallow Basin. Trends for the oxygen consumption (b), long-term oxygen decline and density reduction (D) in the Deep Basin (from Aksnes et al., 2019; Darelius, 2020) are also included.

It is clear that σ_Θ decreases for all depths in the Deep and Shallow Basin below the Inner sill depth during the observational period. The reduction rate of σ_Θ at the bottom is larger in the Shallow Basin (-0.024 $\mathrm{kg\,m^{-3}\,year^{-1}}$ for 280 m) than in the Deep Basin (-0.0085 $\mathrm{kg\,m^{-3}\,year^{-1}}$ for 450 m) between March 2019 and March 2021. The only increases in σ_Θ is found at 120 m in the Shallow Basin, where it increases from March to October in 2019 and from June to September in 2020 (Figure 4.5).

The O_2 concentration in the Upper layer (200 m) is similar to the observations from Shallow Basin (at 200 and 280 m), both in concentration and in evolution. O_2 increases at 200 m in the Deep Basin from March to October in 2019, and from June to September in 2020. In the Shallow Basin, O_2 increase between March and October 2019 are seen at 200 and 280 m. Between March and September 2020, O_2 increases at 120, 200 and 280 m. Small changes in O_2 concentration are seen in the Deep basin at 350 m and 450 m during the observational period. O_2 decreases from 2.7 mL L^{-1} to 2.5 mL L^{-1} at 350 m over the observational period. At 450, the O_2 concentration increases with 0.16 mL L^{-1} over the full observational period, from 2.26 to 2.42 mL L^{-1}. Between March 2019 and March 2020, O_2 increases with 0.22 mL L^{-1} (Figure 4.5).

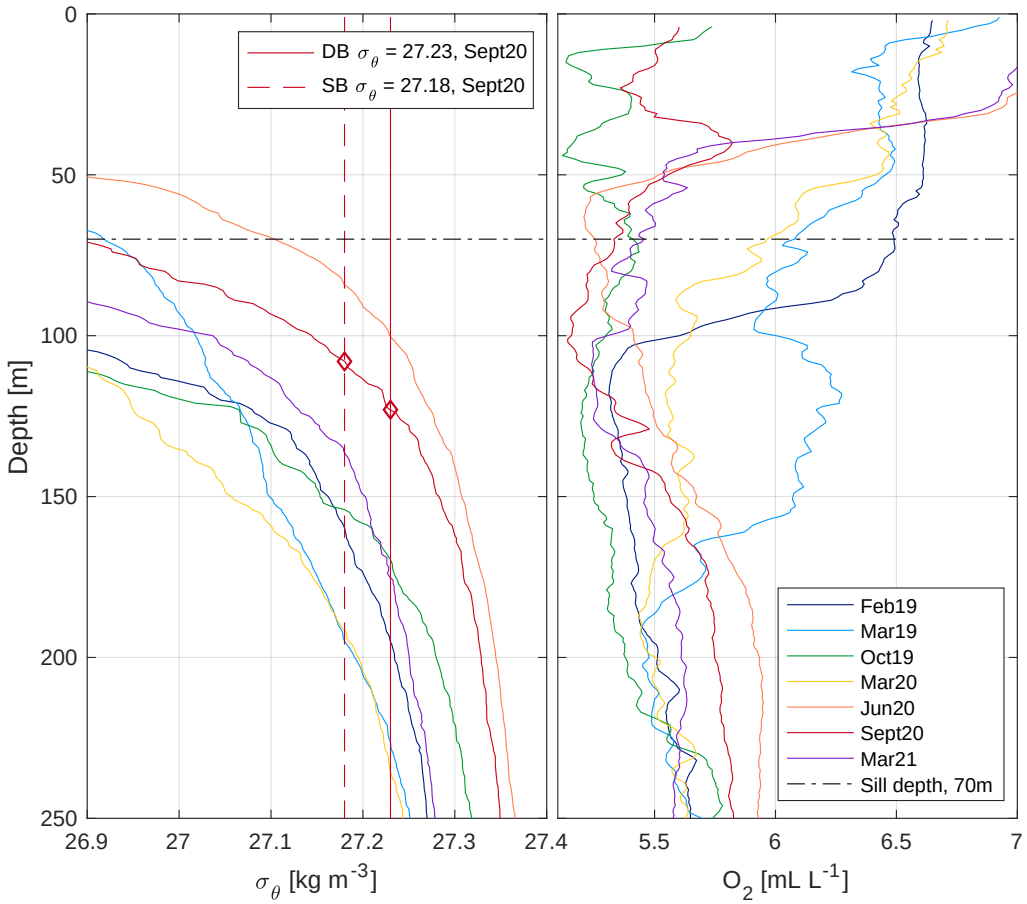

Figure 4.6: Profiles of σ_Θ and O_2 in the upper 250 m of Fensfjorden/mouth of Masfjorden (station M04). The profiles are color coded and represent the cruises (and time) they were obtained. A horizontal line representing the sill depth at 70 m. The density of the Shallow Basin (SB) and Deep Basin (DB) from Sept20 are represented as vertical lines, along with points indicating the where the intersection between SB/DB density and density in Fensfjorden.

In addition to the hydrography in Masfjorden, the water masses at sill depth of the Outer Sill in Fensfjorden (station M04) are of interest in regards to renewal of the basin layer in Masfjorden. Lighter and more oxygen-rich water is found at the sill depth (70 m) compared to the Deep and Shallow Basin (Figure 4.6). Both the density and the oxygen

concentration vary with time. The water masses with the same density as the Deep and Shallow Basin are typically found between 150 - 200 m (compared with σ_Θ in the basins from September 2020). In June 2020, these water masses were found between ca 80 - 100 m, and at 123 m and 108 m in September 2020.

4.1.2 Inner Mooring results and stagnation periods

The Inner Mooring observations of CT, SA, σ_Θ and O_2 concentrations from February 2019 to March 2020 were used in addition to the CTD data to identify renewal episodes in the Deep Basin. The O_2 time series show a clear oxygen increase at 190 m between June 2019 and mid-August 2019. Here, the O_2 concentration increases from 3.98 $\mathrm{mL\,L^{-1}}$ to 4.38 $\mathrm{mL\,L^{-1}}$ (Panel D, Figure 4.7). From mid-August 2019 to October 2019, O_2 is stable before it starts to decrease. Small O_2 variations were observed at 340 m and 455 m, which agrees with the O_2 observations seen in Figure 4.5. While the O_2 concentration at 340 m is relatively stable, the concentration at 455 m increase by about 0.21 $\mathrm{mL\,L^{-1}}$ over the deployment period, from 2.25 $\mathrm{mL\,L^{-1}}$ to 2.46 $\mathrm{mL\,L^{-1}}$, which agrees with the CTD observations.

The time series of SA and σ_Θ show a decrease at all three depths from October 2019 to the end of time series, which also agrees with the CTD observations. A small increase in SA and a larger increase in CT is seen at 190 m in June/July, which is coherent with the timing of O_2 increase. σ_Θ at 190 m does not show the same increase signal, but the density reduction slow down compared to the rest of the time series. At 455 m, an increase in SA and σ_Θ is detected between June 2020 and mid September 2019 (Panel B and C, Figure 4.7).

The CTD measurements and uncertainty in O_2 and σ_Θ from February, March, and October 2019, and March 2020 are also plotted with the Inner Mooring time series (Figure 4.5). We see that SA, and σ_Θ, measurements are higher in the mooring data than in the CTD data, especially at 190 m, and for October 2019 (Panel B and C, Figure 4.7). For the O_2 correction, the mooring data from February 2019 are higher compared to the CTD. Otherwise, the CTD and mooring measurements agree for O_2, as well as for the CT measurements (Panel A and D, Figure 4.7). The offsets observed between the CTD and mooring measurements implies that the conductivity corrections applied to the instruments (Table 7.1) have not been the best choice. The vertical O_2 profile from Oct19 shows a gradient at 190 m (Figure 4.3), which could explain why this CTD measurement does not overlap with the mooring measurement at this depth.

The findings from the CTD and mooring data show that shallow, partial renewals occurred during the summer months of 2019 and 2020 in the Upper layer of the Deep Basin.

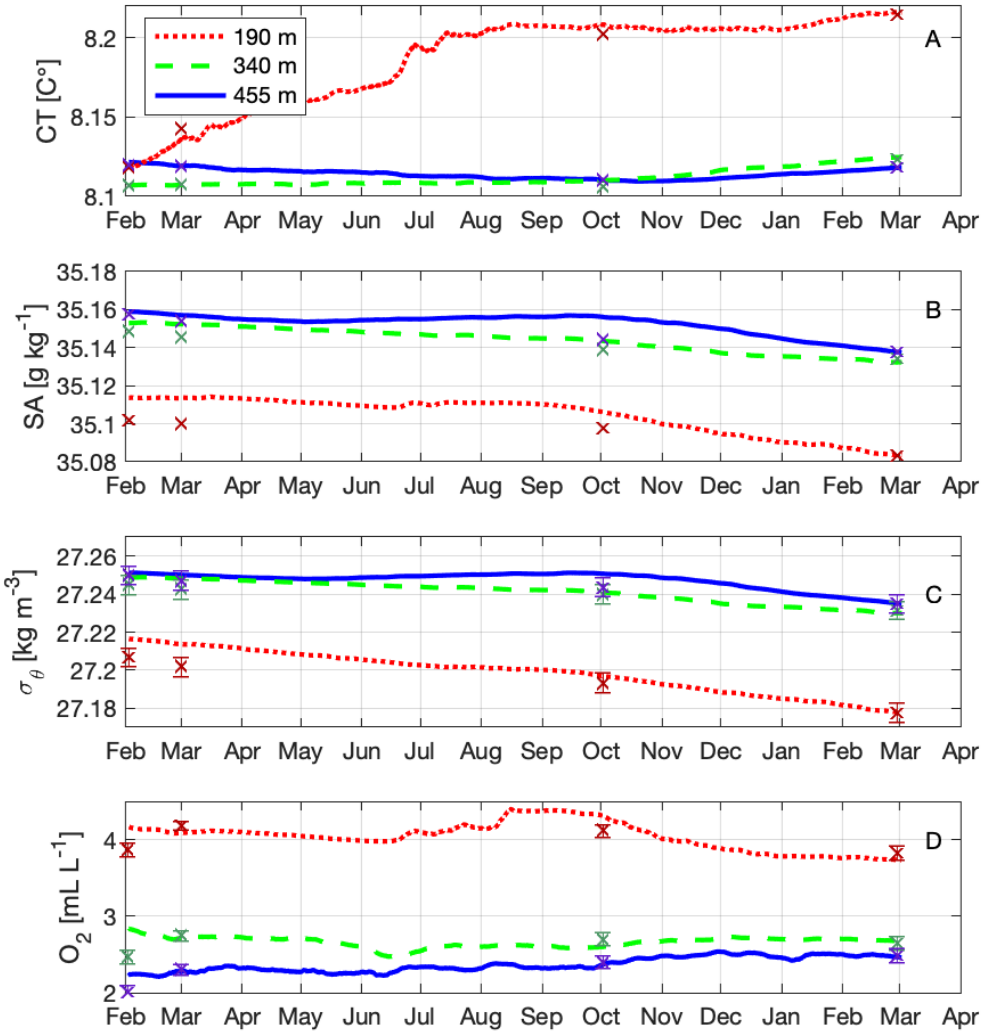

Figure 4.7: Low-passed (7 days) time series of A) CT, B) SA, C) σ_Θ and D) O_2 from the Inner Mooring at 190 m, 340 m and 455 m. The CTD measurements of CT, SA, σ_Θ ($\pm$ 0.005 kg m^{-3}) and O_2 ($\pm$ standard deviation as in Table 3.3) from Mar19, Oct19 and Mar20.

According to the CTD data, the partial renewals took place between March and October 2019, and June and September 2020, as O_2 concentration increased in between these cruises at around 200-220 m (Figure 4.3). The findings from 2019 are supported by the Inner Mooring data. The timing of the increase in O_2, CT, and SA at 190 m suggests that water with higher oxygen concentration entered the basin at the end of June. Another O_2 increase is seen in the middle of July. There are no signs of a partial renewal in the Lower layer.

With the two partial renewals identified, three stagnant periods during the observation period can be established: Feb19-Mar19, Oct19-Mar20 and Sept20-Mar21.

4.2 Vertical Diffusivity

I estimated the vertical diffusivity in the Deep Basin for the three stagnant periods in the Deep Basin with the method described in Chapter 3.4.1. For these calculations, I worked with CTD data from Feb19, Mar19, Oct19, Mar20, Sept20 and Mar21 (Figure 4.8).

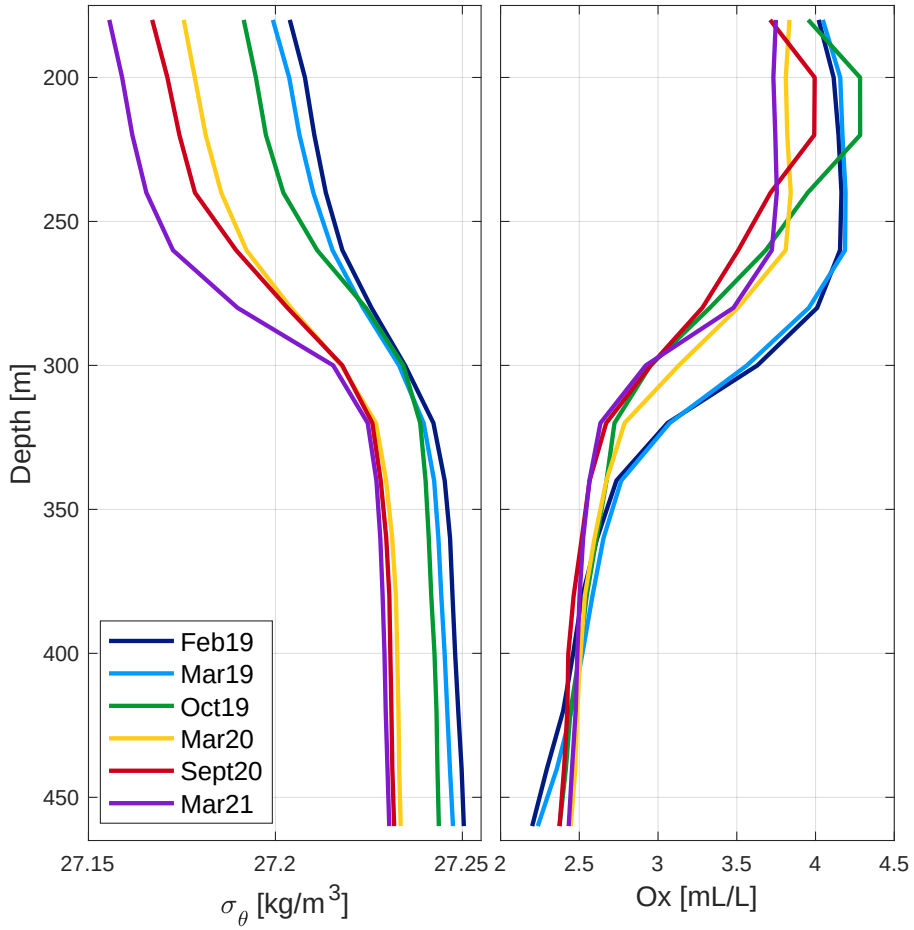

Figure 4.8: Example of smoothed density and oxygen profiles from the Deep Basin (M26). A moving mean over 20 m between 180 m and 460 m was applied to each profile before they were used in calculations of κ_{Mean}, and in calculations of oxygen concentration in the deep basin.

I used data from the M26, M24 and M28, the three deepest stations in the Deeb Basin. The amount of CTD casts available from these stations varied between the cruises, so the profiles calculated from each station in each stagnant period varied (Table 4.1). In total 12 κ-profiles were calculated for the Deep Basin; 4 profiles from Feb19-Mar19, 6 profiles from Oct19-Mar20 and 2 profiles from Sept20-Mar21 (Panel A, Figure 4.9). Generally, the κ-profiles follow the same shape. The largest values are located between 150 - 250 m and 350 - 450 m, and the smallest values are found at around 300 m. The largest spread is found in the areas with the largest values, and close to the bottom (Figure 4.9).

In an attempt to estimate one κ-profile representing the vertical diffusivity in the Deep

Stagnant period	Kappa profiles from each station
Feb19 - Mar19	M24 (1), M26 (2), M28 (1)
Oct19 - Mar20	M24 (2), M26 (4)
Sept20 - Mar21	M24 (1), M26 (1)

Table 4.1: List of CTD stations used for calculations of vertical diffusivity from the stagnant periods Feb19-Mar19, Oct19-Mar20 and Sept20-Mar21. The amount of κ-profiles calculated at each station for the time periods in question are given in parenthesis.

Basin, I calculated a κ_{Mean} profile. There are two ways we can obtain κ_{Mean}. One way is to find the mean of all the individual κ-profiles calculated (Panel A, Figure 4.9). This profile is called $\kappa_{Mean(Individual)}$ (Panel C, Figure 4.9). Another way is to find the average of each stagnant period, $\kappa_{Average}$ (Panel B, Figure 4.9), and then find the mean profile from the $\kappa_{Average}$-profiles. This profile is the $\kappa_{Mean(Group)}$ (Panel C, Figure 4.9).

If the amount of CTD casts from each stagnant period were the same, $\kappa_{Mean(Individual)}$ and $\kappa_{Mean(Group)}$ would be equal. This is not the case for the data I have available (Table 4.1). Due to this, my initial thought was to find the unweighted $\kappa_{Mean(Group)}$ so all three stagnant periods are given the same weight, independent of the casts available from each period. But the results show that the profiles from Sept20-Mar21 are lower than from Feb19-Mar19 and Oct19-Mar20. This is probably due to the conductivity calibration of Mar21, as discussed in Chapter 5.2.1. Therefore, I decided to find $\kappa_{Mean(Individual)}$ as all profiles are given the same weight. The two profiles from Sept20-Mar21 become less important, and $\kappa_{Mean(Individual)}$ is less affected by the error in Mar21 calibration than in $\kappa_{Mean(Group)}$.

When comparing $\kappa_{Mean(Individual)}$ and $\kappa_{Mean(Group)}$, we see they resemble each other. $\kappa_{Mean(Individual)}$ being slightly larger than $\kappa_{Mean(Group)}$. This is because Sept20-Mar21 is given more weight in $\kappa_{Mean(Group)}$, pulling the mean towards the lower values observed in Sept20-Mar21 . The profiles differs the most between 180 m - 220 m, and between 400 m and the bottom. The largest difference is 1.9×10^{-4} m^2 s^{-1} at 460 m (Panel C, Figure 4.9).

As discussed above, I will $\kappa_{Mean(Individual)}$ as κ_{Mean} since all profiles are equally weighted. The range for κ_{Mean} is 1.6×10^{-4} m^2 s^{-1} to 1.1×10^{-3} m^2 s^{-1}, and the volume mean vertical diffusivity in the basin is 6.5×10^{-4} m^2 s^{-1}. By using a mean profile, we assume the vertical mixing due to diffusivity is constant over time during stagnation periods.

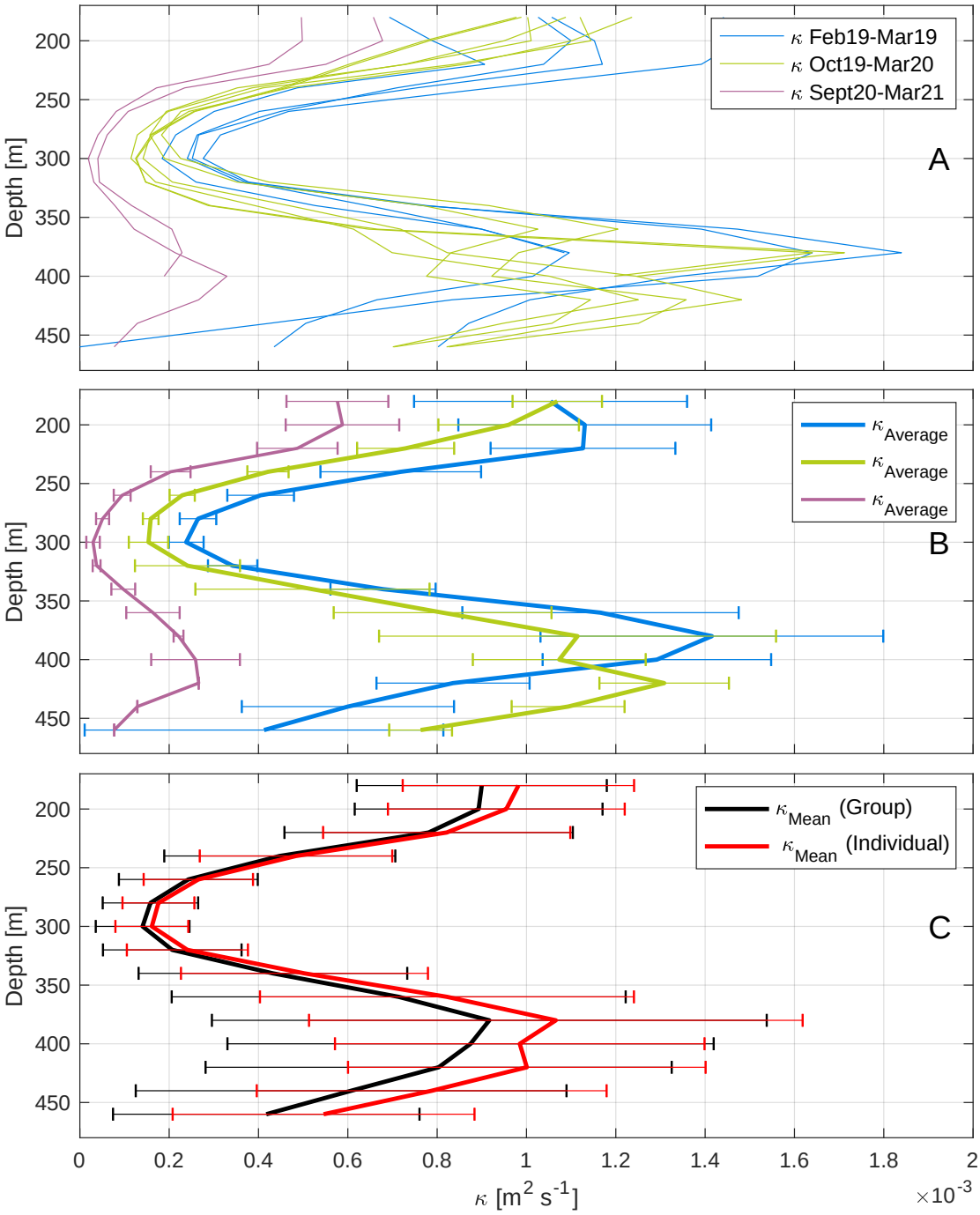

Figure 4.9: Results from estimation of κ-profiles from the Deep Basin. Panel A shows all estimated profiles, color coded depending on which time period they were calculated from. Panel B shows the average κ-profiles from each time period along with the standard deviation. Panel C shows two mean κ-profiles; one calculated from the profiles in panel A (Individual) and one calculated from profiles in panel B (Group).

4.3 Stagnant periods and vertical diffusivity in NorFjords160

To compare the vertical diffusivity from NorFjord160 with the observations, I followed the same procedure as for the observations: first analyze the hydrographic conditions and identity renewal episodes in the basin, and then calculate κ (Chapter 3.4.1).

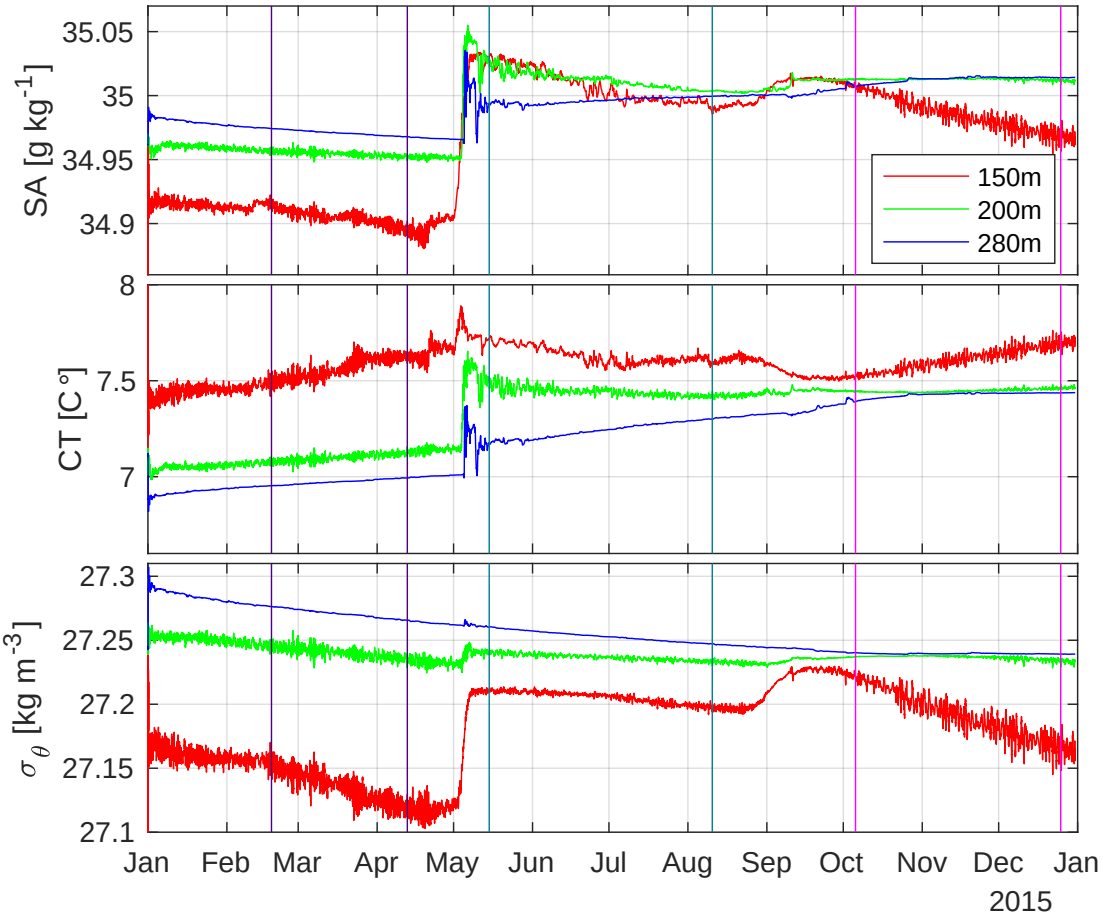

Figure 4.10: Time series of SA, CT and σ_Θ at 150 m, 200 m and 280 m for the NorFjords160 model run of 2015. SA, CT and σ_Θ are calculated from the temperature and salinity data from the NorFjords160 model results. The vertical lines are color coded and indicate the beginning and end of stagnant period.

The model results of CT, SA and σ_Θ time series show two renewals, one in the beginning of May, and the second in the beginning of September (Figure 4.10). This is clear from the increase in SA and σ_Θ, most apparent at 150 m. At 200 m and 280 m, the increases in SA and σ_Θ are weaker. Except for the renewal episodes, SA and σ_Θ decreases over time. CT generally increases over time for all three depths.

I identified three stagnant periods: the first from February - April, the second from May - August and the third from October - December. With these established, I extracted vertical profiles of temperature and salinity from the beginning and the end of each stagnant period, all profiles from the same station in the model (same location as M24)

(Table 3.5). The temperature and salinity data were converted to CT and SA, from which potential density (σ_Θ) were found (Figure 4.11).

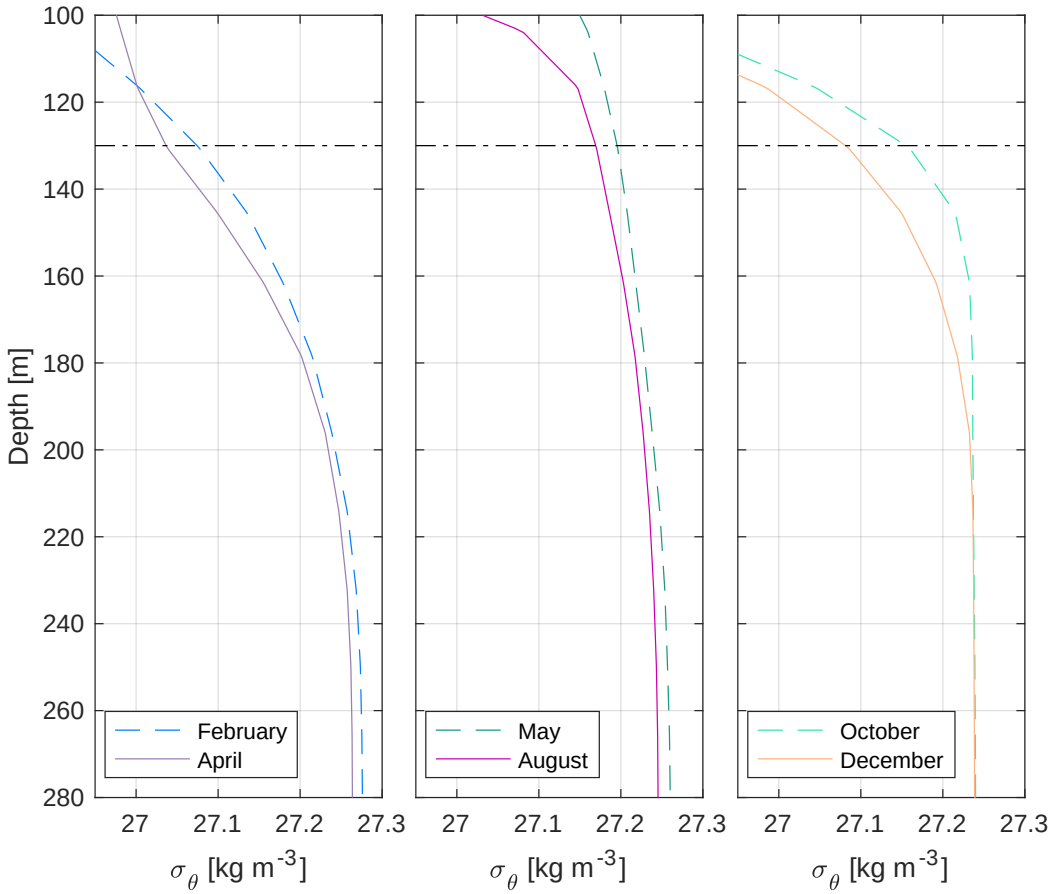

Figure 4.11: Vertical profiles of potential density (σ_Θ) from NorFjords160. These profiles will be used to calculate vertical diffusivity for three different stagnant periods. The horizontal black line indicates the sill depth (130 m) of the Inner Sill in the model grid.

I calculated 6 κ-profiles, two profiles from each stagnant period (Figure 4.12). The κ-results from Feb-Apr15 increase with depth, and have the largest values close to the bottom. The results from May-Aug15 show similar behaviour to Feb-Apr15, but does not increase as much as seen for Feb-Apr15. The results Oct-Dec15 profiles differ, and have the largest values for κ at 190 m, and smallest values found close to the bottom.

Due to the differences in the depth profile between the model grid and the bathymetric maps (Figure 3.2, a direct comparison of κ-results from the observations and the model does not work. In stead, I compare the volume mean vertical diffusivity, as the volume of the basins are of comparable size (Table 3.6). For the basin in NorFjords160, the volume mean vertical diffusivity is $\kappa_{ModelMean} = 1.9 \times 10^{-4}$ m^2 s^{-1}, with a range of $1.4 - 2.7 \times 10^{-4}$ m^2 s^{-1}.

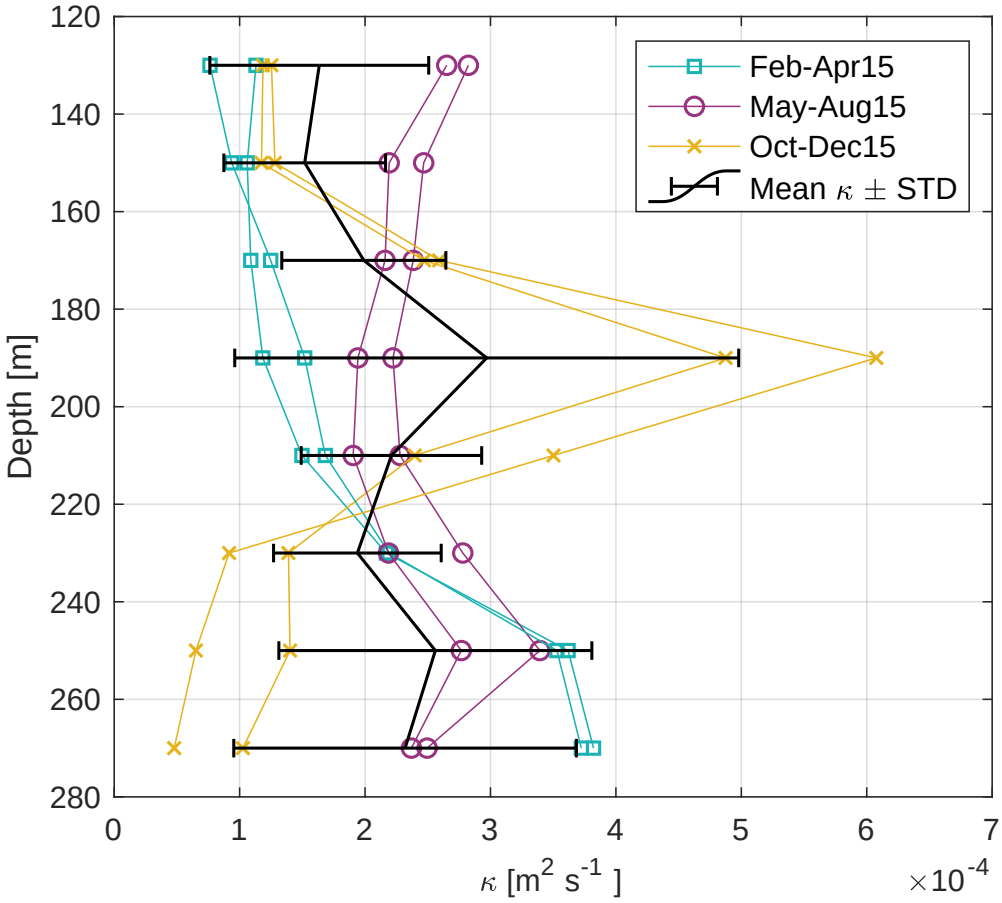

Figure 4.12: κ-profiles from NorFjords160 data. The results from each stagnant period is color coded. The $\kappa_{ModelMean}$-profile is also included alongside the standard deviation.

4.4 Oxygen calculations with estimated vertical diffusivity

4.4.1 Observed initial profiles and oxygen consumption rate

I calculated theoretical O_2-concentrations in the Deep Basin based on κ_{Mean} and the observed initial profile by using Equation 5. The calculations estimate the changes in O_2 due to diffusive processes, where the initial profile is the start O_2-concentration. The standard deviations from κ_{Mean} (Panel C, Figure 4.9) define a range for the upper and lower limit for the O_2 calculations. The time interval for the calculations were determined by the length of the stagnant periods; Feb19-Mar19, Oct19-Mar20 and Sept20-Mar21, i.g. I calculated three O_2-profiles from stagnant period. The estimated profile at the end of each stagnant period represents the O_2 concentration in the basin when the effects of biology are neglected. The end profile is the observed O_2-profile at the end of the stagnant periods, where both diffusive processes and biological oxygen consumption have affected the O_2 concentration in the Deep Basin. The biological oxygen consumption were estimated from the difference between the observed O_2-profile and the estimated O_2-profile.

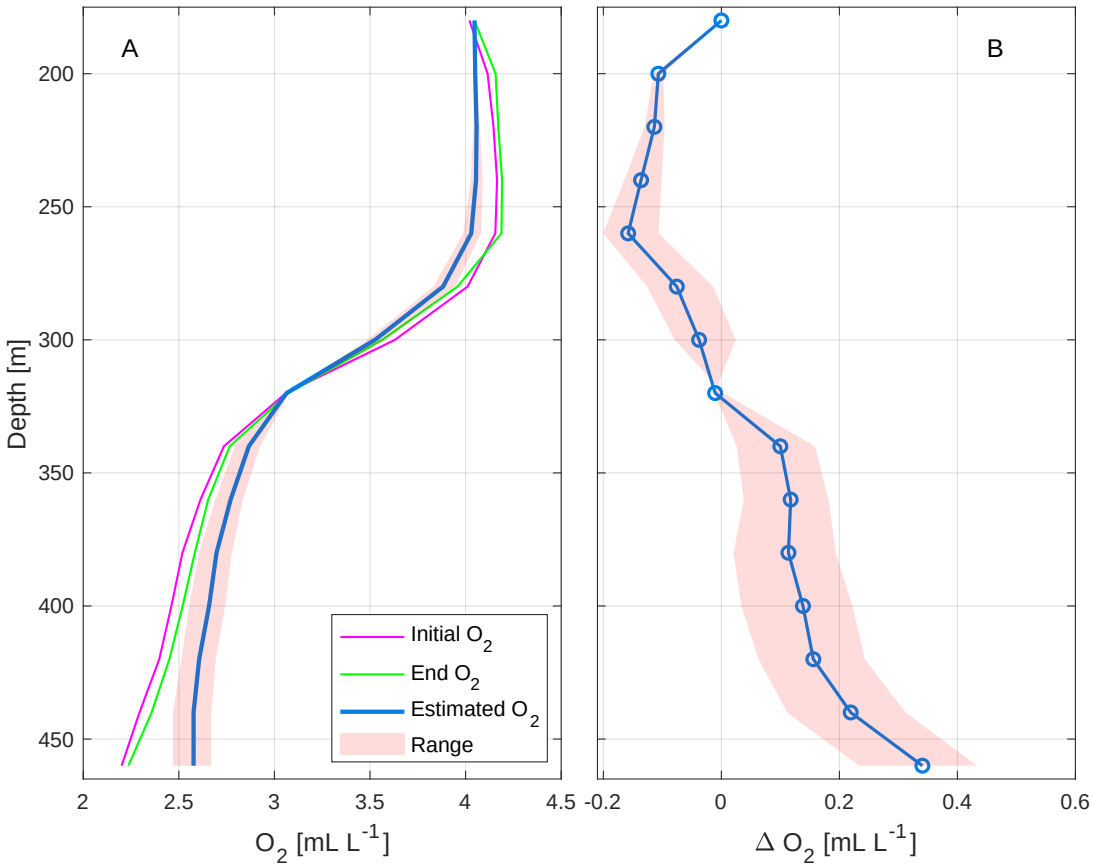

Figure 4.13: Panel A shows the results from the calculation of O_2 profiles by the use of κ_{Mean} for Feb19 - Mar19. Initial and End O_2 are from observation at M26. In Panel B, Δ O_2 = Estimated profile - End profile is shown.

The results from all three stagnant periods show that the estimated O_2 concentration is smaller than the observed concentration above 300 m, and larger than the observed below 300 m. Larger O_2-concentrations for the estimated profile are expected since biological oxygen consumption is neglected in Equation 5. The upper boundary condition, which is dependent on the oxygen concentration of the end profile, causes the difference between computed and observed oxygen, ΔO_2 to be 0 at 180 m. From 180 m ΔO_2 slowly increase towards a minimum at 260 m, where the computed values are about 0.13 - 0.17 mL L^{-1} larger than the observed oxygen. Below 260 m Δ O_2 increases with depth, and the maximum is found at 460 m in all three cases (Panel B, Figure 4.13, 4.14, 4.15).

For the one-month period Feb19-Mar19, the estimated profile is the closest to the observed, as Δ O_2 are closer to 0 compared to the results from the other stagnant periods. At 260 m, Δ O_2 is -0.16 mL L^{-1} and at 460 m Δ O_2 is 0.34 mL L^{-1} (Panel B, Figure 4.13).

Oct19-Mar20 and Sept20-Mar21 are similar to each other, both in terms of the results from the estimated profile, and the observed initial and end profile. The initial profiles

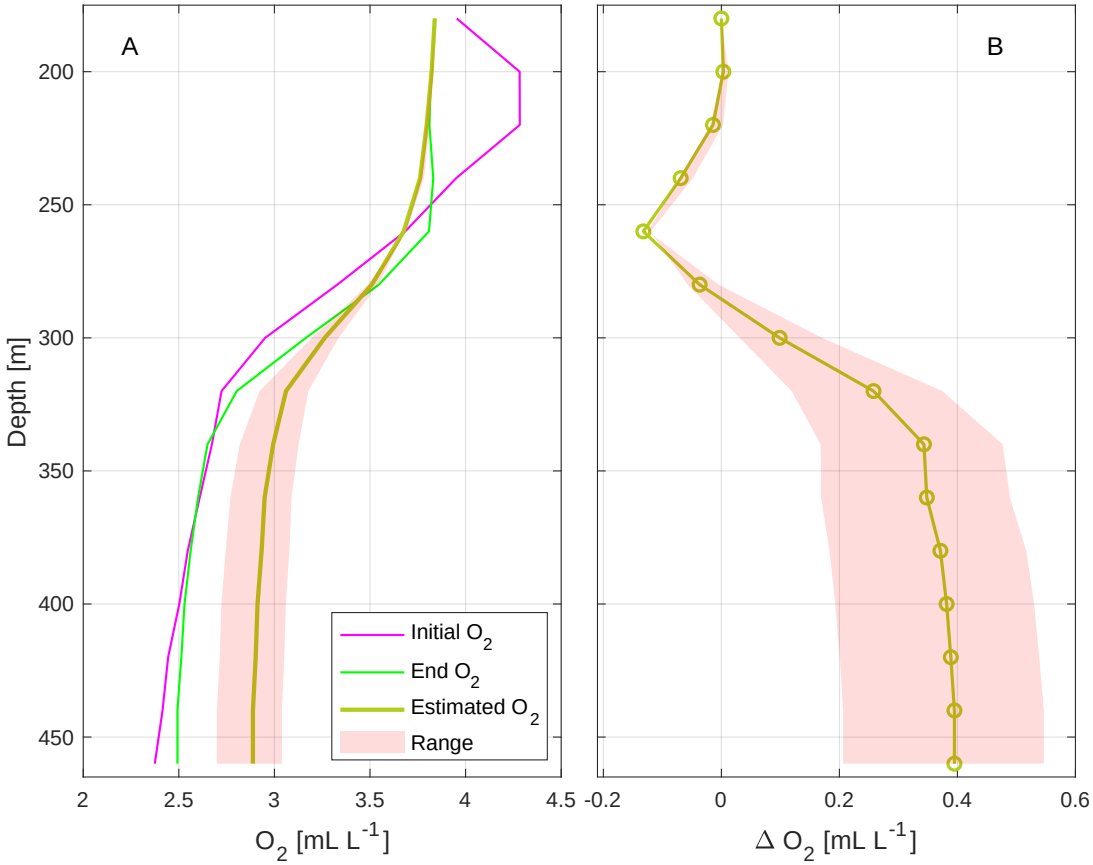

Figure 4.14: Panel A shows the results from the calculation of O_2 profiles by the use of κ_{Mean} for Oct19 - Mar20. Initial and End O_2 are from observation at M26. In Panel B, Δ O_2 = Estimated profile - End profile is shown.

from Oct19 and Sept20 both have an increased oxygen signal at 200 - 200 m compared to the end profiles in Mar20 and Mar21. Slightly higher oxygen values are found in Oct19 than Sept20 (4.3 mL L^{-1} compared to 4 mL L^{-1} at 200 m) (Figure 4.8). The estimated oxygen profile in both cases is also very similar. It increases with depth below 300 m, with oxygen concentrations being 0.2 - 0.4 mL L^{-1} higher oxygen concentration compared to the observed in both cases (Panel B, Figure 4.14 and 4.15).

Then I calculated the oxygen consumption rates in the Lower layer (below 300 m) by following the two methods described in Chapter 3.5.1. First, I found the vertical profile of the biological oxygen consumption rate $b_{t,z}$. This rate was estimated by $b_{t,z}$ = Δ O_2 / $\Delta time$, where $\Delta time$ is the length of each stagnant period. For Feb19-Mar19, $b_{t,z}$ does not differ much from Δ O_2. For this period, $\Delta time$ for this period is slightly less than a month (about 28 days) (Figure 4.16). For Oct19-Mar20 and Sept20-Mar21, $b_{t,z}$ follows the same shape, which is not surprising as Δ O_2 was similar for each case, and $\Delta time$ is only 9 days shorter for Oct19-Mar20 than Sept20-Mar21 (152 and 163). At 460 m $b_{t,z}$ = 0.077 mL L^{-1} $month^{-1}$ from the Oct19-Mar20, and $b_{t,z}$ = 0.072 mL L^{-1} $month^{-1}$ from

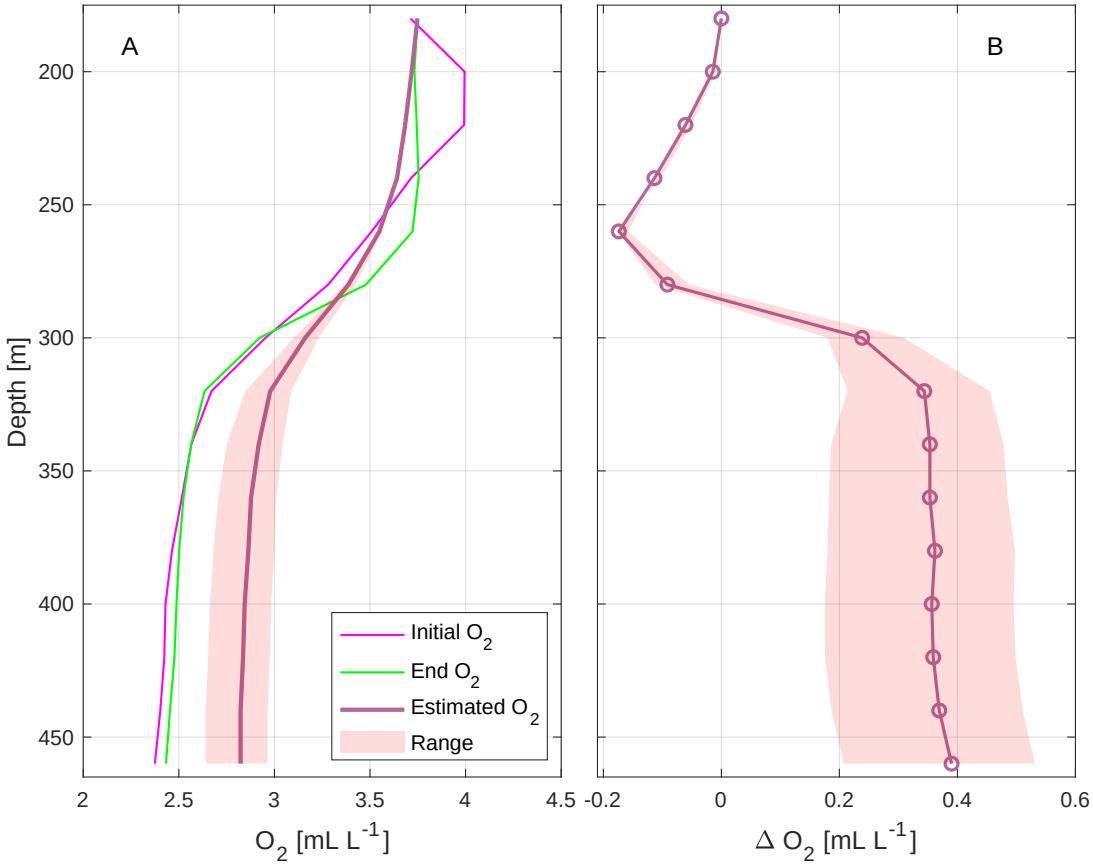

Figure 4.15: Panel A shows the results from the calculation of O_2 profiles by the use of κ_{Mean} for Sept20 - Mar21. Initial and End O_2 are from observation at M26. In Panel B, Δ O_2 = Estimated profile - End profile is shown.

Sept20-Mar21 (Figure 4.16).

In order to be able to compare the oxygen consumption rates with the results from the method used in Aure and Stigebrandt (1989), I also found the volume mean oxygen consumption rate Mean $b_{t,z}$. It was calculated from $b_{t,z}$ (Figure 4.16) between 300 m and 460 m in the Deep Basin. In addition, I found Mean $b_{t,z}$ min and max by calculating the O_2 calculations for the upper and lower limit set by the range. I also found the total oxygen consumption rate, Total $b_{t,z}$, in the basin below 300 m during the stagnant period by

$$\sum_{460m}^{300m} b_{t,z}$$

and Total $b_{t,z}$ min and max were also found in a similar way as for Mean $b_{t,z}$ min and max. All values for Mean and Total $b_{t,z}$ are found in Table 4.2.

The method from Aure and Stigebrandt (1989) finds the mean oxygen consumption rate in the basin directly, without finding a vertical profile, by the use of the parameters CONS, DEPL and DIFF (as described in Chapter 3.5.1). I found DEPL and DIFF in the basin

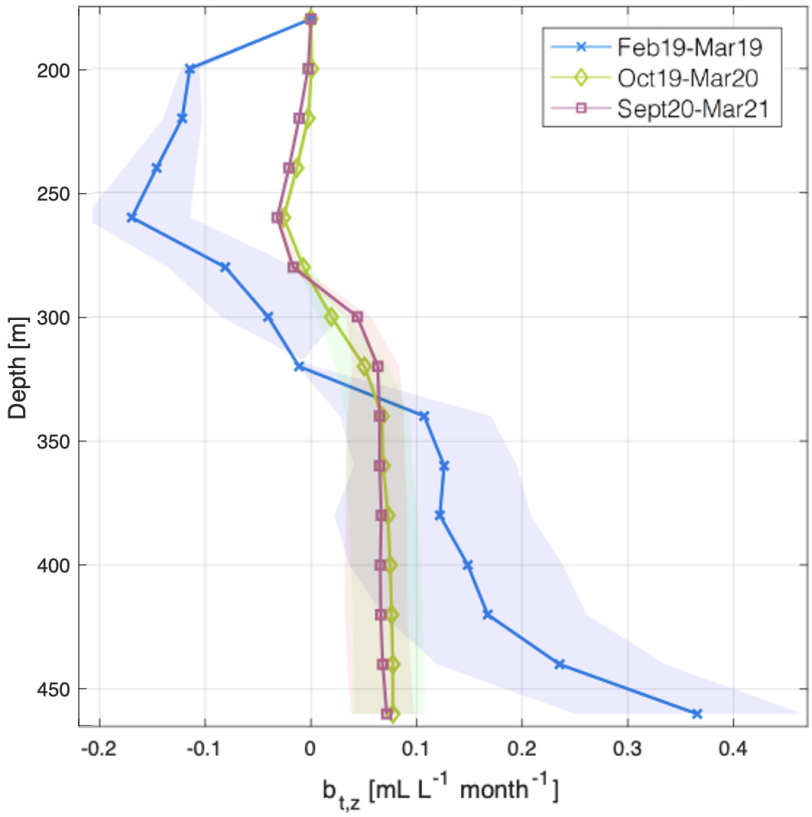

Figure 4.16: Results of the estimated biological oxygen consumption rate, $b_{t,z}$, based on $\Delta\ O_2$ and $\Delta time$. $\Delta time$ for the stagnant periods are 28 days (Feb19-Mar19), 152 days (Oct19-Mar20) and 163 days (Sept20-Mar21).

Oxygen consumption rate parameter	**Feb19-Mar19** [mL L^{-1} month^{-1}]	**Oct19-Mar20** [mL L^{-1} month^{-1}]	**Sept20-Mar21** [mL L^{-1} month^{-1}]
Total$b_{t,z}$	1.22	0.59	0.57
Total$b_{t,z}$ min	0.58	0.29	0.31
Total$b_{t,z}$ max	1.79	0.82	0.78
Mean $b_{t,z}$	0.14	0.065	0.061
Mean $b_{t,z}$ min	0.06	0.032	0.035
Mean $b_{t,z}$ max	0.20	0.091	0.0.87
CONS	0.13	0.063	0.050
DEPL	0.035	0.012	0.0040
DIFF	0.092	0.051	0.046

Table 4.2: Results of estimated biological oxygen consumption rate, $b_{t,z}$ and CONS, from below 300 m in the Deep Basin. $b_{t,z}$ was found from the difference between computed and observed oxygen profile, and CONS were from the parameters DEPL and DIFF.

layer between 300 m and 460 m, and calculated CONS from them (Table 4.2). Some interesting observations from the oxygen consumption rate results are that the results from Feb19-Mar19 differ from Oct19-Mar20 and Sept20-Mar21, and that Mean $b_{t,z}$ and

CONS show similar values for the volume mean oxygen consumption rate.

4.4.2 Idealized initial profiles and partial renewals

To study the effect of the observed shallow, partial renewal on the O_2 concentration in the Deep Basin, I modified the initial profile from Sept20 to three idealized, or artificial, initial profiles (presented in Table 3.7, shown in Panel A, Figure 4.17). Each of the initial profiles represent different scenarios.

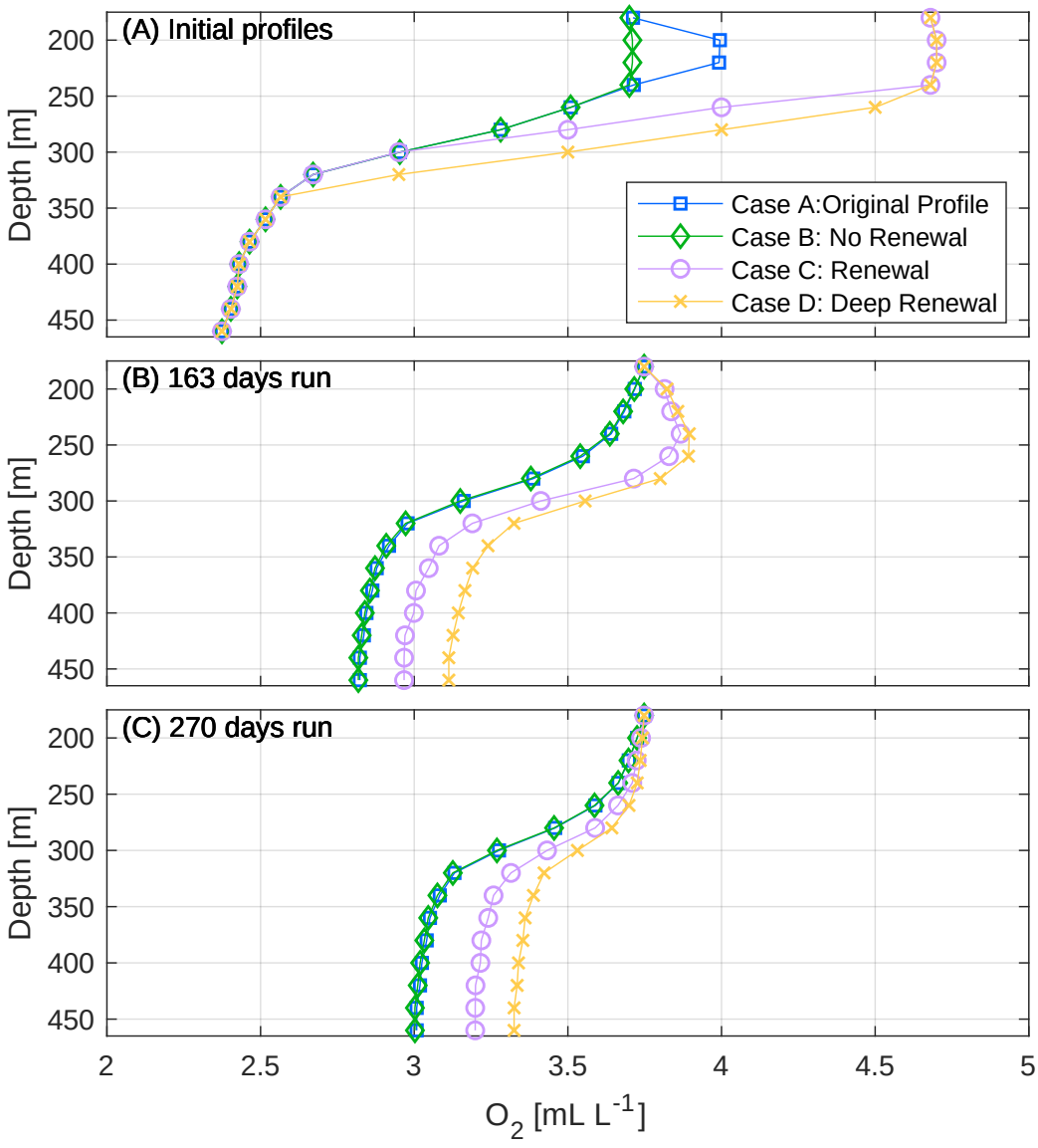

Figure 4.17: Panel A shows four initial oxygen profiles; observed and three artificial. They represent four different cases: Original profile (Sept20), No Renewal, (partial) Renewal and Deep (partial) Renewal (as described in Table 3.7). Panel B shows the estimated oxygen profile from each initial profile in Panel A at the end of the stagnation period Sept20-Mar21.

Case A is the original profile from Sept20 which shows a small renewal at 200 - 220

m depth. A situation with no partial renewal is represented in Case B, and it was made as a reference profile for when no renewal has occurred. Case C and D represent partial renewals, and what differentiate them is the depth of the layer with increased O_2 concentration, i.e. the renewed layer. Both Case C and D have the same O_2 concentrations between 180 and 240. At 280 m they start to differ from each other, where the profile in Case D is 0.5 mL L^{-1} higher compared to Case C. The renewal layer reaches down to 340 m in Case D, and to 300 m in Case C. Case D is therefore called Deep Renewal.

I did the calculations for the stagnant period Sept20-Mar20, which is 163 days (Panel B, Figure 4.17), and for a longer time period, where the length increased from 163 days to 270 days (Panel C, Figure 4.17). From observations we saw that partial renewals occurred during the summer. Increasing the length from 163 days to 270 days would suggest the end of the calculations to be sometime in June when the initial profile is from Sept20. This length seemed realistic for vertical mixing in the basin to occur without any interruption of partial renewals. The upper boundary condition at 180 m was set to have a linear behaviour given by $O_{n+1}(180m) = O_n(180m) + \frac{O_{Mar21}(180m) - O_{Sept20}(180m)}{m}$. The O_2 concentration is reduced with the same amount for each time step, given by the observed O_2 concentration in September 2020 and March 2021. Since I had no information about the O_2 concentration after Mar21, I set the upper boundary condition for the calculations after the stagnant period Sept20-Mar21 to be equal to the observations seen in March 2021 $O_{n+1}(180m) = O_{Mar21}(180m)$.

The estimated O_2 concentrations after 163 days were largest for the renewal cases, Case D and C. Below 340 m, the O_2 in Case C and D were respectively 0.7 mL L^{-1} and 0.5 mL L^{-1} larger than Case B, the reference profile for no renewal event. At the end of the stagnant period, the estimated profiles from Case A and Case B are identical (Panel B, Figure 4.17). This indicates that the small renewal seen in Case A did not significantly affect the oxygen concentration in the basin at the end of the stagnant period. After 270 days, the estimated O_2 concentrations below 300 m have increased further for all four cases, but Case D still has the highest O_2 values and Case A and B the lowest. Case A and B has reached 3 mL L^{-1} at the bottom (Panel C, Figure 4.17). There are no longer signs of the partial renewals for Case C and D, as it is at 250 m after 163 days.

In addition to the final results of O_2 at the end of the calculations, the temporal evolution of O_2 at given depths are also of interest. I chose to look at the evolution at 200 m, 260 m, 340 m and 460 m as these depths represent the renewed layer, a point above and below the pycnocline, and at the bottom. At 200 m, the O_2 signal of the small partial renewal in Case A quickly vanishes, and Case A and B are identical after about 60 days. The O_2 concentration of Case C and D decreases linearly due to the upper boundary condition (200 m, Figure 4.18). Note that the boundary condition is set at 180 m, and Figure 4.18

show the development at 200 m.

The effects of the small renewal in Case A are seen at both 200 m and 260 m, but not at 340 m or 460 m. The small renewal effects at 260 m peaks after about 15 days, and it takes about 150 days before Case A and B overlaps compared to at 200 m. Case C and D differs from each other at 260 m, as a linear reduction is seen in Case D. In Case C, O_2 concentrations after about 30 days before it is gradually reduced. A bigger gradient in O_2 is between 240 m and 260 m in Case C than Case D, which would explain this difference behaviour which indicate that higher oxygen concentrations are mixed down before in Case C before the gradients have been reduced.

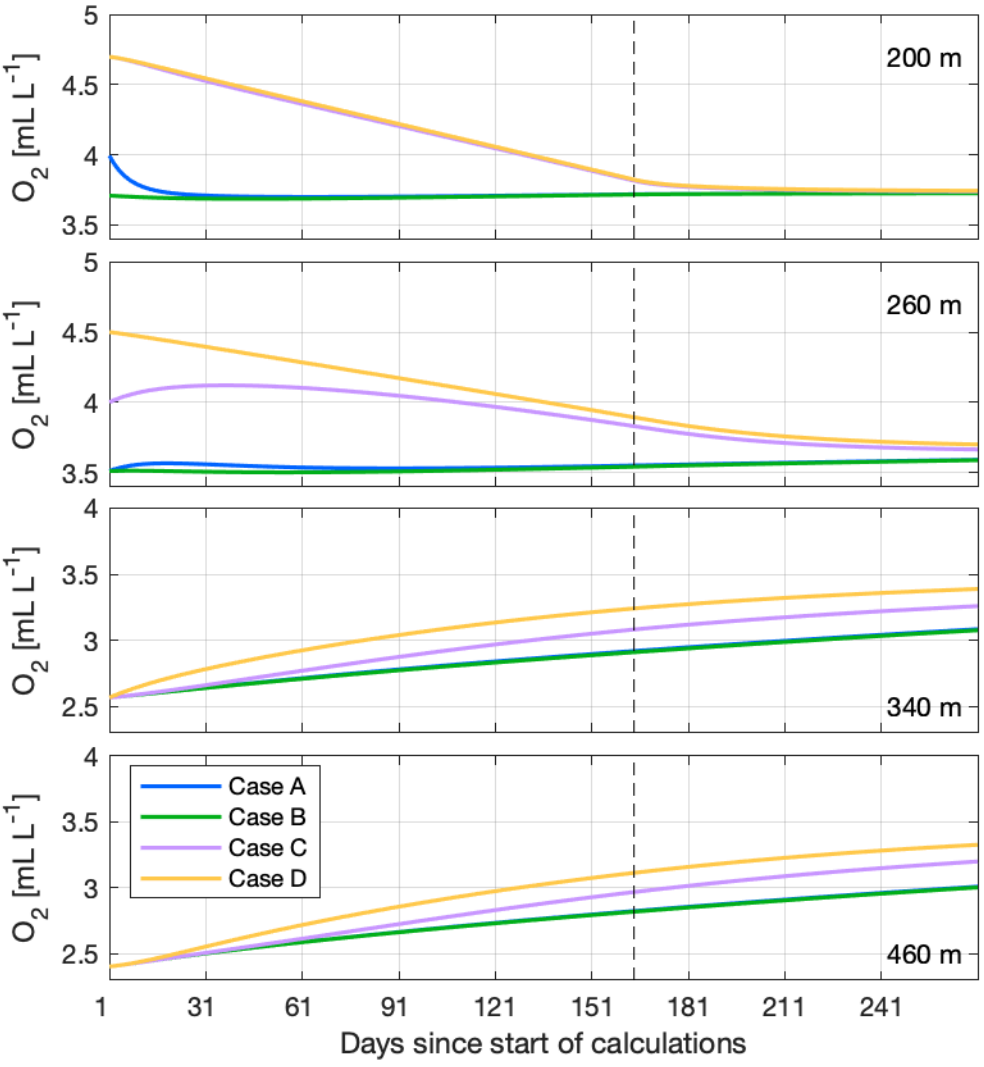

Figure 4.18: The time evolution of the oxygen concentration at 200 m, 260 m, 340 m and 460 m during the stagnation period Sept20-Mar21, and the following 107 days (270 days in total). The end of the stagnant period is indicated in with vertical, black dashed lines. The oxygen concentrations are shown for each renewal case.

At 340 m and 460 m, the oxygen concentration increases over time for all cases. Oxygen

from above is continuously mixed downwards, which over time will increase the concentration close to the bottom. The effects of the deep Case D reaches the depths at 340 m and 460 m first, followed by Case D. An immediate response is seen for Case D at 340 m because the renewed layer reaches all the way down to this depth. A response in Case C is seen after about 45 days. The effects of the small renewal in Case A are not seen at these depths, and follows Case B as if no renewal occurred. The behaviour at 460 m is similar to 340 m, but the response in Case D and Case C lags with about 20 days.

The time evolution after the stagnant period, meaning from day 163 to day 270, show that the O_2 concentration at 200 m does not change with time as seen from day 1 to day 163. The effects of the partial renewals fades out and the concentrations becomes stable, clearly seen at 200 m and 260 m. The O_2 continues at 340 m and 460 m continues to increase, but less quickly.

5 Discussion

Oxygen concentrations in the deep basin of Masfjorden, a sill-fjord in western Norway, have declined since the 1970s (Aksnes et al., 2019). The low-oxygen concentrations have been linked to a reduced renewal frequency of the basin water, which is likely caused by a reduction of the annual maximum density at the coast (Darelius, 2020).

In this thesis, I use hydrographic data from Masfjorden to map the hydrography and identify renewal episodes in the Deep Basin. I follow the budget method to estimate the vertical diffusivity during stagnant periods (from Stigebrandt and Aure, 1989) in the Deep Basin with observational and model data from NorFjords160. The vertical diffusivity results from observations and the model are compared in order to determine if the model produces realistic results of vertical mixing in the fjord basin. Based on the vertical diffusivity from observations, I estimate the amount of oxygen supplied to the deep basin through diffusion (Equation 5). Finally, I estimate the oxygen consumption rate in the basin due to biological activity in the basin.

5.1 Observations of oxygen in the Deep Basin

5.1.1 Oxygen calibration and errors

Before the oxygen data from observations could be analyzed, it was important to calibrate the CTD and mooring instruments. The sensors on the instruments will drift over time, so calibration of the sensors is a necessary step to make sure the measurements available are of good quality and can be trusted (Thomson and Emery, 2014). For this thesis, I calibrated the CTD oxygen measurements from Jun20, and the Inner mooring instruments with suitable calibrated CTD data (Appendix, Chapter 7.1 and 7.2). The mean dO were typically on the order of 0.1 - 0.2 $\mathrm{mL\,L^{-1}}$ with a standard deviation of dO generally between 0.06-0.08. The highest standard deviation value (0.098 $\mathrm{mL\,L^{-1}}$) was found for Jun20, and lowest for Sept20 (0.016$\mathrm{mL\,L^{-1}}$) (Table 3.3).

There are a couple of plausible explanations for why the standard deviation for mean dO was large for Jun20. The first is that there are errors related to the sampling process of the water samples and the Winkler titration method. The sampling process for the oxygen samples are in need of attentiveness due to oxygen being a reactive component. If air bubbles enter the sample at some point before the titration starts, the sample is ruined as the air bubble changes the oxygen concentration. The Winkler titration method is either manually or automatically, but the standard deviation for the oxygen corrections are not affected by the choice of method (Table 3.3). The errors would be related to the accuracy of adding and measuring the volume of reagent that goes into the sample during the titration. During the student cruises, the Winkler titration of were carried out by

several students with little experience in both sampling and titration.

During the Jun20 cruise, we experienced troubles with the equipment used for adding chemicals to the oxygen samples. The equipment often caused air bubbles to enter the sample together with the chemicals. Several samples had to be redone in order to add the chemicals without air bubbles. There is a possibility that small air bubbles entered some samples unnoticed. This could have caused the oxygen concentration from the samples to vary more even though the samples were analyzed on board and by the automatic Winkler titration system.

The second explanation for the large standard deviation in dO was the water sample location in the water column, or more specifically located in gradients where the oxygen concentration changes quickly with depth. Since the CTD sensor and the Niskin flasks are not located at the exact same depth, they might measure different oxygen concentration when water samples are collected from such areas. This might results in higher offsets when comparing the CTD and sample concentration. During the Jun20 cruise, we sampled oxygen from the entire column which included area with gradients. I removed samples from the upper 100 m from the calibration, as this was the layer where offset was the largest, most likely due to the gradients present here.

The observed oxygen concentration in the Deep Basin changes over time, and largest changes between each cruises are about 0.5 $\mathrm{mL\,L^{-1}}$ at 200 m and 300 m (Figure 4.5). At 350 m and 450 m, the variations are smaller, and the changes between each cruise are typically around 0.1 $\mathrm{mL\,L^{-1}}$. The typical standard deviation of 0.06 - 0.08 $\mathrm{mL\,L^{-1}}$ are close to the changes we see in oxygen concentration over time in the Lower Layer.

5.1.2 Oxygen observations in the Deep Basin

From the hydrography data, we identified the surface, intermediate and basin layers in Masfjorden (Figure 4.1 and 4.2). In the Deep Basin, we saw two layers present, the Upper layer (180 m - 280 m) and the Lower layer (340 m - 480 m) (Figure 4.3). The oxygen concentrations in the Lower layer was observed to be around 2.5 $\mathrm{mL\,L^{-1}}$ below 340 m from February 2019 to March 2021. Based on the classification limits for oxygen, the Lower layer is oxygen stressed (Table 2.1) and the environment based on the oxygen conditions are on the limit between Moderate and Poor. This indicates that the oxygen concentrations below 340 m in the Deep Basin most likely will affect the marine life. In the Upper layer and in the Shallow Basin, the oxygen concentrations observed are between 3.6 $\mathrm{mL\,L^{-1}}$ and 4.3 $\mathrm{mL\,L^{-1}}$. This is classified as Good for the ecological conditions (Table 2.2), and the oxygen concentration does not affect marine life. As the oxygen consumption rate with the vertical diffusivity for the Deep Basin is known, it would have been possible to calculate when the Lower layer would become hypoxic, given that no DWR events

occur by Equation 4.

The density reduction during stagnant periods at the bottom of Masfjorden are typically D = 0.010-0.015 $\mathrm{kg\,m^{-3}\,year^{-1}}$ (Darelius, 2020). The density reduction observed during the observation period 2019 - 2021 suggested a density reduction of 0.0085 $\mathrm{kg\,m^{-3}\,year^{-1}}$ at 450 m (Figure 4.5). The observed density reduction is found from a period where shallow partial renewals occurred, but no full DWR was observed. The observed reduction is close to, but slightly lower than the values given in Darelius (2020).

The results from the oxygen data from 2019 - 2021 showed that the oxygen concentration varied at different depths throughout the observation period (Figure 4.5 and Figure 4.7). Shallow partial renewals were observed during the summer months of 2019 and 2020 between 180 m - 220 m. The oxygen concentration at 350 m decreases over time, which agrees with the observations of declining oxygen during stagnant periods Aksnes et al. (2019). At 450 m, the oxygen concentration increases over the observational time period. This an unexpected finding since no major DWR event occurred in the basin, and the observations of oxygen concentration and density in the basin layer decreased in the basin layer during the stagnant periods (Figure 4.5). Changes in the oxygen consumption rate close to the bottom could be an explanation for why the oxygen concentration increases at 450 m. The oxygen consumption rate may decrease when the oxygen concentration becomes less than 2 $\mathrm{mL\,L^{-1}}$ (Aure and Stigebrandt, 1989), as the low oxygen concentrations affect the ecosystem. Even though the oxygen concentration at 450 m is not observed to be below 2 $\mathrm{mL\,L^{-1}}$ in the Lower layer during the observation period, the Lower layer is oxygen stressed and on the limit between Moderate and Poor for the environmental classification. If the concentrations are low enough to affect the ecosystem in the Deep Basin, the biological consumption rate could be reduced so that the diffusive processes become more important.

An interesting research question regarding the oxygen increase at 450 m would be to check if there is a link between reduced fish farming activities, a reduced oxygen consumption rate and increase in the oxygen concentration close to the bottom. Fish farms produce waste in form of organic matter which sinks down to the bottom of the basin and increases the oxygen consumption rate below the fish farms (Stigebrandt, 2012). Activity from fish farms in Masfjorden had to be reduced due to the observations of low-oxygen concentrations (Andersson et al., 13.02.2017; Aarre, 16.05.2017), and there are currently no fish farms operating in the inner part of the fjord, though IMR's research station is still active. The biological oxygen consumption may have decreased as a result of reduced fish farming activities due to less organic waste. By comparing the temporal evolution of the oxygen concentration and biological consumption rate before and after fish farms were relocated, one could potentially determine if the reduction in fish farm activity has

reduced the biological consumption rate in the basin.

A decreasing trend for oxygen concentration (0.014 - 0.047 mL L^{-1} $year^{-1}$) in the Masfjorden basin was observed during 1975 - 2017 (Aksnes et al., 2019). The oxygen concentrations observed during 2019-2021 decrease with larger rates than the decreasing trend suggests. From Mar19 to Mar21, the reduction rate for oxygen is 0.32 and 0.078 mL L^{-1} $year^{-1}$ at 300 and 340 m (Figure 4.5. But comparing the observed reduction rates observed with the trend from Aksnes et al. (2019) does not work well for two reasons. The first reason is that the observations from 2019-2021 are data from a short time period where no DWR event has occurred, while the long-term trend is based on observations from several decades, including years with DWR renewal events. During the 2019-2021 time period, the oxygen reduction rate would be better explained by the biological oxygen consumption rate.

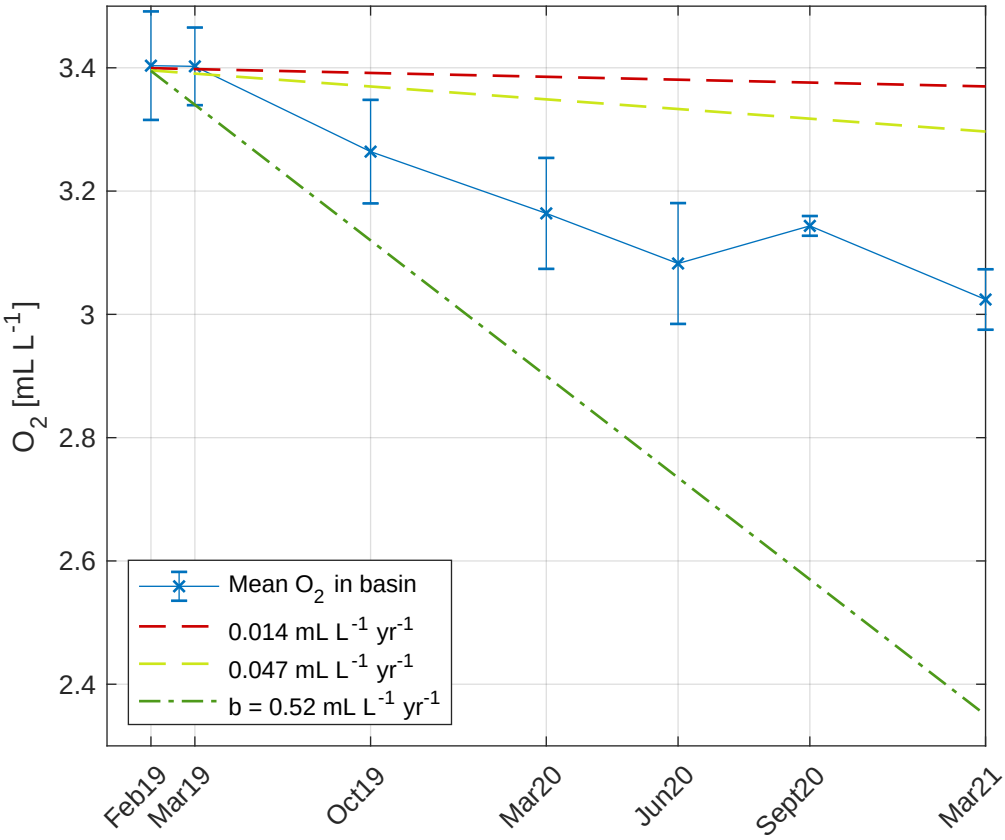

Figure 5.1: Temporal evolution of the mean O_2 concentration in the Deep Basin (M26) based on measurements from 200, 300 and 400 m. The observed long-term trend for oxygen decline (0.014 - 0.047 mL L^{-1} $year^{-1}$) and the biological consumption rate from Aksnes et al. (2019) are also included. The standard deviations from each cruise is listed in Table 3.3.

The second reason is that the oxygen concentrations in Aksnes et al. (2019) are based on the average of oxygen measurements from 200, 300 and 400 m measured in the Deep Basin in October or November. The oxygen concentration in represent a mean concentration

for the basin. The observations in Figure 4.5 are not the mean concentration, but the concentration at specific depths. To compare the data set from 2019-2021 with Aksnes et al. (2019), I calculated a mean O_2 for the basin from the oxygen measurement at 200, 300 and 400 m for the 2019-2021 (Figure 5.1). The temporal evolution of mean O_2 decreases with time, except between Jun20 and Sept20. The increase is explained by the shallow partial renewal that occurred during 2020, which affected the oxygen concentration at 200 m. Mean O_2 decreases with 0.24 mL L^{-1} between Mar19 and Mar20, and with 0.12 mL L^{-1} between Mar20 and Mar21. For the two-year period between Mar19 and Mar21, the decrease is of 0.38 mL L^{-1} gives a reduction rate of 0.19 mL L^{-1} yr^{-1} in the basin. Thus, the reduction rate in 2019-2021 data is larger than the decreasing trend of 0.014 - 0.047 mL L^{-1} $year^{-1}$ found in Aksnes et al. (2019). But it is less than the mean biological consumption rate of b = 0.52 mL L^{-1} yr^{-1} found in (Aksnes et al., 2019). The partial renewals affect the the oxygen reduction rate, as seen for Jun20 - Sept20.

The oxygen concentration in Aksnes et al. (2019) between 2015-2017 is between 2 - 3 mL L^{-1}, while the concentration is between 3 - 3.5 mL L^{-1} for the data from 2019-2021 (Figure 5.1). An increase in the mean oxygen concentration must have occurred between 2017 and 2019 to explain the increase in mean O_2. If oxygen and density data from 2018 indicate a renewal event in Masfjorden, it would explain the increased the oxygen concentration from 2017 to 2019.

5.1.3 Partial renewal

The results from hydrography in Masfjorden suggest that no full DWR event occurred during the observation period February 2019 - March 2021 because the density decreases over time at all depths in the Deep Basin. Oxygen concentrations at 180-240 m increased between March and October 2019, and June and September 2020, which indicates that shallow, partial renewals occurred during summer months of 2019 and 2020 (Figure 4.3 and Figure 4.7). This is supported by the findings in the Shallow Basin, where the oxygen concentrations increased during the summer months (Figure 4.4). The Inner Mooring observations of O_2, CT and SA at 190 m from show that warmer and slightly more saline water with higher oxygen concentrations entered the Upper layer in June/July 2019 (Figure 4.7).

The timing of the partial renewals can be explained by density variations observed at the coast outside of Masfjorden. Temperature and salinity are regularly measured at a IMR station in Sognesjøen (obtained from `http://www.imr.no/forskning/forskningsdata/stasjoner/view?station=Sognesjoen`). These measurements represent the coastal water masses found outside of Masfjorden and Fensfjorden. The density at 75 m in Sognesjøen was observed to be the highest during the summer months of 2019, which coincide

with the observation of the partial renewal in Masfjorden (Sagen and Aguiar, 2020).

Aksnes et al. (2019) defined the high density (HD) frequency as the percentage of all of σ_θ observations at 75 m in Sognesjøen that are above 27.25 in a year. They then set up an empirical model, where the fraction of the water in Masfjorden that is renewed depends on HD. When HD = 0 % of the observations in Sognesjøen are below 27.25 kg m^{-3} and no new water enters the basin in Masfjorden. The density observed during summer of 2019 and 2020 at 75 m in Sognesjøen is lower than the proxy (Figure 5.2), i.e. HD = 0. The observed potential density in Masfjorden in the upper, partially renewed, layer were 27.2 kg m^{-3} and 27.18 kg m^{-3}, while the maximum density observed in Sognesjøen were 27.15 kg m^{-3} and 27.18 kg m^{-3} in 2019 and 2020 respectively. The coastal water masses were not dense enough for a DWR event in the basin layer, but still dense enough to renew a smaller part of the Upper layer in the basin. Because partial renewals were observed in Masfjorden, the density in Sognesjøen must have been higher than the bi-weekly observations at some point. So, the resolution of observations in Sognesjøen did not capture the density peak. The density peak signal does not need to be very long, as a renewal event in Masfjorden of 1-3 days is enough to renew the basin layer, given a density difference of 0.06 kg m^{-3} (Darelius, 2020).

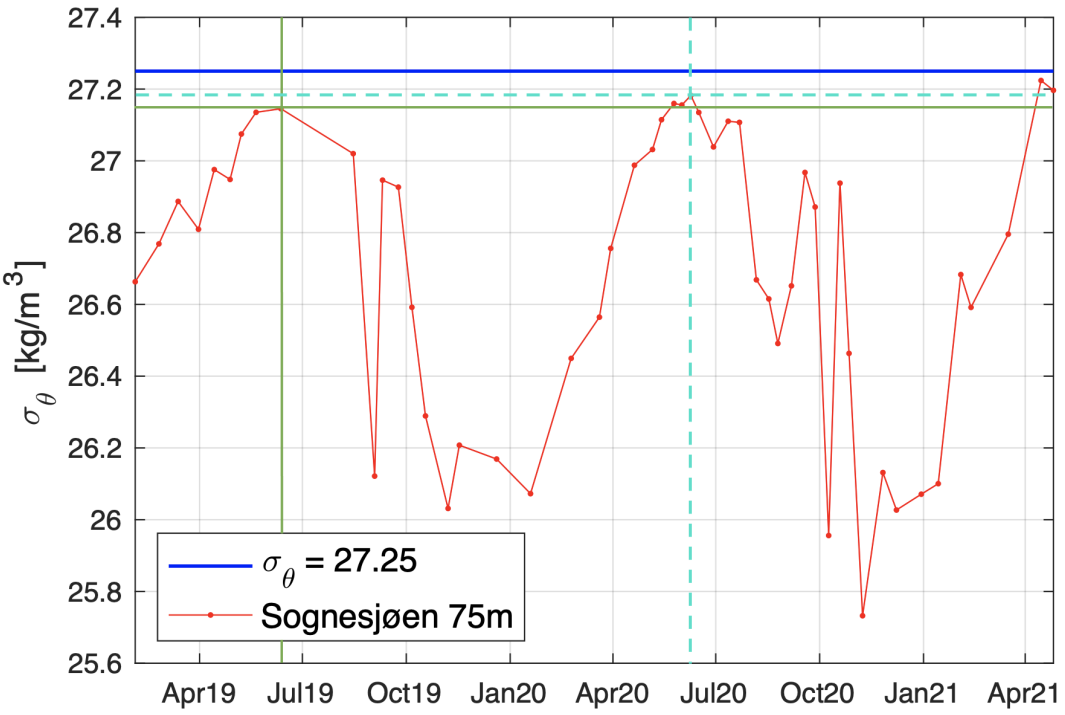

Figure 5.2: Time series of σ_Θ at 75 m in Sognesjøen between 1. January 2019 and 26. April 2021. Partial renewal in 2019 (green line) and 2020 (blue dashed line) marked. σ_Θ = 27.25 is a proxy used in Aksnes et al. (2019) to determine if a renewal will occur in Masfjorden based on the potential density at 75 m in Sognesjøen.

Since I have used oxygen as the main indicator of a partial renewal, I chose to not go into

further work with the Sill Mooring time series, or include current data from a mooring located in the mouth of Masfjorden (IMR Mooring). These moorings provided data from the summer months of 2019, and it would have been interesting to combine data from these moorings and try to identify the water masses that entered the fjord in relation to the observed renewal profile in the Deep Basin. There were no apparent changes in density during the renewal events from the Inner Mooring and CTD data, it is likely that the density of the coastal water masses at sill level have had similar density as the basin layer. But since the Sill Mooring only provided density data and no oxygen data, I chose not go into further details regarding this.

5.2 Vertical Diffusivity from observations and NorFjords160

5.2.1 From observations

The establishment of stagnant periods is a requirement for using Equation 2 to estimate the vertical diffusivity, and had to be done before the calculations were made. If the vertical diffusivity were calculated during a period where a renewal occurred, the changes in density would no longer be solely due to diffusion. The results would therefore not represent the diffusive processes that take place in the basin layer. This is why the diffusivity could only be estimated from the stagnant periods Feb19-Mar19, Oct19-Mar20 and Sept20-Mar21. The vertical diffusivity profiles, κ-profiles, estimated with Equation 2 from the three stagnant periods all follow the same shape (Figure 4.9), even though the stagnant period Feb19-Mar19 lasts for 1 month, and Oct19-Mar20 and Sept20-Mar21 last for about 5 months. Feb19-Mar19 and Oct19-Mar19 are similar to each other, while lower values were found for Sept20-Mar21.

While working with Equation 2, it became clear that the κ results are sensitive for small errors in the potential density profiles. A correct calibration of the conductivity sensors is of great importance as salinity is calculated from conductivity, and salinity largely determines the density. The κ results from Sept20-Mar21 may be a good example of the sensitivity in density profiles. All conductivity corrections were based on IMR's conductivity calibration except for Mar21, which was based on the conductivity calibration done by the GFI students. In order to have time to include results from a third stagnant period in the results, I used the conductivity corrections from GFI since they were available first. I later got the results from the IMR, but I did not have time to redo all calculations with the new correction. Ideally, I would have used the conductivity corrections from IMR to be consistent.

The conductivity calibration from GFI suggested dC = 0.013 $\mathrm{S\,m^{-1}}$, while the results from IMR suggested dC = 0.006 $\mathrm{S\,m^{-1}}$. The difference in dC could be explained by the difference in calibration method. The conductivity calibration by IMR only uses

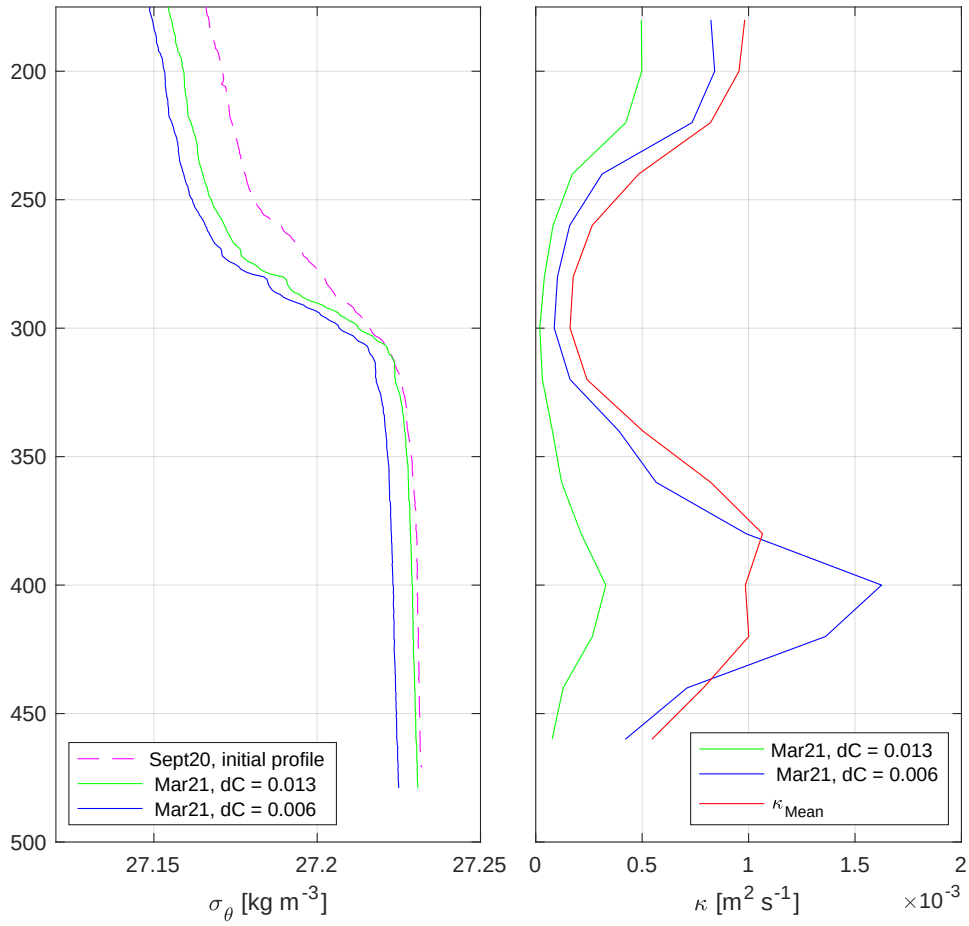

Figure 5.3: Illustration of the effect of the different conductivity corrections (dC = 0.013 S m^{-1} from GFI and dC = 0.006 S m^{-1} from IMR) on density profiles and resulting κ profiles.

water samples from the bottom of a CTD cast, while the GFI calibration includes water samples from several depth. When comparing the density profiles corrected with dC = 0.013 S m^{-1} and dC = 0.006 S m^{-1}, the difference in density were 0.006 kg m^{-3} (at 450 m). Thus, when using dC = 0.006 S m^{-1}, the resulting κ-profile would be larger, since density profile in Mar21 were lighter than when using dC = 0.013 S m^{-1} (Figure 5.3). The order of magnitude of κ with IMR correction is more similar to results from other stagnant periods (Figure 4.9).

Since I determined κ_{Mean} from each individual profiles (Panel A, Figure 4.9) and only 2 out of 12 profiles are from Sept20-Mar21, I assume that κ_{Mean} is still a fairly good representation of the vertical diffusivity in the basin. But if I were to do calculations again, I would use the correction suggestion from the IMR calibration for Mar21 for more accurate Sept20-Mar21 κ-results.

It is clear from κ_{Mean}-profile that the lowest values for diffusivity is found between ca 250-350 m (Figure 4.9). This means that in this area we find the lowest mixing intensity

in the Deep Basin. This can be explained by the observation of the gradient between 280 m and 340 m, which separates the Upper and Lower layer (Figure 4.3). In this area, the stratification works against the vertical mixing and reduces the intensity of the mixing. The largest κ_{Mean} values are found between 180-240 m and 340-450 m. Here, the water masses are well mixed and the vertical gradients are small. The lack of gradients in density in these areas makes mixing easier, and the intensity of mixing is greater.

5.2.2 In the model

The $\kappa_{ModelMean}$-profile from NorFjords160 results does not show any similarity with the results from the observations other than the order of magnitude (Figure 4.12). The $\kappa_{ModelMean}$-profile lacks a minimum in the middle of the model basin, which is explained by the fact that there is one homogeneous layer found below sill depth in the model data (Figure 4.11), as opposed to the Upper and Lower layer identified from observations (Figure 4.3). Instead, a local maximum is located at 190 m for the Oct-Dec15 period. This is not seen in the calculations for Feb-Apr15 or May-Aug15. The explanation for the maximum at 190 m can be found when looking into the parameters of Equation 2. As $\frac{\delta\rho}{\delta z}$ is in the denominator in Equation 2, large (small) values for $\frac{\delta\rho}{\delta z}$ will give small (large) values for κ. Physically, this means that when vertical density gradients are present, the mixing intensity becomes smaller. Between 170 - 190 m for Oct15, $\frac{\delta\rho}{\delta z}$ is small while $\frac{\delta\rho}{\delta t}$ is relatively large. This gives rise to the maximum found at 190 m.

The results from observations and the model are not directly comparable because the fjord basin in the model grid is made shallower in order to smooth the steep walls of the fjord basin (Figure 3.2). The fjord basins were defined as described in Table 3.6, and the basin volume in the model grid and from the observations were of the same order of magnitude. Therefore, I compared the volume mean of κ. The volume mean of κ_{Mean} were 6.5×10^{-4} $\mathrm{m^2\,s^{-1}}$, and for $\kappa_{ModelMean}$ it was 1.9×10^{-4} $\mathrm{m^2\,s^{-1}}$. They are of the same order of magnitude, and are comparable to the typical magnitude for vertical diffusivity in Norwegian fjords (Gade and Edwards, 1980).

The vertical diffusivity in the model is 4.6×10^{-3} $\mathrm{m^2\,s^{-1}}$ lower compared to the observations. Thus, the mixing coefficients in the model produce realistic results for the fjord basin. But, lower diffusivity means that the density in the basin reduces slower and the renewal frequency is lower in the model compared to the observations. If the vertical diffusivity in the model had been larger than the observed, it could be part of the explanation why the renewal frequency observed in the model results are higher than observed. The renewal frequency depends on the density reduction rate within the fjord and the off-shore density variability at sill level (Gade and Edwards, 1980). If the vertical diffusivity reduces the basin density quicker in the model compared to the observations,

the difference between coast and fjord basin becomes smaller faster in the model, and a renewal event is more likely to occur in the model. A smaller the vertical diffusivity and higher renewal frequency in the model compared to the observations, indicate that the error in the modeled renewal frequency is due to errors in the coastal forcing. The off-shore density variability at the coast is reduced in the model compared to reality.

5.3 Estimates of oxygen concentrations and consumption rates

5.3.1 Oxygen consumption in the Deep Basin

κ_{Mean} from observations was used in Equation 5 and Equation 6 to calculate the oxygen consumption rate for each of the stagnant period in the Lower layer in the Deep Basin. I used two methods for finding oxygen consumption rates which resulted in the rates Mean $b_{t,z}$ and CONS (Table 4.2).

I found the vertical oxygen consumption rate profile, $b_{t,z}$, from ΔO_2, as the effects of biological activity is neglected in the estimated profile. The results of $b_{t,z}$ show that the oxygen consumption rate is largest close to the bottom (Figure 4.16). The larger consumption rates close to the bottom help sustain the gradients in the O_2-profile, which again drive diffusive transport of O_2 from above. Negative $b_{t,z}$ are observed in the Upper layer between ca 180 m - 280 m. This is where $\Delta O_2 < 0$, meaning that the estimated O_2 concentrations are lower than observed (Panel A, (Figure 4.13, 4.14 and 4.15). The negative oxygen consumption rates indicate that the oxygen concentration increases here. These results are not realistic, as O_2 concentrations in a stagnant basin can only increase close in the euphotic layer where photosynthesis occur. After closer examination of the O_2-profiles (Panel B, Figure 4.13, 4.14 and 4.15), we see the oxygen increases with depth between 180m - 240 m, and decreases with depth below ca 240 m. This is important to note, as diffusion is a gradient-driven process, so the vertical gradients determines the direction oxygen is transported by diffusion. The diffusive flux of oxygen is directed upwards where oxygen increases with depth, and downwards when oxygen decreases with depth. A better upper limit for the calculations would have been at a deeper level, e.g. 260 m, where the vertical O_2 gradients, and hence the diffusive fluxes, are negligible.

The volume mean oxygen consumption rate, Mean $b_{t,z}$, was calculated from $b_{t,z}$-values in the Lower layer (300 m - 460 m). This was done in order to compare the results with the oxygen consumption rates found with the method presented in Aure and Stigebrandt (1989). The oxygen consumption rates found with this method, CONS, was found from volume mean quantities as given in Equation 6. The results of Mean $b_{t,z}$ and CONS from each stagnant period agree with each other within each time period. Mean $b_{t,z}$ and CONS for the Feb19-Mar19 were about two times larger than Oct19-Mar20 and Sept20-Mar21 (Table 4.2).

In Aksnes et al. (2019), the oxygen consumption rate was estimated to be 0.52 mL L^{-1} yr^{-1}, ranging between 0.42-0.75 mL L^{-1} yr^{-1}. These findings were based on oxygen observations from 1975-2015. By converting Mean $b_{t,z}$ and CONS to an annual oxygen consumption rate, my findings suggests rates between 0.6-0.78 mL L^{-1} yr^{-1} for Oct19-Mar20 and Sept20-Mar21. For the Feb19-Mar19 results, the consumption rates are between 1.56 - 1.68 mL L^{-1} yr^{-1}. The results for the oxygen consumption rates in Oct19-Mar20 and Sept20-Mar21 are comparable, but a little higher, to the results in Aksnes et al. (2019). I used data from 300 - 460 m to find Mean $b_{t,z}$ and CONS, but the rate of 0.52 mL L^{-1} yr^{-1} is based on oxygen data from 200-400 m. As seen for the vertical profile of $b_{t,z}$, the oxygen consumption rate is larger closer to the bottom in the Lower layer (Figure 4.16). This increases the estimates of Mean $b_{t,z}$ and CONS. The results for Feb19-Mar19 are to be too high compared to the results found in Aksnes et al. (2019).

Results from other sill fjords in western Norway show that CONS varied between 0.14 - 1.46 mL L^{-1} $month^{-1}$, DEPL between 0.11 - 1.41 mL L^{-1} $month^{-1}$ and DIFF between 0.01 and 0.24 mL L^{-1} $month^{-1}$ (Aure and Stigebrandt, 1989). While DIFF in Masfjorden is comparable to other fjords, the CONS is lower (0.13-0.050 mL L^{-1} $month^{-1}$) because DEPL in Masfjorden is one order of magnitude less than in other sill fjords. In my results, DIFF is the largest contributor to CONS, but in the other fjords, DIFF typically contributed with 20 % to to CONS, and DEPL 80 % (Aure and Stigebrandt, 1989). Masfjorden is a deeper fjord, with both a larger sill depth and a larger mean depth compared to the other fjords in Aure and Stigebrandt (1989). In addition to being a deeper fjord, I did the calculations for the Lower layer (below 300 m). Since the Lower layer is further away from the surface and sill depth, it might explain why the results for Masfjorden differ from other fjords.

Potential errors in the oxygen calculations may follow from the estimated vertical diffusivity. If the estimated κ is too high or too low, the oxygen supply through diffusive processes will be over- or underestimated. This error would also affect the oxygen consumption rates, resulting in too high or too low rates. The boundary condition used to calculate the oxygen profiles with Equation 5 is another factor that affects the calculations of oxygen profiles. The only information we have about the behavior of the oxygen concentration at the sill level is the initial and end value of each stagnant period. By definition, a renewal does not take place during a stagnant period, so I set the upper boundary condition to linearly decrease from the initial profile to the end profile in the stagnant period. This is a plausible boundary condition, and it was the best fit with the available information. The upper limit boundary was located at 180 m because I used the Inner Sill depth to define the basin layer. The findings of the negative oxygen consumption rates between 180 m - 240 m suggests that a better choice of upper limit would have been at 260 m rather than at 180 m.

5.3.2 Effects of partial renewal on oxygen concentration

The investigation of how a partial renewal affects the oxygen concentrations in Lower layer in the Deep Basin was possible due to idealistic initial profiles. These initial profiles represented different situations, including both non-renewal and renewal scenarios (Table 3.7 and Panel A, Figure 4.17). According to the calculations, the small renewal observed at 200 - 220 m (Case A) did not affect the Lower layer (Figure 4.17). The time evolution at 260 m show that the small renewal caused a slight increase in the beginning of the calculations, but no signal is seen at 340 or 460 m (Figure 4.18). This would imply that the partial renewals observed in 2019 and 2020 most likely did not significantly affect the oxygen concentration in the Lower layer in the Deep Basin. In order for a partial renewal to increase the oxygen concentration in the Lower layer, higher oxygen concentrations in the renewed layer are needed. Increasing the depth of the renewal layer will also give an additional oxygen increase (Figure 4.17 and 4.18).

We can link these findings to the stratification and vertical diffusivity profile. The pycnocline between the Upper and Lower layer reduces the mixing intensity at around 300 m, which explain why the signal from the small partial renewal does not reach the Lower layer. The two other renewal cases have both higher oxygen concentrations and renewal layers that reaches down to 300 and 340 m, so the renewal layer intrudes the pycnocline and is less affected by the stratification.

The oxygen concentrations estimated with the artificial profiles were also found by neglecting biology, so the oxygen concentrations are too high compared to the true value, which should be around 2.5 $\mathrm{mL\,L^{-1}}$. The oxygen consumption rate for Sept20-Mar21 was Mean $b_{t,z} = 0.061\ \mathrm{mL\,L^{-1}\,month^{-1}}$ (Table 4.2). This would mean that below 300 m, 0.33 $\mathrm{mL\,L^{-1}}$ would have been consumed during Setp20-Mar21 period, and 0.55 $\mathrm{mL\,L^{-1}}$ consumed after 270 days. If this was subtracted from estimated oxygen concentration below 300 m, the estimated profiles would give a more realistic oxygen concentration since the effects of biology would be included.

5.4 On the oxygen observations in Masfjorden

Deoxygenation in sill fjords is a part of a global problem for oceanic waters. Declining oxygen concentrations have been observed in both coastal waters and open ocean since the 1950s (Breitburg et al., 2018), and is predicted to decrease by 2-3 % over the next century (Chu et al., 2018). The oxygen concentrations in coastal area and fjords are important for the health of fjord, the ecosystem and biodiversity. If fjords are to be used sustainably, it is vital observe the environment and hydrography in the fjord in order to evaluate whether the fjord are suitable for aquaculture activity etc.

The low-oxygen concentrations of 2.5 $\mathrm{mL\,L^{-1}}$ observed during February 2019 - March 2021 suggest oxygen-stressed conditions in the Lower layer in Masfjorden (Table 2.1). Based on the oxygen concentrations, the environmental classification is on the limit between Moderate and Poor for the ecosystem here (Table 2.2). The layer becomes hypoxic if the oxygen concentration reduces additionally with ≥ 1 $\mathrm{mL\,L^{-1}}$. In hypoxic conditions we expect animals and organisms to be affected by the low-oxygen concentrations, (Breitburg et al., 2018; Chu et al., 2018), and the classification of the ecosystems would be Very Poor (Table 2.2). The oxygen increase observed over the observation period at 450 m might be an indication that the ecosystem already is affected and altered, as oxygen concentrations below 2 $\mathrm{mL\,L^{-1}}$ can alter the oxygen consumption rate (Aure and Stigebrandt, 1989).

Aksnes et al. (2019) estimated that if a stagnation period lasts for 7-12 years, Masfjorden will become anoxic due to the biological oxygen consumption. The findings in Darelius (2020) showed that the likelihood for Masfjorden to become anoxic increased as a consequence of reduced coastal density, which increased probability for stagnant periods in Masfjorden to last longer than 10 years. With this in mind, alongside the long-term declining oxygen (from Aksnes et al., 2019), the low-oxygen concentrations in Masfjorden, and similar sill fjords, are of concern and might continue to be so in the future.

6 Summary and conclusions

The observations of oxygen concentrations in the Deep Basin in Masfjorden during February 2019 to March 2021 show that Upper and Lower layer in the basin have different oxygen concentrations. The the oxygen concentrations vary differently in the Upper and Lower layer. Close to the bottom, at 450 m, the oxygen concentration increased with 0.16 $\mathrm{mL\,L^{-1}}$ over the observation period. No (full) renewal occurred during the observation period, as the density at 450 m decreased with 0.0085 $\mathrm{kg\,m^{-3}\,yr^{-1}}$, similar to the density reduction rate of D = 0.01 $\mathrm{kg\,m^{-3}\,yr^{-1}}$ mentioned in Darelius (2020). The oxygen increase at 450 m is believed to be caused by changes in the ecosystems close to the bottom or the supply of organic matter, but this has to be verified through further research.

The mean oxygen concentration in the Deep Basin (obtained from 200, 300 and 400 m) decreased during stagnant periods, as expected from theory. The mean oxygen concentration from 2019-2021 decreased faster than the declining oxygen trend (from Aksnes et al., 2019), and similarly, but slightly slower slower than the biological consumption rate of 0.52 $\mathrm{mL\,L^{-1}\,yr^{-1}}$ during the stagnant periods. The long-term trend was based on data from years with and without DWR events. Two shallow partial renewals were observed during 2019-2021, but no DWR events occurred.

The partial renewals were shallow, and observed a layer between 180 m - 220 m depth. They were identified by an oxygen increase, and occurred during the summer months of 2019 and 2020. The timing of the partial renewals can be linked to the coastal density variations, as annual density maximum at the IMR station in Sognesjøen coincides with partial renewals observed during 2019 and 2020. Calculations of how partial renewals affect the oxygen concentration close to the bottom suggest the observed partial renewals in 2019 and 2020 did not affect the oxygen concentration in the Lower layer. For a partial renewal to significantly affect the oxygen concentration in the Lower layer, the renewal needs to extend deeper into the basin, and have higher oxygen concentrations. This is probably due to the stratification in the basin, which works against the vertical diffusive processes in the basin.

The vertical diffusivity was calculated in the Deep Basin with the method from Stigebrandt and Aure (1989) from observations, κ_{Mean}, and for NorFjords160, $\kappa_{ModelMean}$. The results are of realistic order of magnitude compared to the typical values in Norwegian fjords. The κ_{Mean}-profile shows that presence of the Upper and Lower layer in the Deep Basin influence the diffusive processes, as lower mixing intensity is found where the pycnocline between the layers are located. The model results from NorFjords160 show a higher renewal frequency than observations do, as two renewal episodes occurred within the model run of 1 year. The the volume mean in the model, $\kappa_{ModelMean} = 1.9 \times 10^{-4}$ $\mathrm{m^2\,s^{-1}}$, is lower than observed $\kappa_{Mean} = 6.5 \times 10^{-4}$ $\mathrm{m^2\,s^{-1}}$. The high renewal frequency in

the model is therefore likely due to coastal boundary settings.

The oxygen consumption rate in the basin was calculated with two different methods, using the vertical diffusivity from observations. The results from the methods agree with each other for the each stagnant periods, and the results from Oct19-Mar20 and Sept20-Mar21 they are similar to the oxygen consumption rate found in Aksnes et al. (2019). When comparing the results from oxygen consumption rate with other sill fjords in western Norway, the oxygen consumption rate in Masfjorden is lower (Aure and Stigebrandt, 1989), which might be because Masfjorden is a deep sill fjord, and the oxygen consumption rate was calculated for an isolated layer far from the sill depth.

6.1 Recommendations for future work

As mentioned throughout the discussion, there are a few things I would have done differently if I were to start the work with this thesis over. Regarding calibration and corrections of data, I would recommend being thoroughly with the calibration work, as the results for the vertical diffusivity is sensitive for the density observations. For the oxygen calibration, the location where the water samples are from is wise to think through. I think several water samples from the basin layer, or at least away from gradients, are a good choice as the standard deviation offset might become smaller. I would also recommend obtaining deeper CTD profiles from the basin, so that κ can be estimated for depths below 460 m. Then oxygen concentrations and oxygen consumption rate could be estimated closer to the bottom.

For future work, I believe a continuation of regular observations will be very useful for further research and assessments of the physical and environmental conditions in Masfjorden. One could investigate if the observed oxygen increase at 450 m continues, and if this is caused by changes in the oxygen consumption due to environmental changes or aquaculture activity. When a full renewal occurs, it would be interesting to look into the effects of the renewal on the oxygen consumption rates and the diffusive processes in the Deep basin. Data from the sill and fjord mouth region, such as data from Sill mooring and IMR mooring, could be analyzed to get information about the water masses that entered Masfjorden in June-August 2019.

References

Aarre, E. (16.05.2017), 'To oppdrettsanlegg må forlate masfjorden', *Bergens Tidene* .
URL: *https://www.bt.no/nyheter/lokalt/i/rx40m/to-oppdrettsanlegg-maa-forlate-masfjorden*

Aksnes, D. L., Aure, J., Johansen, P. O., Johnsen, G. H. and Vea Salvanes, A. G. (2019), 'Multi-decadal warming of Atlantic water and associated decline of dissolved oxygen in a deep fjord', *Estuarine, Coastal and Shelf Science* **228**(September), 106392.
URL: *https://doi.org/10.1016/j.ecss.2019.106392*

Albretsen, J., Sperrevik, A. K., Staalstrøm, A., Sandvik, A. D., Vikebø, F. and Asplin, L. (2011), 'NorKyst-800 Report No. 1: User Manual and technical descriptions', *Fisken og Havet* (2), 1–48.

Andersson, A. (06.07.2020), 'Denne fjorden lider av oksygenmangel', *Bergens Tidene* .
URL: *https://www.bt.no/nyheter/lokalt/i/8meAjE/denne-fjorden-lider-av-oksygenmangel*

Andersson, A. (24.01.2021), 'Fisk forsvinner. bunnen er råtten og livløs. det foregår noe skummelt i flere av fjordene våre.', *Bergens Tidene* .
URL: *https://www.bt.no/nyheter/lokalt/i/AlllOz/fisk-forsvinner-bunnen-er-raatten-og-livloes-det-foregaar-noe-skummelt*

Andersson, A., Aarre, E. and Lambrechts, L. (13.02.2017), 'Oppdrettsanlegg kan bli tvunget ut av masfjorden', *Bergens Tidene* .
URL: *https://www.bt.no/nyheter/lokalt/i/vBMMm/oppdrettsanlegg-kan-bli-tvunget-ut-av-masfjorden*

Asplin, L., Johnsen, I. A., Sandvik, A. D., Albretsen, J., Sundfjord, V., Aure, J. and Boxaspen, K. K. (2014), 'Dispersion of salmon lice in the Hardangerfjord', *Marine Biology Research* **10**(3), 216–225.
URL: *https://doi.org/10.1080/17451000.2013.810755*

Asplin, L., Salvanes, A. G. V. and Kristoffersen, J. B. (1999), 'Nonlocal wind-driven fjord-coast advection and its potential effect on plankton and fish recruitment', *Fisheries Oceanography* **8**(4), 255–263.

Aure, J. and Stigebrandt, A. (1989), 'On the influence of topographic factors upon the oxygen consumption rate in sill basins of fjords', *Estuarine, Coastal and Shelf Science* **28**(1), 59–69.

BKK (2021), 'Våre kraftverk - Matre', `https://energi.bkk.no/artikkel/6dfa5dca-5e1a-4696-9906-393f3e839c32`. [Online; accessed 23. February 2021].

Boone, W., Rysgaard, S., Carlson, D. F., Meire, L., Kirillov, S., Mortensen, J., Dmitrenko, I., Vergeynst, L. and Sejr, M. K. (2018), 'Coastal Freshening Prevents Fjord Bottom Water Renewal in Northeast Greenland: A Mooring Study From 2003 to 2015', *Geophysical Research Letters* **45**(6), 2726–2733.
URL: *https://agupubs.onlinelibrary.wiley.com/doi/abs/10.1002/2017GL076591*

Breitburg, D., Levin, L. A., Oschlies, A., Grégoire, M., Chavez, F. P., Conley, D. J., Garçon, V., Gilbert, D., Gutiérrez, D., Isensee, K., Jacinto, G. S., Limburg, K. E., Montes, I., Naqvi, S. W. A., Pitcher, G. C., Rabalais, N. N., Roman, M. R., Rose, K. A., Seibel, B. A., Telszewski, M., Yasuhara, M. and Zhang, J. (2018), 'Declining oxygen in the global ocean and coastal waters', **7240**(January).

Broecker, W. S. and Peng, T. H. (1983), *Tracers in the Sea*, Lamont-Doherty Geological Observatory of Columbia University, Palisades, NY.

Bye-Ingebrigtsen, E., Isaksen, T. and Dahlgren, T. (2019), Bye-Ingebrigtsen, E., Isaksen, T.E., Dahlgren, T.G., Technical report, NORCE Norwegian Research Centre AS. NORCE Miljø 2019/026.

Chu, J. W., Curkan, C. and Tunnicliffe, V. (2018), 'Drivers of temporal beta diversity of a benthic community in a seasonally hypoxic fjord', *Royal Society Open Science* **5**(4).

Conley, D. J., Carstensen, J., Aigars, J., Axe, P., Bonsdorff, E., Eremina, T., Haahti, B. M., Humborg, C., Jonsson, P., Kotta, J., Lännegren, C., Larsson, U., Maximov, A., Medina, M. R., Lysiak-Pastuszak, E., Remeikaitè-Nikienè, N., Walve, J., Wilhelms, S. and Zillén, L. (2011), 'Hypoxia is increasing in the coastal zone of the baltic sea', *Environmental Science and Technology* **45**(16), 6777–6783.

Cushman-Roisin, B., Asplin, L. and Svendsen, H. (1994), 'Upwelling in broad fjords', *Continental Shelf Research* **14**(15).

Cushman-Roisin, B. and Beckers, J.-M. (2011), *Introduction to Geophysical Fluid Dynamics - Physical and Numerical Aspects*, second edn, Academic Press.

Dale, T., Bahr, G., Harendza, A., Velvin, R., Palerud, R. and Szczuciński, W. (2019), Miljøovervåkning i Sørfjorden ved Osterøy, Technical report, NIVA.

Darelius, E. (2020), 'On the effect of climate trends in coastal density on deep water renewal frequency in sill fjords—A statistical approach', *Estuarine, Coastal and Shelf Science* **243**(January), 106904.
URL: *https://doi.org/10.1016/j.ecss.2020.106904*

Direktoratsgruppen vanndirektivet (2018), 'Veileder 02:2018. Klassifisering av miljøtilstand i vann'.

Farmer, D. M. and Freeland, H. J. (1983), 'The physical oceanography of Fjords', *Progress in Oceanography* **12**(2), 147–220.

Gade, H. (1973), 'Deep Water Exchanges in a Sill Fjord: A Stochastic Process', *Journal of Physical Oceanography* **3**(2), 213–219.
URL: *https://doi.org/10.1175/1520-0485(1973)003<0213:DWEIAS>2.0.CO;2*

Gade, H. and Edwards, A. (1980), Deep Water Renewal in Fjords, *in* H. J. Freeland, D. M. Farmer and C. D. Levings, eds, 'Fjord Oceanography', Plenum Publishing Coro., New York, pp. 453–489.

Galarnyk, M. (12.09.2018), 'Understandig Box Plots', `https://towardsdatascience.com/understanding-boxplots-5e2df7bcbd51`. [Online; accessed 6. February 2021].

Honrath, R. (1995), 'CE251 - Environmental Engineering Fundamentals Part I: Mass Transport Processes', `https://pages.mtu.edu/~reh/courses/ce251/251_notes_dir/node4.html`. [Online; accessed 26. April 2021].

ICES (n.y), 'Unit Conversion', `https://ocean.ices.dk/tools/unitconversion.aspx`. [Online; accessed 19. January 2021].

IMR (2020), 'Matre Research Station', `https://www.hi.no/en/hi/laboratories/matre-research-station`. [Online; accessed 19. November 2020].

Inall, M. E. and Gillibrand, P. A. (2010), 'The physics of mid-latitude fjords: a review', *Geological Society, London, Special Publications* **344**(1), 17–33.
URL: *http://sp.lyellcollection.org/lookup/doi/10.1144/SP344.3*

Liang, Z., Siegert, M., Fang, W., Sun, Y., Jiang, F., Lu, H., Chen, G. H. and Wang, S. (2018), 'Blackening and odorization of urban rivers: A bio-geochemical process', *FEMS Microbiology Ecology* **94**(3), 1–12.

Müller, M., Homleid, M., Ivarsson, K.-I., Køltzow, M. A. Ø., Lindskog, M., Midtbø, K. H., Andrae, U., Aspelien, T., Berggren, L., Bjørge, D., Dahlgren, P., Kristiansen, J., Randriamampianina, R., Ridal, M. and Vignes, O. (2017), 'AROME-MetCoOp: A Nordic Convective-Scale Operational Weather Prediction Model', *Weather and Forecasting* **32**(2), 609–627.
URL: *https://journals.ametsoc.org/view/journals/wefo/32/2/waf-d-16-0099_1.xml*

Nerheim, M. S. and Lusher, A. L. (2020), 'Investigating microsized anthropogenic particles in Norwegian fjords using opportunistic nondisruptive sampling', *Anthropocene Coasts* **3**(1), 76–85.

Nordberg, K., Gustafsson, M. and Krantz, A. L. (2000), 'Decreasing oxygen concentrations in the Gullmar Fjord, Sweden, as confirmed by benthic foraminifera, and the possible association with NAO', *Journal of Marine Systems* **23**(4), 303–316.

Polovodova Asteman, I. and Nordberg, K. (2013), 'Foraminiferal fauna from a deep basin in Gullmar Fjord: The influence of seasonal hypoxia and North Atlantic Oscillation', *Journal of Sea Research* **79**, 40–49.
URL: *http://dx.doi.org/10.1016/j.seares.2013.02.001*

Sagen, T. S. and Aguiar, V. (2020), Deep water renewal in Masfjorden forced by nonlocal winds, Technical report, Geophysical Institute, University of Bergen.

Sandvik, A. D., Asplin, L. and Skardhamar, J. (2019), Modellering av smittsomme lakseluslarver — bakgrunnsdata for Havforskningsinstituttets modellprodukt til Trafikklyssystemet, 2019, Technical report.
URL: *https://www.hi.no/hi/temasider/arter/lakselus/overvaking-av-lakselus*

Sarmiento, J. and Gruber, N. (2006), *Ocean Biogeochemical Dynamics*, Prinston Univeristy Press.

Spall, M. A., Jackson, R. H. and Straneo, F. (2017), 'Journal of Geophysical Research : Oceans Katabatic Wind-Driven Exchange in Fjords', *Journal of Geophysical Research : Oceans* **122**, 8246–8262.

Stigebrandt, A. (2012), Hydrodynamics and Circulation of Fjords, *in* L. Bengtsson, R. W. Herschy and R. W. Fairbridge, eds, 'Encyclopedia of Lakes and Reservoirs', Springer Netherlands, Dordrecht, pp. 327–344.
URL: *https://doi.org/10.1007/978-1-4020-4410-6_247*

Stigebrandt, A. and Aure, J. (1989), 'Vertical Mixing in Basin Waters of Fjords', *Journal of Physical Oceanography* **19**(7), 917–926.

Talley, L., Pickard, G., Emery, W. and Swift, J. (2011), *Descriptive Physical Oceanography - An introduction*, sixth edn, Elsevier.

Thomson, R. E. and Emery, W. J. (2014), *Data analysis methods in Physical Oceanography*, third edn, Elsevier.

Thorpe, S. (2007), *An Introduction to Ocean Turbulence*, Cambridge University Press.

United Nations (n.d.), 'Sustainable Development Goals - Life below water', `https://www.un.org/sustainabledevelopment/oceans/`. [Online; accessed 19. April 2021].

7 Appendix A: Calibration work

7.1 Oxygen calibration of CTD for Feb19 and Jun20

The water samples serves as the true value of the quantity we want to calibrate, in this case dissolved oxygen concentration. To correct the CTD data, I calibrated the CTD sensor measurements with respect to the water samples. I calculated the offset, dO,

$$dO = O_{2(Bottle)} - O_{2(CTD)} \tag{8}$$

which represents the error between the water samples, $O_{2(Bottle)}$, and the CTD sensor, $O_{2(CTD)}$. Oxygen measurements tends to be pressure dependent, and can also be time dependent i.e. due to sensor drift. In such cases, a linear correction is needed to correct for time or pressure dependency of the oxygen measurements. For Feb19 and Jun20, the oxygen data were corrected with the mean offset found from the data set, and I corrected the data by $O_{2(CTD)} + dO = O_{2(Bottle)}$.

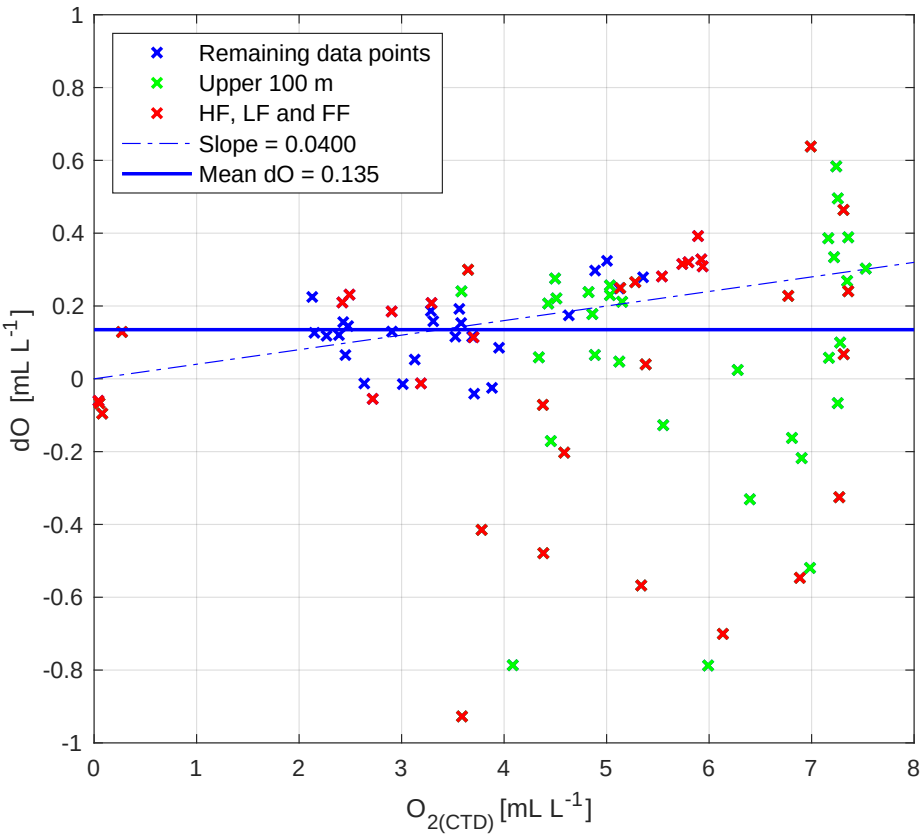

Figure 7.1: The offset, dO, plotted against $O_{2(CTD)}$. All available oxygen data from the Jun20 (MF, FF, HF, LF) is included in the plot . As described in Chapter 7.1, data points from upper 100 m (green) and from LF, FF and HF (red) have been removed. Mean dO was calculated from the remaining data points (blue).

For Jun20, the oxygen data included water samples and CTD measurements from Masfjorden (MF), Fensfjorden (FF), Haugsværfjorden (HF) and Lysefjorden (LF). At first, *dO* was calculated by Equation 8 and plotted against $O_{2(CTD)}$. The data show a large spread in offset ranging from -0.9273 mL L^{-1} to 0.6381 mL L^{-1} (Figure 7.1). I investigated potential time and pressure dependency of dO, and possible errors due to leaking Niskin flasks (Figure 7.2). A leaking Niskin flask should be removed from the analysis, since the water sampled would be contaminated with water from other depths. There were no signs in the data that there were any time or pressure dependency (Panel A and B, Figure 7.2).

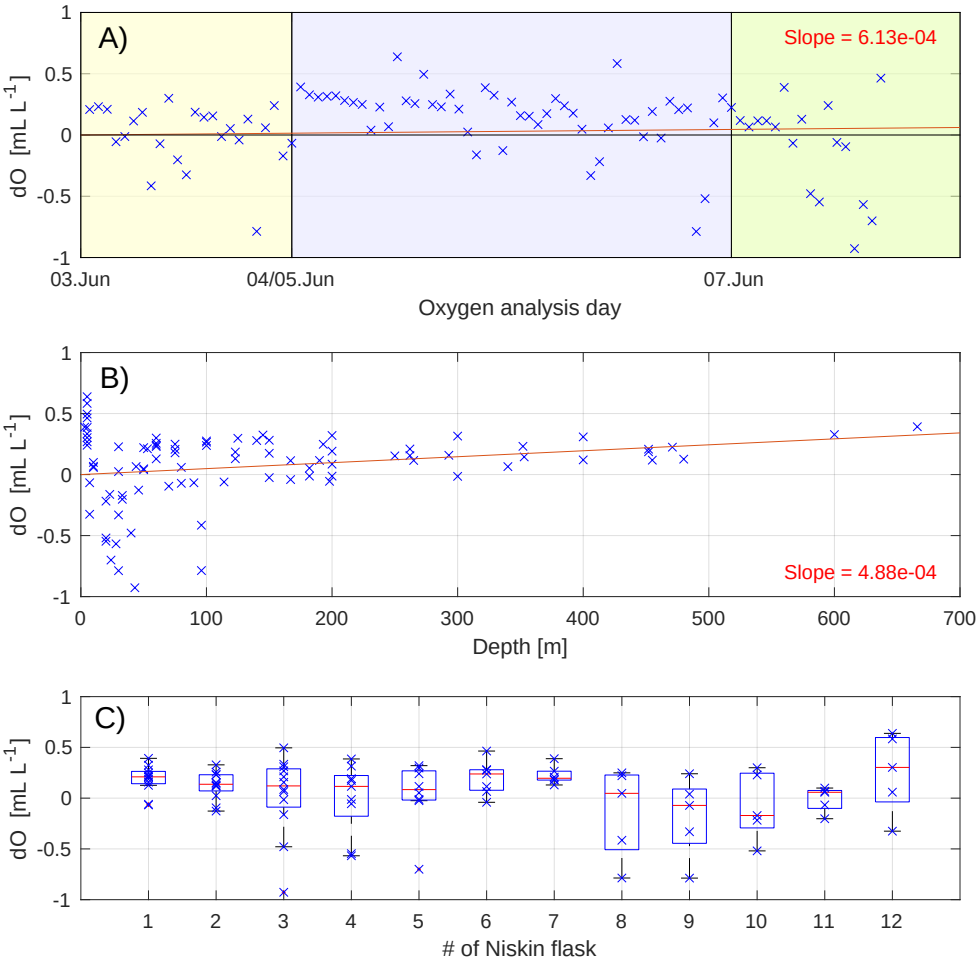

Figure 7.2: Offset plotted against time (Panel A), depth (Panel B) and Niskin flask (Panel C) for Jun20. All available data from the cruise is included (Lysefjorden, Fensfjorden, Masfjorden and Haugsværfjorden). The color background in Panl A represents the different days oxygen samples were analyzed: 3. June (yellow), 4.-5. June (blue), 7. June (green). Panel C shows boxplots of dO for each Niskin flask.

However, the largest spread in data points and most of the negative offsets occur in the

upper 100 m (Panel C, Figure 7.2). Below 100 m, the spread is more confined with a range from -0.0605 to 0.3921 mL L^{-1}. The two data points below 500 m are from Fensfjorden, as this is the only fjord deeper than 500 m. The Niskin flasks with the largest spread is seen for flasks number 3, 4, 5, 8, 9, 10 and 12 . This agrees with the observation that the largest spread is found above 100 m, since Niskin flasks with high numbers collects water closer to the surface.

The basin layer is area of study for this thesis, and the surface waters are not of interest. By removing the data points located in the upper 100 m, the large spread in data points and most of the negative data points are reduced. Consequently, Niskin flask 8, 9, 10 and 12 are completely removed. Thus, the wide spread observed for the Niskin flasks is not likely due to leakage, but because the samples are from the upper 100 m. Close to the surface we find shear in the vertical oxygen profiles. As the CTD sensor and Niskin flasks are samples at slightly different depths, the gradients in the upper 100 m can cause the offset to be larger then at greater depths where shear is absent.

I also removed the data points from Haugsværfjorden, Lysefjorden and Fensfjorden from the analysis, still justified by the fact that Masfjorden is the area of study. Haugsværfjorden is a special case since hypoxic and anoxic conditions are observed below 50 - 60 m. Oxygen samples from such conditions are difficult to measure accurately by Winkler titration.

Altogether 66 data points were removed, and the remaining 25 data points from below 100 m in Masfjorden were used to find the mean dO (Figure 7.1). The data suggested mean dO $= 0.135 \pm 0.098$ mL L^{-1} (also listed in Table 3.3). Accordingly to the discussion of Equation 8, this dO was used to correct the CTD measurements.

I followed the same procedure for the calibration of oxygen data from Feb19. Neither time nor pressure dependency were detected, and there were no indications of leaking Niskin flasks (Figure 7.4). Similarly to the Jun20 calibration, the largest spread in data points were found close to the surface. For Feb19, the largest spread were found in the upper 50 m (Panel B, Figure 7.4), so the data from this layer were removed. To be consistent with the argumentation from Jun20, the data from Fensfjorden were also removed. In total 51 data points were removed, and 44 remained for the further calibration. The remaining data suggested a mean offset of dO $= 0.243 \pm 0.088$ mL L^{-1} (Figure 7.3), which was used to correct the oxygen data for Feb19 (Table 3.3).

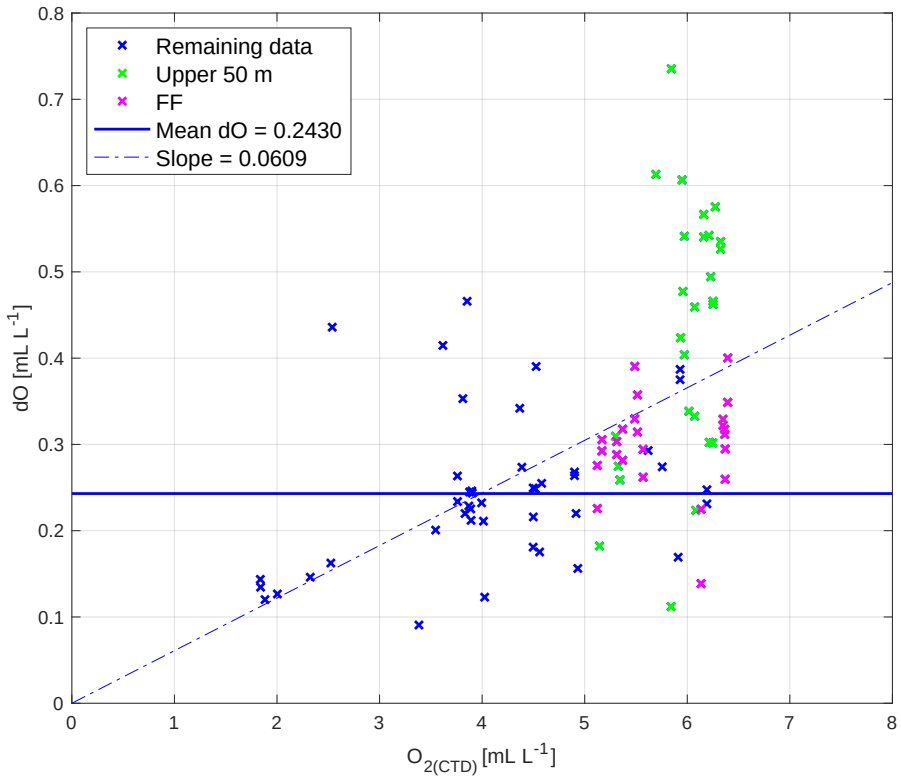

Figure 7.3: Offset plotted against CTD oxygen measurements. Colors indicate remaining data, and the data which has been removed (upper 50 m and Fensfjorden). The regression line and the mean offset of the remaining data are also shown in the plot.

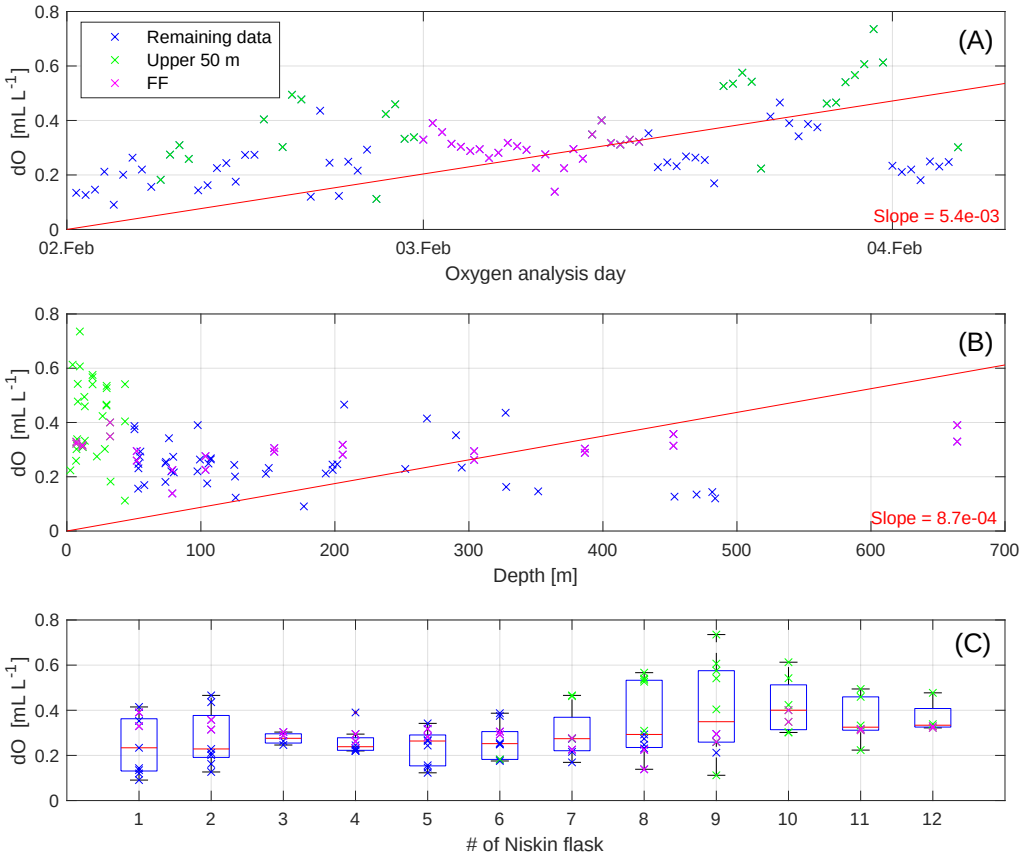

Figure 7.4: Offset from Feb19 plotted against time (Panel A) and depth (Panel B). Panel C shows box plots of dO for each Niskin flask. All available data from the cruise is included (MF and FF). Regression line from all data are included in Panel A and Panel B. Panel A shows the time development of the offset, with the x-grid showing the separate analysis days, with the regression line. The colors indicate the remaining data and the removed data.

7.2 Calibration and data from the Inner Mooring

Similarly to CTD calibration, we wanted to find the offset between the mooring instruments and the CTD cast for the parameter in question. For the correction of the mooring instruments I looked at the time evolution of the offset to see how the instrument drifts over time. From the time evolution, I decided if a linear or constant correction should be applied to the time series. The closest CTD station to the Inner Mooring is station M24, and the relevant cruises for the mooring calibration are Feb19, Mar19, Oct19, and Mar20.

The mooring data gives time series from certain depths, while CTD measures the full water column, but at a specific point in time. Due this difference, vertical and temporal means were introduced in order to compare them. The temporal mean of the mooring time series was found from an interval of ± 1 day around the time of which the CTD profile was obtained. The vertical mean from the CTD data was found for an interval of ± 10 m around the mooring instrument depths. This was done for conductivity, oxygen and temperature. The temperature sensor on SBE37 was assumed to be good and stable, but was calibrated for consistency. From the temporal and vertical means, the offset between the mooring instruments and the CTD was calculated by $dX = X_{Mooring} - X_{CTD}$, where X is the parameter to be calibrated. Either a linear of constant correction was chosen for each instrument, depending on the time evolution of the offset for parameters (Table 7.1).

	190 m	**340 m**	**455 m**
Conductivity corrections	-0.0015 to 0.00054 $\mathrm{S\,m^{-1}}$	0.0013 $\mathrm{S\,m^{-1}}$	0.00077 to -0.0011 $\mathrm{S\,m^{-1}}$
Oxygen corrections	-0.315 to -0.215 $\mathrm{mL\,L^{-1}}$	-0.502 to -0.313 $\mathrm{mL\,L^{-1}}$	-0.428 to -0.283 $\mathrm{mL\,L^{-1}}$
Temperature corrections	-0.0007 C°	0.0037 to -0.0022 C°	-0.0084 C°

Table 7.1: The conductivity, oxygen and temperature corrections applied to different instruments on the Inner Mooring. If one value is listed, a constant correction was applied. If two numbers are listed, a linear correction was applied.

I plotted the temporal means for the original and corrected time series of conductivity, temperature and oxygen, and compared them to the CTD casts from Mar19, Oct19 and Mar20 (Figure 7.5). I excluded the results from Feb19 since it was similar to Mar19. The corrected data are closer to the CTD profiles than the original data, as expected since they were calibrated against the CTD casts. The corrected data fits nicely with the CTD profile, especially for the instruments at 340 m and 455 m. At 190 m, the the instrument is located in a gradient, which influence the vertical mean. Therefore are the corrected data at this depth the most off from from the CTD profiles.

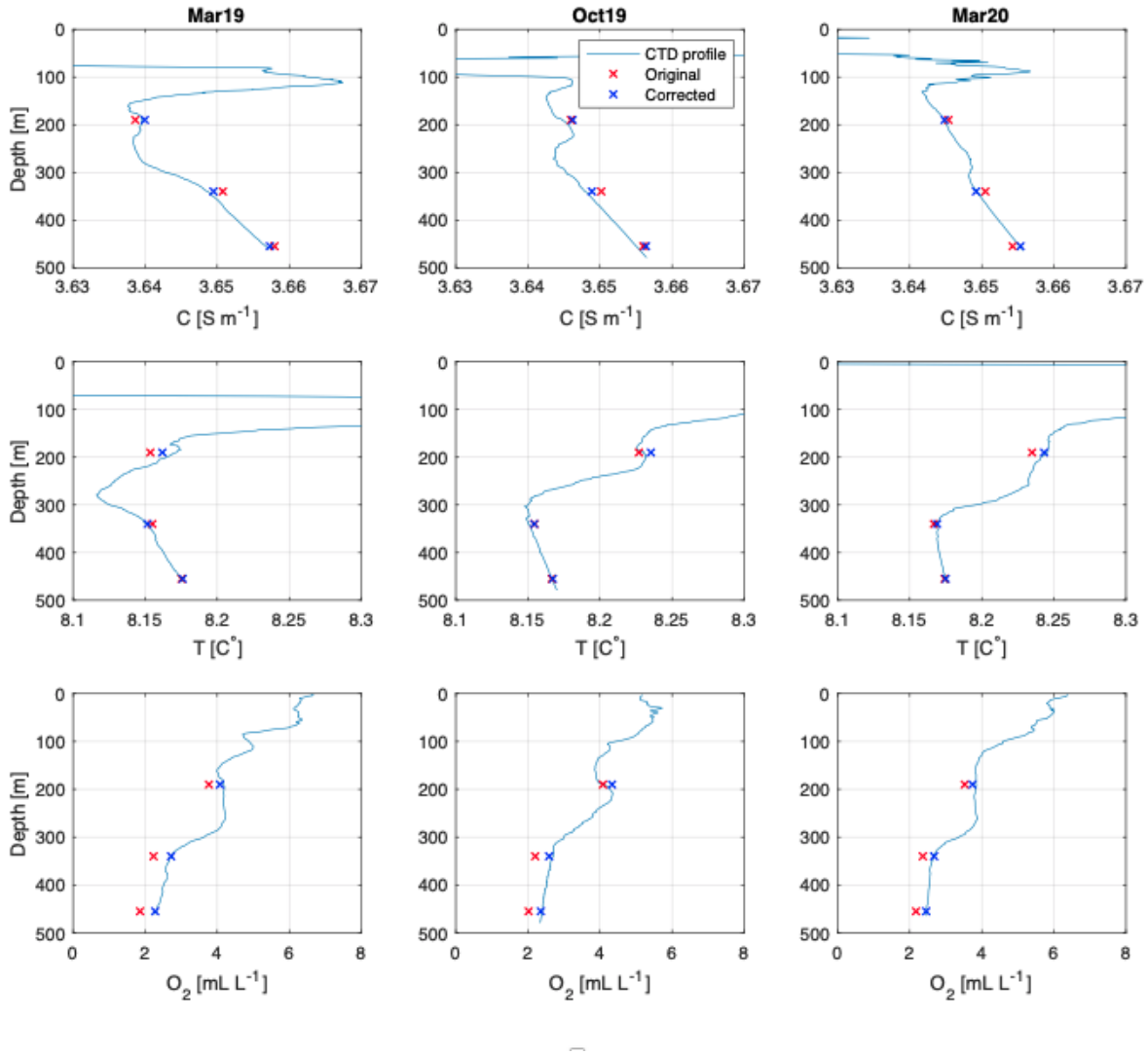

Figure 7.5: The corrected (blue) and non-corrected (red) temporal mean of the Inner Mooring data plotted against CTD casts from the cruises Mar19, Oct19 and Mar20. The upper panel shows the conductivity, middle panel show temperature and and the lower panel shows the oxygen.

To display the distribution of the data from each instrument, box plots of temperature, oxygen and salinity were created. The central statistical features shown in the box plots are the median, 25th and the 75th percentiles. 25th (75th) percentile is the middle value between the median and smallest (largest) number of the data set, and the range between them is the interquartile range. It also plots the outliers, which are datapoints outside of the whiskers. The whisker extends for 1.5 times the interquartile range away from the 25th or the 75th percentiles, and an outlieres is a datapoint outside of this range (Galarnyk, 12.09.2018). I also added the mean of the data for comparison.

According to the box plots (Figure 7.6), outliers were detected for all instruments. When removing the outliers found in the box plots, the interesting signals in the time series

disappeared . So, instead of removing the outliers detected with the box plot, I removed spikes from the data set with a despike-function that removed short-duration spikes from the time series.

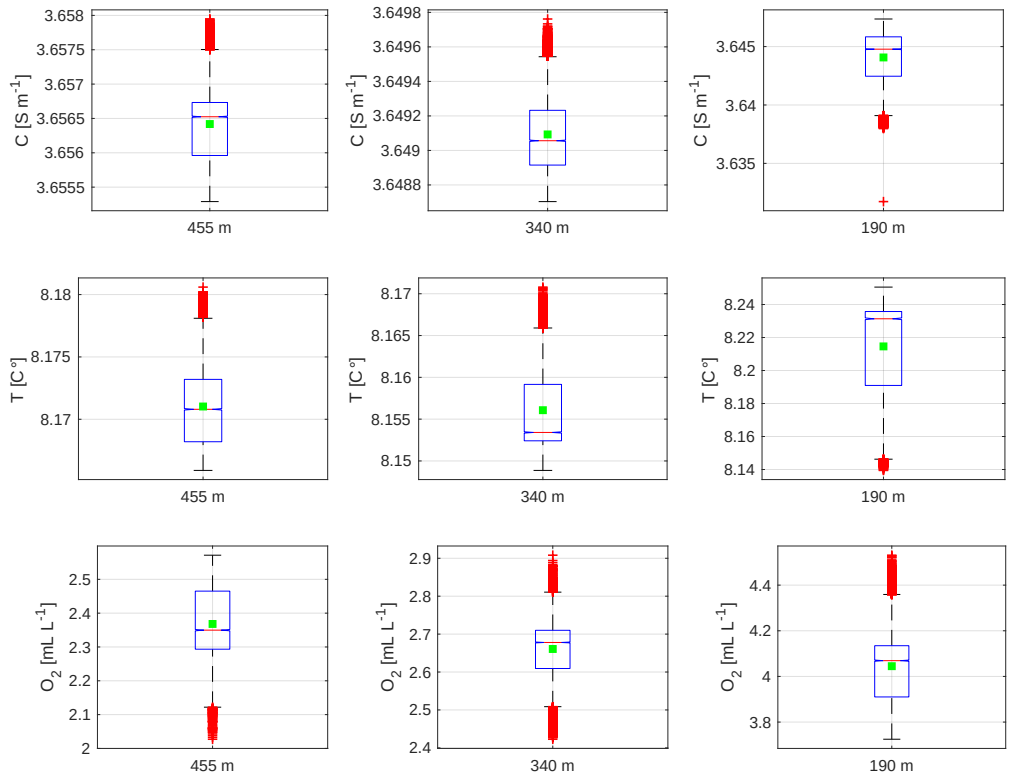

Figure 7.6: Box plots of Inner Mooring instruments. Data from conductivity (C), temperature (T) and oxygen (O_2) from each instrument at 455 m, 340 m and 190 m. The red line is the median, and the green square represent the mean for each instrument.

Since I was interested in the temporal evolution of temperature, salinity and oxygen, I applied a low-apss filter to smooth the time series. I used the moving mean filter as it is a simple and common filter to use to create weekly time series (Thomson and Emery, 2014). The moving mean was calculated for a box containing 48*7 data points, as the sampling interval for all instruments were 30 min which results in 48 samples each day (Figure 7.7).

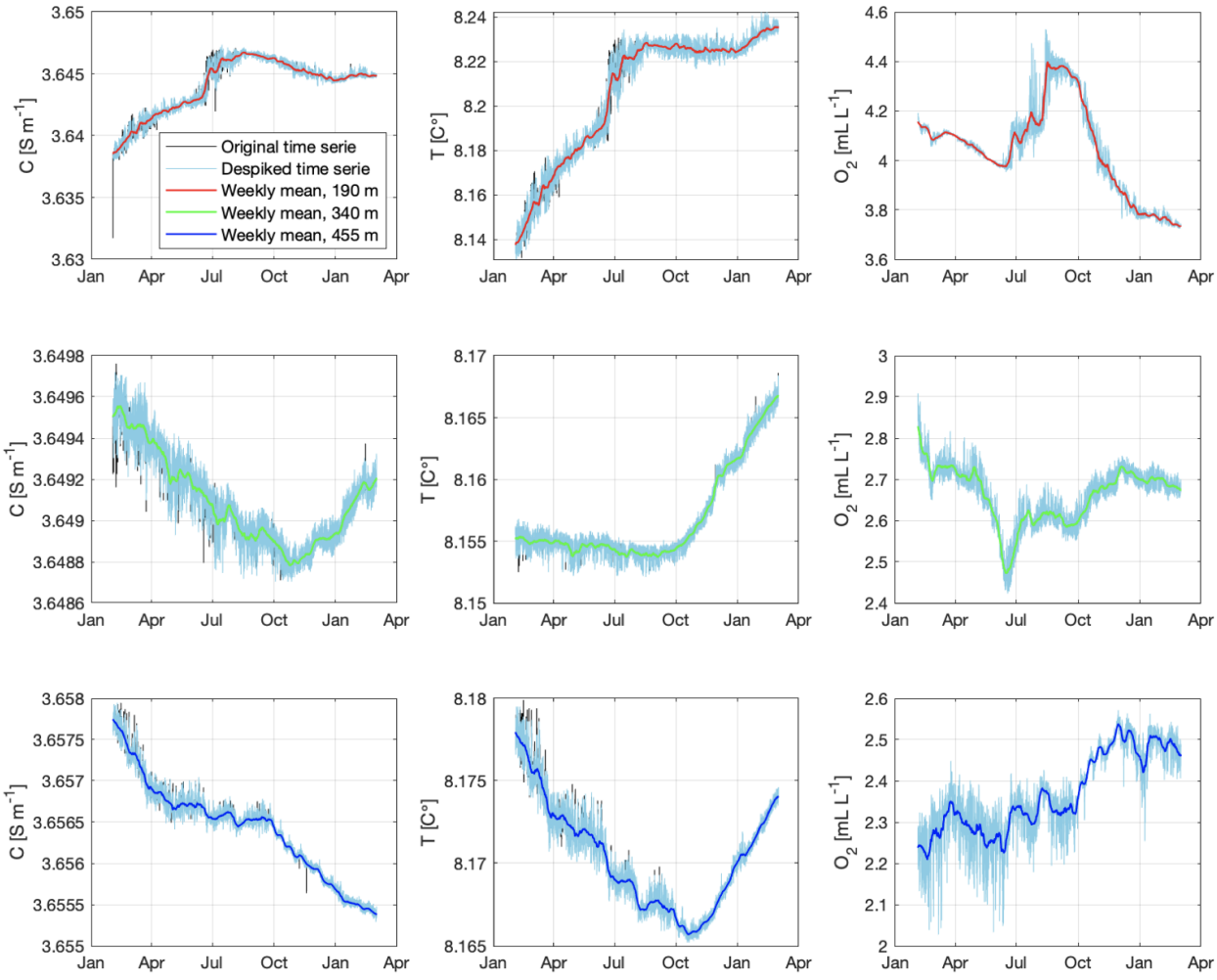

Figure 7.7: Time series of conductivity (C), temperature (T) and oxygen (O_2) from the Inner Mooring. Each subplot shows the original and the despiked time series together with the weekly mean. Note that scale differs from each subplot, and thus are not directly comparable.